Study of Scalars and Fermions in Models Beyond the Standard Model

Deepanjali Goswami

A thesis
submitted for the degree of
Doctor of Philosophy

Department of Physics
Indian Institute of Technology Guwahati
Guwahati 781039, India

June 2019

Study of Scalars and Fermions in Models Beyond the Standard Model

Deepanjali Goswami

A thesis
submitted for the degree of
Doctor of Philosophy

Supervisor:
Prof. Poulose Poulose

Department of Physics
Indian Institute of Technology Guwahati
Guwahati 781039, India

June 2019

Declaration

The work contained in the thesis entitled "**Study of Scalars and Fermions in Models Beyond the Standard Model**" has been carried out at the Department of Physics, Indian Institute of Technology Guwahati, India by me under the supervision of Prof. Poulose Poulose. The material of this thesis has not been submitted elsewhere for any other degree. Works presented in the thesis are all my own unless referenced to the contrary in the thesis.

Date:

(Deepanjali Goswami)
June, 2019
Department of Physics
Indian Institute of Technology Guwahati
Guwahati - 781039, India

Disclaimer

The bibliography included in this thesis is, by no means complete but contains the ones which are consulted thoroughly by me. I apologize for inadvertently missing out some of the research papers, review articles and other scientific documents pertaining to the focus of this thesis which should also have been cited.

Prof. Poulose Poulose

Department of Physics

Indian Institute of Technology Guwahati

Guwahati-781039, INDIA

Email: poulose@iitg.ac.in

Certificate

It is to certify that the work contained in the thesis entitled "***Study of Scalars and Fermions in Models Beyond the Standard Model***" by Ms. Deepanjali Goswami (Roll No -136121013), a PhD student in the Department of Physics, Indian Institute of Technology Guwahati is carried out under my supervision and has not been submitted elsewhere for the award of any degree.

Date:

Poulose Poulose

(Professor)

Dedicated

to

My parents and motherland...

Acknowledgements

I would like to express my gratitude, respect and appreciation to the Almighty before writing this page!

This page takes me to the onset of my deep involvement of pursuing PhD degree which begins from the picturesque and the utmost naturally beautiful campus, my beloved institution, to whom I would like to thank for giving me an opportunity to be a part of it with one of the most prestigious affiliations, the Indian Institute of Technology Guwahati. I feel myself very fortunate and honoured to get such an institute to spend couple of years with wonderful people around, surrounded by scenic beauty of mother nature. The presence of mighty Brahmaputra, the beautiful hills around the campus, with its lakes inside and flowers serve as a splendid feat to make it even more exquisite. Its collective contribution has inculcated in me slowly and silently, and immensely helped me in my learning process throughout this journey.

Having said that, now firstly and foremost, I would like to express my indebtful gratitude toward my thesis supervisor Prof. Poulose Poulose for giving me an opportunity to work under his esteemed and profound guidance. His continuous support, inspiration, constant motivation, encouragement and his immense knowledge have contributed towards successful completion of my PhD research work. He has always been motivating me to learn the deeper aspects of physics and his inspirational words immensely helped me to get the high spirit to do the research and to be able to move over all the ups and downs of research life. Alongwith, I would like to thank Ms. Stavelin Ma'am for her inspirational words and their two adorable kids Hasvid and Onella for sharing many beautiful moments with me.

I would also like to express my sincere gratitude to my doctoral committee members: Dr. Arunansu Sil (Chairman), Dr. Udit Raha, and Dr. Soumitra Nandi, for reviewing my yearly progress with their valuable suggestions and for giving me their insightful comments and encouragement, and also for their positive critics which aspired in me to widen my research process from various prospectives. I would also like to thank, all former and current, Head of Department of Physics (Prof. Saurabh Basu, Prof. Poulose Poulose and Prof. Subhradip Ghosh), for their support and providing me various departmental facilities. It is my pleasure to thank all the faculty members of the Department of Physics, IIT Guwahati for their support and help during this journey. Specially, I would like to express my grateful thanks to Dr. Subhaditya Bhattacharya, Dr. Tarak Nath Dey, Prof. Sunil K Khijwania, Dr. Debaprasad Maity, Dr. Malay Kumar Nandy, Prof. Perumal Alagarsamy, Prof. Girish Sampath Setlur. I thank all scientific officers of Department of Physics, IITG, specially Dr. Sidananda Sarma for his motivational words and Mr. Basab Bijoy Purkayastha for his continuous support and all time help at any emergency situation with all my technical issues. I would also like to acknowledge my department office staff members for their kind help.

It is my honour to reserve my special thanks to Prof. Benjamin Fuks, Dr. Debasish Borah for providing me an opportunity to work and having wonderful experience of learning while collaborating with them, I have learned several analysis techniques of my research work from Prof Fuks and my knowledge treasure has been benefitted immensely with the discussions I had with Dr. Debasish Borah. I greatly owe a lot to Prof Daniel Jeans for providing me valuable opportunity to work with him at KEK, Japan. I would like to sincerely thank him, as with him I learned the basics of the ILC study.

It is my privilege to thank all my teachers, starting from my school days, whose efforts and blessings have helped me in reaching to the current position. The person who holds a special place in my heart is my father cum my teacher Prof D. D. Goswami, for teaching me motivational lesson of life and to pursue my carrier in physics. I would remain indebted for his uncountable contribution in my life as a result of which I could achieve upto this stage. I also express my grateful thanks to my brother cum teacher Dr. Umananda Dev Goswami, for his help in making me wade through the challenging times of my life

and pursue the research. I am also highly thankful to Prof Bipul Bhuyan for his help and providing me a working space in a conducive ambience of his High Energy Physics Laboratory. He was also very kind to allow me to access his HEP cluster to carry out the necessary high speed computation for my research work. I am also thankful to him for having several insightful discussions about current physics scenarios in experimental high energy physics.

I extend my acknowledgement to DAE-BRNS, Govt of India for the research fellowship, International Travel Support under DST, Govt. of India for presenting a paper at the APS April Meeting 2016 held at Utah, USA. I also acknowledge Govt. of Japan, for selecting me for the Invitation Fellowship Program for Young Women Researchers in Asia Pacific Countries under Athena Program to visit KEK, Japan in January 2019.

I thank my research group friends: Dr. Satendra Kumar, Dr. Biswaranjan Das, Dr. Shibananda Sahoo, Subhasish Behera, Dr. Rashidul Islam, Suresh Chand and Sreemanti Chakraborti for their help and many fruitful discussions. I would also like to thank my senior research fellow members Dr. Deepanwita Dutta, Dr. Biswajit Karmakar and lab mates and friends Dr. Kamal Jyoti Nath, Maharnab, Dibyajyoti, Devender, Jyotirmoi, Shubhangi, Sunayana and Pulak for their kind help. A special thanks goes to my beloved friends Dr. Chandita Baruah, Dr. Prahlad Baruah, Niharika Baruah, Biju Bharali and Dr. Sushma Chityala for sharing the beautiful moments in the lovely IITG campus and always staying by my side in all my sad and happy times. The memories collected with them are as precious as they are.

This acknowledgement would remain incomplete without the mention of the love, the care, the hard work and the sacrifice of my ancestors, my grandparents, my beloved parents, my relatives and Guruji in bringing me up and also the utmost affection, given by my entire family, specially my sister Dr. Rupanjali Goswami and brother in law Mr. Nripen Mahanta for their constant support and keeping the faith in me to allow me to do what I like. I feel myself to be extremely fortunate to gain such unimaginable strength from Mummyji, my sisters Dr. Neelima Yadav, Teshma Di and Anamika, for supporting me unconditionally, and any degree of acknowledgment to the God's gifts: Dr. Nitin Yadav,

Krishna, Raj, Ruchi, Lucky, Kanha, Dolcy, would somewhere, definitely, leave in me a void of ungratefulness.

June, 2019 *Deepanjali Goswami*

Abstract

The Standard Model (SM) of particle physics is well established with the discovery of the Higgs boson by the independent experiments, ATLAS and CMS at LHC in 2012. The properties of the discovered Higgs boson is very similar to the proposed one in the SM and the discovery is considered as a remarkable success of this model. Inspite of this success, many experimental evidences provide hints of some fundamental issues; mainly absence of dark matter (DM), non-zero neutrino mass and hierarchy problem, which shows that the SM is not a complete theory. A possible way out of this situation is to look beyond the SM(BSM) to resolve these issues by accommodating new particles in the spectrum or extending the gauge sector of the SM. Out of many attractive proposals of BSM, models governing seesaw mechanism could explain the non-zero masses of neutrinos. Similarly, DM issue is addressed by many multi-Higgs models with or without addition of extra fermionic sector in the particle spectrum. Among the seesaw models, we consider Type III seesaw model, which is a simple extension of the SM with an additional $SU(2)_L$ fermion triplet and Minimal Left Right Symmetric Model(MLRSM) with additional Higgs fields and right-handed neutrino, and extending the gauge group by a additional $SU(2)_R$ symmetry. Alongside, we also consider Inert version of the Two Higgs Doublet Model with a charged fermion singlet as partner to it. But the fate of these BSM scenarios will be decided by the observation or non-observation of these new particles at collider experiments. Our main aim in this thesis is to focus on the collider signatures of Type III seesaw model, MLRSM, and Dark Matter Models in the context of Large Hadron Collider(LHC) and Future Leptonic Colliders(FLC).

In the first work of the thesis, we consider the Type III seesaw model to probe the heavy fermions arising in this model at high energy electron-positron collider through their direct production and subsequent decays. We study the single production of charged as well as neutral fermions in association with leptons at 1 TeV center of mass energy and pair production of charged fermion at 2 TeV center of mass energy. Our study establish that final states arising from single production of heavy fermions can probe electron type mixing very well with heavy fermions. $2j + e^- + \not{E}$ in the final state is the best channel providing 5σ sensitivity using less than 2 fb^{-1} luminosity. On the other hand, in the case of pair

production we consider both electron and muon type mixing, taking once at a time. The final state $4b + 2l$ comes out to be the best channel and can be probed with 5σ significance using around 50 fb^{-1} luminosity. Thus, clearly, the leptonic collider can fingerprint the mixing very efficiently, unlike the case of LHC. The mass reach of around 1 TeV can be achieved for the considered center of mass energy.

In the second work, we perform a collider study of the rich scalar sector of the Minimal version of the Left Right Symmetric Model. We consider the four-leptonic final state arising from the pair production of doubly charged Higgs boson and trileptonic final states arising from associated production of doubly charged Higgs boson with singly charged Higgs boson at 14 TeV LHC. A full set of signal and SM background analysis for a selected benchmark point is performed using 1000 fb^{-1} integrated luminosity. We generalise the study for upcoming High Luminosity -LHC and obtained required luminosity to probe four leptonic final state is around 350 fb^{-1} with 5σ sensitivity. For the trileptonic case, the required luminosity with 5σ sensitivity is quite larger, around 800-1200 fb^{-1}. We demonstrate the 5σ mass reach of doubly charged Higgs boson around 980 GeV and 960 GeV using 3000 fb^{-1} luminosity for four-leptonic and trileptonic final states, respectively.

In the last work, we consider Inert Higgs Doublet Model (IHDM) added with a charged partner fermions, which are considered as fermionic dark matter candidate along with scalar dark matter candidate originating from the Inert Higgs doublet. We emphasise the discovery possibility of such charged fermions arising in Multi Component Dark Matter Models at International Linear Collider(ILC) with its baseline center of mass energy of 250 GeV. The charged fermions are produced at ILC in pairs with gauge coupling and decays to tau lepton and lightest dark matter candidate. We perform a complete signal versus background study using ILCsoft. The outcome of the study is very impressive with the potential of discovering charged fermions using 50 fb^{-1} integrated luminosity.

Summarising, we focus on the models beyond the SM to probe the discovery potential of additional scalars and fermions at LHC and FLC.

List of Publications

1. "Direct searches of Type III seesaw triplet fermions at high energy e^+e^- collider", **Deepanjali Goswami**, P. Poulose, *Published in Eur. Phys. J. C78 (2018) no.1, 42.* arXiv:1702.07215.

2. "Investigating the scalar sector of left-right symmetric models with leptonic probes", Debasish Borah, Benjamin Fuks, **Deepanjali Goswami**, P. Poulose, *published in Phys.Rev. D98 (2018) no.3, 035008* . arXiv:1805.06910.

3. "Study of Charged Dark Fermions at ILC250", **Deepanjali Goswami,** Daniel Jeans, P. Poulose. (manuscript with collaborator).

4. "Probing the type-III seesaw model through $e^+e^- \to \Sigma^+\Sigma^-$ at ILC ", Sumit K. Garg, **Deepanjali Goswami**, P. Poulose, *published in the Journal of Physics-Conference series, IOP publishing with volume 481 on 5th March,2014.*

5. "Identification of Type-III Seesaw Fermionic Triplet at the International Linear Collider", **Deepanjali Goswami**, P. Poulose, *published in the Springers Pro. Phys. 174 (2016) 611-617.*

6. "Type-III Seesaw fermionic triplets at the International Linear Collider", **Deepanjali Goswami**, P. Poulose, *published in arXiv.org [arXiv:1507.04186].*

7. " Studying the Left Right Symmetric Model through Higgs production at the LHC", **Deepanjali Goswami**, P. Poulose, Debasish Borah, *published in the proceeding of CICAHEP, Dibrugarh University, 2015.*

Conferences/Workshops/Schools/visits

1. Paper entitled "Probing the type-III seesaw model through $e^+e^- \to \Sigma^+\Sigma^-$ at ILC" in the National Conference on Contemporary Issues in High Energy Physics & Cosmology 2013 at Gauhati University, Assam, India, February 12-14, 2013.

2. SERC PREPARATORY SCHOOL in Theoretical High Energy Physics organized by Department of Physics, Tezpur University, sponsored by DST, New Delhi, June 17- July 13, 2013.

3. Discussion meeting on EWSB and Flavors in the light of LHC at IIT Guwahati, Guwahati, India, February 20-22, 2014.

4. Paper entitled "Type III see saw fermionic triplets at International Linear Collider" in the "National Conference on Current Trends in Particle Physics Research" organized by Department of Physcics, University of Kalyani, March 13-15, 2014.

5. The Second Asia-Europe-Pacific School of High Energy Physics (AEPSHEP 2014) held in Puri, India, 4-17 November, 2014.

6. Paper entitled "Identification of Type-III seesaw fermionic triplet at the International Linear Collider" in the "XXI DAE-BRNS HIGH ENERGY PHYSICS SYMPOSIUM 2014" held at the Indian Institute of Technology Guwahati, 08-12 December, 2014.

7. XXIX SERC Main School in Theoretical High Energy Physics held at BITS Pilani, K K Birla Goa Campus, 20th December, 2014 - 8th January, 2015.

8. Paper entitled "Studying the Left Right Symmetric Model through charged Higgs Production at the LHC" in CICAHEP'15 at Dibrugarh University, 2-5 November, 2015.

9. Paper entitled "Type-III seesaw fermionic triplet at high energy e^+e^- collider" in the APS April Meeting 2016 in Salt Lake City, Utah, USA, 16-19 April, 2016.

10. School-cum-workshop on "Collider Physics: Events, Analysis and QCD", Department of Physics, IIT Guwahati, 27-31 March, 2017.

11. First Vietnam School on Neutrino at Quy Nhon, Vietnam during 10-21 July, 2017.

12. Attended Neutrino at Quy Nhon, Vietnam, 16-22 July, 2017.

13. GIAN course on Electroweak Symmetry Breaking, Flavour Physics and BSM at Indian Institute of Technology Guwahati, 18-22 December, 2017.

14. Visited KEK with an Invitation Fellowship for Young Women Researchers in Asia -Pacific Countries under Athena Program and worked under Prof. Daniel Jeans for three weeks, 20th January 2019 - 8th February 2019.

Contents

List of Figures

List of Tables

Chapter 1

Introduction

Understanding the mystery of Nature is one of the main engagements of mankind from the very beginning of its evolution. In particular the Particle Physics community focuses on answers to all the pertinent questions related to the characteristics of the elementary particles and their dynamics. Such elementary particles are expected to be the building blocks of the universe. Thus their dynamics and characteristics play an important role in the origin and evolution of the universe. A series of developments, in the 20th century, including the revolutionary ideas of quantum mechanics and special theory of relativity lead to deeper understanding of the world of subatomic particles. These further developed into the insightful mathematical framework of Quantum Field Theory incorporating the principle of gauge symmetry to guide particle interactions. The resulting theory is beautifully manifested to summarise all the elementary particles and fundamental interactions with their dynamics is widely known as **Standard Model (SM)** of Particle Physics. While it successfully explains most of the experimental results at high precision, there are compelling reasons to go beyond the SM (BSM). The lack of explanation for tiny neutrino mass and the requirement of a dark matter (DM) candidate are two of the major concerns of the present Particle Physics. There are many attempts to address these issues with extensions of the SM proposed to include higher gauge symmetries or larger particle spectrum. This thesis will mainly focus on some of the BSM scenarios, especially considering

the signatures of such models in the collider experiments like the Large Hadron Collider (LHC).

The arrangement of this chapter is in the following manner. First, we present the short description of the Standard Model and then we provide the main reasons to go beyond the Standard Model. Then we give a brief description of some of the BSM, which follows by the outlines of the main chapters of the thesis.

1.1 The Standard Model

SM, combining the electroweak theory proposed by Glashow, Weinberg and Salam [1, 2] to describe the electromagnetic and weak interactions, and quantum chromodynamics (QCD) describing the strong interaction, provides a beautiful description of the properties and interactions of the elementary particles. The SM is based on the following gauge group

$$SU(3)_C \times SU(2)_L \times U(1)_Y.$$

Here the subscript C represents color, the strong interaction charge, L represents left-handed chirality and Y represents weak-hypercharge. There are total twelve gauge bosons with spin 1 related to the local symmetry of the above gauge group. They can be described in the following way:

- $SU(3)_C$ is the special unitary gauge group representing color charges with eight gluons (G^A_μ), as gauge bosons (G^A_μ) describe strong interactions among quarks.
- $SU(2)_L$ is the gauge group of weak isospin, with three gauge bosons W^a_μ, describing weak interaction quarks and leptons.
- $U(1)_Y$ is the unitary gauge group of hypercharge (Y) with one gauge boson B_μ.

The building blocks of matter are fermions (spin-$\frac{1}{2}$ particles) called leptons and quarks. Both leptons and quarks are divided into three families with different masses. Leptons have only electro-weak interactions while quarks have both electroweak and strong interactions. Left-handed leptons are doublets under $SU(2)_L$ containing one charged lepton l_L and one neutrino ν_L, whereas the right-handed charged leptons (e_R, μ_R, τ_R) are singlets

Field content		$SU(3)_C$	$SU(2)_L$	$U(1)_Y$
Gauge	G^A_μ	8	1	0
	W^a_μ	1	3	0
	B_μ	1	1	0
Lepton	$L_i = \begin{pmatrix}\nu_L \\ e_L\end{pmatrix}_i$	1	2	-1
	e_{Ri}	1	1	-2
Quark	$Q_i = \begin{pmatrix}u_L \\ d_L\end{pmatrix}_i$	3	2	$\frac{1}{3}$
	u_{Ri}	3	1	$\frac{4}{3}$
	d_{Ri}	3	1	$-\frac{2}{3}$
Scalar	$\Phi = \begin{pmatrix}\phi^+ \\ \phi^0\end{pmatrix}$	1	2	1

Table 1.1: *Standard Model fields are represented along with quantum numbers associated with their symmetry groups. Here, i= 1, 2, 3 denotes the generation index; $e_i = e, \mu, \tau; u_i = u, c, t$ and $d_i = d, s, b$ respectively. In the subscript of G_A, the value of A goes from 1 to 8, representing 8 gluon fields, and a = 1, 2, 3 for three weak gauge bosons.*

under $SU(2)_L$. In the SM, there are no right-handed neutrinos. The quarks come in six flavours in the SM. Three of them are up-type quarks, up (u), charm (c), top (t) and rest three are down type quarks, down (d), strange (s) and bottom (b). Here again, the left-handed up type (u) and down type (d) quarks form a doublet under $SU(2)_L$, whereas the right-handed partner of these quarks are singlet under $SU(2)_L$ symmetry. Mass terms of gauge bosons and the fermions in the above set up are not permitted, as they break gauge invariance explicitly. On the other hand, experimentally we know some of these have non-zero mass. A way out of this is the Higgs mechanism, which breaks the symmetry spontaneously, and thereby generate mass terms for gauge boson. Fermions get their mass through their Yukawa interactions with the Higgs field. Higgs mechanism requires introduction of a scalar (spin-zero) field.

The quantum numbers of the SM fields corresponding to various gauge group can be summarised as in Table 1.1. The particle content of the SM with respective masses, electric charges and spins are given in Figure 1.1.

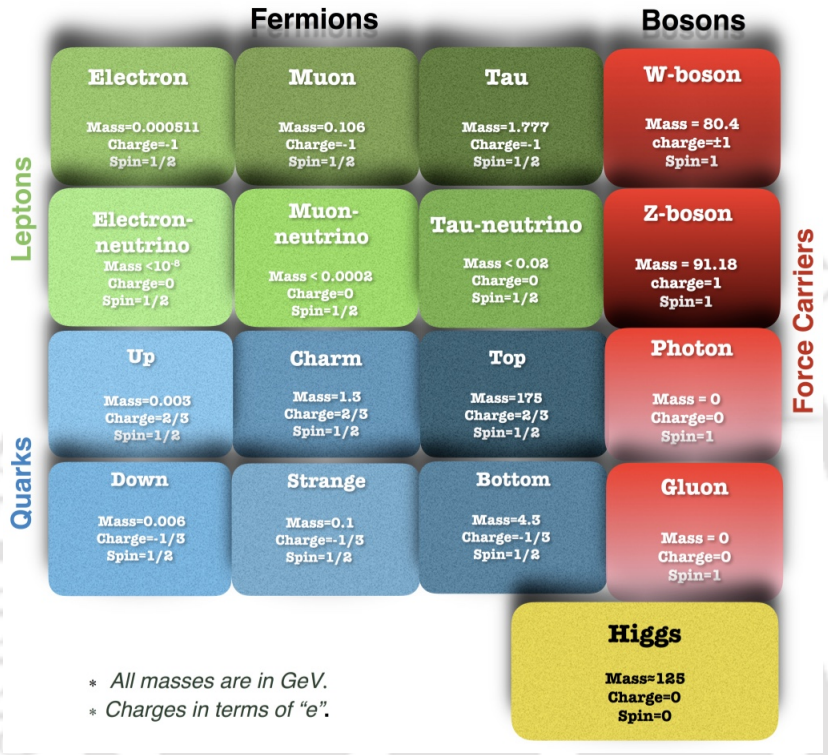

Figure 1.1: *Particle content with mass, charge and spin of the Standard Model.*

The SM Lagrangian that is consistent with the gauge group and the field content may be written as

$$\mathcal{L}_{SM} = \mathcal{L}_{quark} + \mathcal{L}_{lepton} + \mathcal{L}_{Gauge} + \mathcal{L}_{Yuk} + \mathcal{L}_{\phi}. \tag{1.1}$$

The Lagrangian $\mathcal{L}_{quark}$ includes the quark sector of the SM, is represented as follows

$$\mathcal{L}_{quark} = \overline{Q}_j i\gamma^\mu D^Q_\mu Q_j + \overline{q}_j i\gamma^\mu D^q_\mu q_j, \tag{1.2}$$

where

$$D^Q_\mu = (\partial_\mu - ig_s T^A G^A_\mu - ig\frac{\tau^a}{2}W^a_\mu - ig'YB_\mu), \tag{1.3}$$

$$D^q_\mu = (\partial_\mu - ig_s T^A G^A_\mu - ig'YB_\mu), \tag{1.4}$$

with Q_j the left-handed quark doublets and q_j the right-handed quark singlets, and $j = 1, 2, 3$ representing the three families. Similarly, $\mathcal{L}_{lepton}$ for lepton sector can be written as

$$\mathcal{L}_{lepton} = \overline{L}_j i\gamma^\mu D_\mu^L L_j + \overline{\ell}_j i\gamma^\mu D_\mu^\ell \ell_j, \tag{1.5}$$

where

$$D_\mu^L = (\partial_\mu - ig\frac{\tau^a}{2}W_\mu^a - ig'YB_\mu), \tag{1.6}$$

$$D_\mu^\ell = (\partial_\mu - ig'YB_\mu), \tag{1.7}$$

with L_j the left-handed lepton doublets and ℓ_j the right-handed lepton singlets ($\ell_j = e_R, \mu_R, \tau_R$). The kinetic term for the gauge field $\mathcal{L}_{Gauge}$ under the gauge group $SU(3)_C \times SU(2)_L \times U(1)_Y$ can be written as

$$\mathcal{L}_{Gauge} = -\frac{1}{4}G^{A\mu\nu}G^A_{\mu\nu} - \frac{1}{4}W^{a\mu\nu}W^a_{\mu\nu} - \frac{1}{4}B^{\mu\nu}B_{\mu\nu}, \tag{1.8}$$

where the field strength tensor $G^A_{\mu\nu}$, $W^a_{\mu\nu}$ and $B_{\mu\nu}$ represents the field content of $SU(3)_C$, $SU(2)_L$ and $U(1)_Y$ gauge groups, respectively. $G^A_{\mu\nu}$, $W^a_{\mu\nu}$ and $B_{\mu\nu}$ can be defined explicitly in terms of the corresponding gauge field as

$$G^A_{\mu\nu} = \partial_\mu G^A_\nu - \partial_\nu G^A_\mu - g_s f_{ABC} G^B_\mu G^C_\nu \ , \tag{1.9}$$

$$W^a_{\mu\nu} = \partial_\mu W^a_\nu - \partial_\nu W^a_\mu - g\epsilon_{abc} W^b_\mu W^c_\nu \ , \tag{1.10}$$

$$B_{\mu\nu} = \partial_\mu B_\nu - \partial_\nu B_\mu \ , \tag{1.11}$$

where f_{ABC} and ϵ_{abc} are real, called structure constants, antisymmetric under interchange of any two indices.

The $\mathcal{L}_\Phi$ and $\mathcal{L}_{Yuk}$ terms in Eq. 1.1 introduce the interaction of a scalar field, Φ with the gauge bosons and the fermions, thereby generating the masses to the corresponding particles. We describe this in the next subsection.

1.1.1 The standard Higgs mechanism

The symmetry of the electroweak gauge group followed by SM forbids mass terms in the Lagrangian for fermions and bosons. These masses can be generated through the well known Higgs Mechanism proposed by R. Brout, F. Englert, P. Higgs, G. S. Gurlanik, C. R. Hagen and T.W.B. Kibble [3–5] in 1964 preserving the renormalizability of the theory. This is achieved by introducing a $SU(2)_L$ doublet of complex scalar field with hypercharge $Y = 1$,

$$\Phi = \begin{pmatrix} \phi^+ \\ \phi^0 \end{pmatrix}, \tag{1.12}$$

where ϕ^+ and Φ^0 both are complex scalar fields. The Lagrangian involving the scalar field Φ can be written as

$$\mathcal{L}_\Phi = (D_\mu \Phi)^\dagger (D^\mu \Phi) - V(\Phi), \tag{1.13}$$

where the covariant derivative $D_\mu = \partial_\mu + ig\frac{\tau^a}{2}W_\mu^a + ig'\frac{Y}{2}B_\mu$, with g is the $SU(2)_L$ coupling and g' is the $U(1)_Y$ coupling. The scalar potential of the Lagrangian is given by

$$V(\Phi) = \mu^2 \Phi^\dagger \Phi + \lambda(\Phi^\dagger \Phi)^2. \tag{1.14}$$

If $\lambda > 0$ and $\mu^2 < 0$, the minimization condition on the potential V, i.e. $\frac{\partial V}{\partial(\Phi^\dagger \Phi)} = 0$, for the Φ field, gives a non zero *vacuum expectation value* (VEV) which can be expressed as

$$\left\langle \Phi^\dagger \Phi \right\rangle = v^2 = -\frac{\mu^2}{\lambda}. \tag{1.15}$$

Now we can expand the Φ field around the minimum VEV and takes the following form

$$\Phi = \frac{1}{\sqrt{2}} \begin{pmatrix} \phi_1(x) + i\phi_2(x) \\ v + h(x) + i\phi_3(x) \end{pmatrix}. \tag{1.16}$$

Here $\phi_1(x)$, $\phi_2(x)$, $\phi_3(x)$ and $h(x)$ are all real fields with $h(x)$ corresponding to the field of physical Higgs particle. Using a gauge transformation, the fields ϕ_1, ϕ_2 and ϕ_3 can be removed from the scalar field Φ, and transferred to the gauge bosons, W_μ^a and B^μ. Notice that we are now fixing the gauge by our choice of this transformation. This gauge in

which the physical spectrum is explicitly present is known as the unitary gauge or physical gauge. This addition of degrees of freedom is now manifested in the gauge bosons, leaving two massive charged gauge bosons, $W^{\pm} = \frac{1}{\sqrt{2}}(W^1_\mu \mp iW^2_\mu)$ and one massive neutral gauge boson, Z_μ. The neutral gauge boson is a suitable combination of W^3_μ and B_μ given by

$$Z_\mu = W^3_\mu \cos\theta_W - B_\mu \sin\theta_W . \tag{1.17}$$

The orthogonal combination,

$$A_\mu = W^3_\mu \sin\theta_W + B_\mu \cos\theta_W \tag{1.18}$$

corresponds to the massless photon, the mediator of EM interactions. The angle, $\theta_W = \tan^{-1}(\frac{g'}{g})$ is the weak mixing angle, also known as the Weinberg angle.

In this way, the $SU(2)_L \times U(1)_Y$ symmetry is broken down to the $U(1)_{EM}$ symmetry, with the corresponding gauge boson, the photon, indeed massless. The masses of the gauge bosons in terms of the VEV of the Φ and the gauge couplings are given by $M_{W^\pm} = \frac{1}{2}vg$ and $M_{Z^0} = \frac{1}{2}v\sqrt{(g^2 + g'^2)}$. Electromagnetic coupling constant e can be written in terms of parameters g, g' and θ_W :

$$e = g' \sin\theta_W = g \cos\theta_W .$$

The Higgs field itself, in this (unitary) gauge, can be written as

$$\Phi(x) = \frac{1}{\sqrt{2}} \begin{pmatrix} 0 \\ v + h(x) \end{pmatrix} . \tag{1.19}$$

As we mentioned earlier, the three degrees of freedom $\phi_1(x)$, $\phi_2(x)$, $\phi_3(x)$ of the scalar doublet reappear as the longitudinal components of the massive weak-isospin triplet gauge bosons. After the spontaneous symmetry breaking, the mass of the remaining degrees of freedom in Φ appears as SM Higgs boson with mass, $M_h = \sqrt{-2\mu^2}$. Given that $v = 246$ GeV from the measurement of Fermi coupling constant, $G_F = \frac{v^2}{\sqrt{2}}$, all other couplings in the scalar sector are fixed in terms of v and M_h. Thus the trilinear and quartic self interaction couplings of Higgs boson can be written as

$$\lambda_{hhh} = -\frac{\mu^2}{v} = \frac{M_h^2}{2v}, \quad \lambda_{hhhh} = \frac{-\mu^2}{v^2} = \frac{M_h^2}{8v^2}.$$

The interaction between the Higgs field and fermion field, the so called Yukawa coupling, gives masses to the fermions in the SM. The Yukawa Lagrangian

$$\mathcal{L}_{Yuk} = Y_{ij}^d \bar{Q}_i \ \phi \ d_{Rj} + Y_{ij}^u \bar{Q}_i \ \tilde{\phi} \ u_{Rj} + Y_{ij}^\ell \bar{L}_i \ \phi \ \ell_{Rj} + h.c., \tag{1.20}$$

where $\tilde{\phi} = i\tau_2\phi$ and $i, j = 1, 2, 3$ represents three generations of fermions, and $Y_{ij}^{d,u,\ell}$ are the complex Yukawa couplings. In addition to providing masses to the fermions, these terms also dictate the interaction of the Higgs boson, h, with the fermions. The predicted physical Higgs boson h is discovered by ATLAS and CMS collaborations [6, 7] in 2012, leading to the nobel prize for F. Englert and P. W. Higgs in 2013. The mass of the Higgs boson is measured to be $M_h \sim 125$ GeV. This most awaited discovery of Higgs boson is a grand success for Particle Physics community to complete the SM predictions and has began a new era of Particle Physics.

Inspite of being a very successful model including the very stringent experimental tests, many hints from theory and experiments clearly indicate that there are many unexplainable phenomena which the SM is not capable of addressing. In the next section, we are going to expose some of the open questions as well as limitations of the SM.

1.2 Limitations of the Standard Model

This section provides some of the fundamental physical phenomena in nature that the SM does not adequately explain.

1.2.1 Dark matter and dark energy

There are many observational evidences which show that a large amount of the energy content of the Universe is not visible. Evidences include observations of gravitational lensing, the galactic rotation curve [8] and the anisotropy in the cosmic microwave background radiation [9]. Present estimates show that the visible matter accounts for about

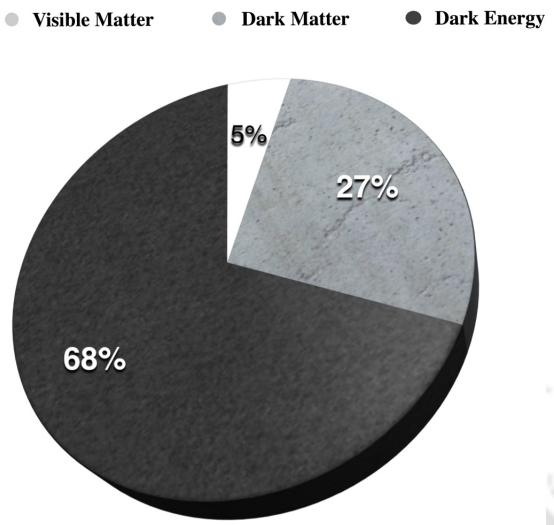

Figure 1.2: *The energy composition of the present universe.*

5% of total content of the universe. The remaining 96% is still unknown called as DM [10] and dark energy (see Figure 1.2). Of the missing 96%, about 27% accounts for DM, which would behave just like other matter, but which only interacts very weakly with the SM fields and therefore not visible, while the remaining 68% is being attributed to the dark energy, a constant energy density of the vacuum of the universe. The SM does not provide any fundamental particle that fits to the properties of DM. However, there are many extensions of the SM, which include viable DM candidates in their mass spectrum.

1.2.2 Matter - antimatter asymmetry

Today we see the universe which is mostly made out of matter consisting of electron, proton and neutrons. We do not find large regions of antimatter [11]. This can only happen when the matter and antimatter are created in a disproportionate ratio during the very early universe. However, the SM predicts that matter and anti-matter should have been created in equal amounts. This clearly indicates the need to go beyond the SM.

1.2.3 Neutrino masses

According to the Standard Model, neutrinos are supposed to be particles without mass. The SM theory can not construct a renormalizable term for neutrino mass due to the absence of the right-handed neutrino of any flavour. One possible solution to acquire neutrino mass is to extend the particle content of the SM. This is one of the shortcomings of the SM which makes extensions necessary as neutrino oscillation experiments [12] have shown that neutrinos do have mass.

1.2.4 Hierarchy problem of the Standard Model

The experimentally measured mass of the Higgs boson is found to be around 125 GeV. The tree level Higgs mass in the SM is given by $M_h^2 = \lambda v^2$. This mass term gets modified

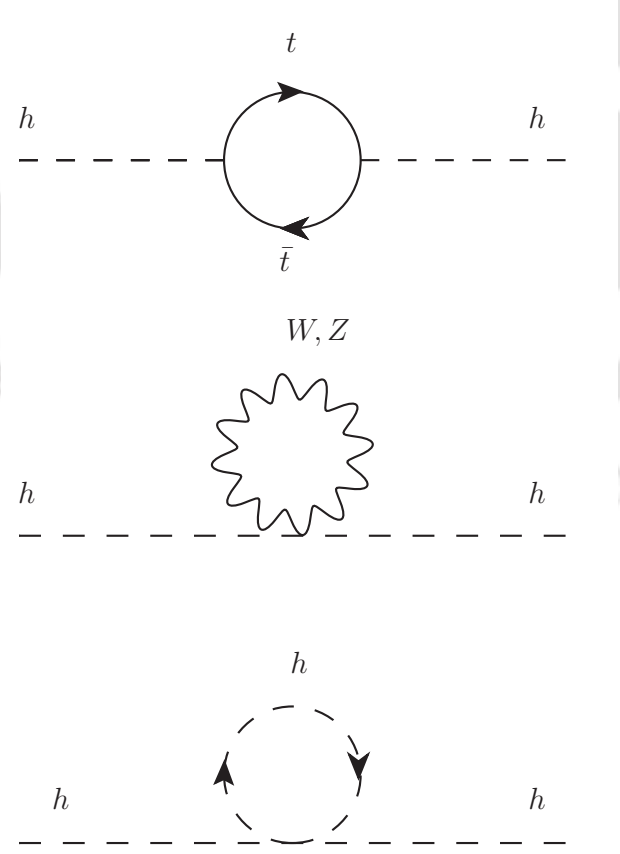

Figure 1.3: *Different loop diagrams contributing to the Higgs mass.*

when higher order perturbative corrections (see Figure 1.3) are included into it. The

modified physical mass of Higgs boson can be written as

$$M_h^2 = M_{0h}^2 + \Delta M_h^2. \tag{1.21}$$

Considering the major contributions due to the top-quark, W/Z bosons and self Higgs itself in the loop, the one loop contributions to the corrections are given by,

$$\Delta M_h^2 = \frac{3\Lambda^2}{8\pi^2}\left[-y_t^2 + \frac{g^2}{6} + \frac{\lambda^2}{6}\right], \tag{1.22}$$

where y_t is the Yukawa coupling to the top quark, g is the $SU(2)_L$ gauge coupling, λ is the quartic coupling of the Higgs and Λ is a cutoff scale.

As clearly seen, ΔM_h^2 gives a very large correction which is proportional to the square of the cut off scale. If the SM is valid upto GUT scale ($M_{GUT} \sim 10^{16}$ GeV) or Planck scale ($M_P \sim 10^{19}$ GeV), then the corresponding coupling must be chosen very precisely $\mathcal{O}(10^{-14} - 10^{-17})$ to have the Higgs mass of the order of EW scale. This suggests that there must be some new physics that become relevant at around a few TeV scale so that the above fine tuning of the coupling is not required.

1.3 Few glimpses of BSM physics

Considering the shortcomings of the SM explained in the previous section we now discuss some of the possible models beyond the Standard Model in this section.

1.3.1 Seesaw model for neutrino mass generation mechanism

The unambiguous evidence of the neutrino oscillation opens up a new window by accounting for their tiny mass, which is about six or more orders of magnitude smaller than electron mass and hence, provide the most compelling reasons to think beyond the SM. One of the most appealing theoretical approaches to generate the neutrino mass, is known as the seesaw mechanism [13–18]. In seesaw mechanism, the tininess of the neutrino mass is attributed to the heaviness of a partner particle, justifying the name of the mechanism.

We discuss the theory behind the seesaw mechanism and its three different types in this section.

In the seesaw mechanism, one assumes the existence of the right-handed neutrinos ν_R besides the SM left-handed neutrinos ν_L. Under this assumption a Dirac mass term for neutrinos can be written in the following form,

$$\mathcal{L}^D_{mass} = m_D \bar{\nu}_R \nu_L + h.c. = \frac{1}{2}(m_D \bar{\nu}_R \nu_L + m_D \bar{\nu}^c_L \nu^c_R) + h.c. \tag{1.23}$$

Since neutrinos have no electric charge, in general Majorana mass terms can also be possible. One can construct the Majorana mass term as follows,

$$\mathcal{L}^M_{mass,L} = \frac{1}{2}\, m_L \bar{\nu}^c_L \nu_L + h.c.\,, \tag{1.24}$$

$$\mathcal{L}^M_{mass,R} = \frac{1}{2} m_R \bar{\nu}^c_R \nu_R + h.c. = \frac{1}{2} m_R \bar{\nu}_R \nu^c_R + h.c. \tag{1.25}$$

Here the subscript c represents the charge conjugation and $\nu_{L/R}$ are left and right-handed neutrino representations. Now one can introduce a mass matrix

$$M = \begin{pmatrix} m_L & m_D \\ m_D^T & m_R \end{pmatrix}, \tag{1.26}$$

so that,

$$\mathcal{L}_{mass} = \mathcal{L}^D_{mass} + \mathcal{L}^L_{mass} + \mathcal{L}^R_{mass} = \frac{1}{2} \bar{n}^c_L M n_L, \tag{1.27}$$

where left-handed neutrino field n_L can be defined as,

$$n_L = \begin{pmatrix} \nu_L \\ \nu^c_R \end{pmatrix}, \bar{n^c_L} = \begin{pmatrix} \bar{\nu}^c_L & \bar{\nu}_R \end{pmatrix}. \tag{1.28}$$

We can now represent all the mass terms together in terms of Mass matrix as follows

$$\mathcal{L}_{mass} = \begin{pmatrix} \bar{\nu_L}^c & \bar{\nu}_R \end{pmatrix} \begin{pmatrix} m_L & m_D \\ m_D^T & m_R \end{pmatrix} \begin{pmatrix} \nu_L \\ \nu^c_R \end{pmatrix}. \tag{1.29}$$

After Diagonalizing the mass matrix M, we get the physical mass corresponds to the eigenvalues of M,

$$m_{1,2} = \left|\frac{1}{2}\left(m_L + m_R \pm \sqrt{(m_L - m_R)^2 + 4m_D^2}\right)\right|. \tag{1.30}$$

Since ν_L and $\bar{\nu}_L^c$ have third component of isospin, $I_3 = +\frac{1}{2}$ and $-\frac{1}{2}$, respectively, the SM gauge symmetries forbid the left-handed Majorana term. This means that m_L is required to be zero. In the seesaw theory, the right-handed neutrino field ν_R is assumed to be with a heavy mass, whereas m_D is of the electroweak scale. Therefore $m_D \ll m_R$. Then the simplified mass eigen values are

$$m_1 \approx \frac{m_D^2}{m_R} \tag{1.31}$$

and

$$m_2 \approx m_R\left(1 + \frac{m_D^2}{m_R^2}\right) \approx m_R. \tag{1.32}$$

This suggests that mass m_1 is suppressed by $1/m_R$, so if m_R is very heavy then m_1 is very light and m_2 is very large. One can remark in the same context, to obtain the low experimental mass limit for the neutrino, right-handed mass scale has to be in the GUT scale. This mechanism provides a natural way of explaining the observed small neutrino masses, known as Seesaw Mechanism.

There are three types of seesaw model on the basis of the way the Majorana mass terms are generated. We briefly discuss three of them below.

Type I seesaw model:

In the Type I seesaw model [14], at least two SM gauge singlet right-handed heavy neutrino fields (N_R) are introduced. These new fields couple to leptons and the Higgs field, through Yukawa interactions. The light neutrino mass is inversely proportional to the heavy right-handed neutrino field and thus it is allowed to be naturally small.

Type II seesaw model:

The Type II seesaw model [16, 19, 20] is introduced by replacing the $SU(2)_L$ singlet fermion as in Type I seesaw case by a scalar triplet, with hypercharge of the scalar fields,

$Y = 2$. The VEV acquired by these triplet scalars induces Majorana mass to the neutrinos.

Type III seesaw model:

The Type III seesaw model [21] introduces a $SU(2)_L$ fermionic triplet field with hypercharge $Y = 0$. The Yukawa term including SM lepton doublet and the SM Higgs field along with the triplet fermion provides the necessary Majorana mass term through the VEV of the Higgs field. The particle spectrum contains both charged and neutral heavy fermionic fields in addition to the SM particles. In one of the works we present in this thesis considers collider searches of heavy fermions in this model. We explain the details of this model in subsection 1.4.2.

1.3.2 Minimal left right symmetric model

The Minimal Left Right Symmetric Model (MLRSM) [22–33] is a well motivated gauge extension of the SM, providing a natural explanation for parity violation. Moreover, many GUT models go through a Left-Right Symmetric stage before finally arriving at the SM gauge symmetry. In the Left-Right Symmetric paradigm, the Abelian hypercharge symmetry group $U(1)_Y$ of the SM is extended to an $SU(2)_R \times U(1)_{B-L}$ gauge group and the right-handed $SU(2)_L$ fermionic singlets are collected into $SU(2)_R$ doublets, which naturally requires the introduction of right-handed neutrino fields in the spectrum. Focusing on minimal model building possibilities (based on Type-I and Type-II seesaws), the extended gauge symmetry is spontaneously broken down to the SM gauge symmetry, thanks to a scalar field that lies in the adjoint representation of $SU(2)_R$.

1.3.3 Two Higgs doublet model

One of the important issues in the SM is mass hierarchy with the fermion sector. Considering this drawback as one of the primary motivation, the SM Higgs sector can be simply extended with one more Higgs doublet, and as a result fermions can get mass from two different doublets. This model is well known as the Two Higgs Doublet Model (THDM) [34, 35]. The extended Higgs doublet respects the symmetries of the SM.

1.3.3.1 Inert Higgs doublet model

This is a modified version of THDM [36] obtained by making the second Higgs doublet decoupled from the rest of the particle spectrum. This model is proposed to address some of the most challenging issues like the presence of dark matter. The second Higgs doublet of this model is considered to be odd under a Z_2 symmetry, while rest of the particle spectrum is even under the same symmetry such that fermions and scalar from SM like Higgs doublet of the model will not have any coupling with the second Higgs doublet. In addition to the SM like Higgs boson, this model contains a charged Higgs, one pseudo scalar, a lightest neutral scalar which is considered as DM candidate. Due to the imposed additional symmetry, second Higgs doublet neither gain VEV nor interact with the fermionic sector of the model. Therefore, this model is named as **Inert Higgs Doublet Model (IHDM)**.

1.3.4 Supersymmetric models

"Hierarchy problem" discussed in the previous section indicates that physics beyond the SM that protects the Higgs mass against large quantum corrections should exist in the multi-TeV regime. One possible way to address the hierarchy problem is the introduction of supersymmetry, which unifies bosons and fermions into one framework, shielding the scalar boson mass from diverging high-energy corrections. Supersymmetry requires essentially the doubling of the particle content compared to the SM, with the lightest super-partner providing a natural candidate for DM. Besides, these models have richer scalar sector, making the electroweak symmetry breaking sector more robust.

1.4 Main focus of the thesis

As we discussed, we have seen that there are many reasons that forces us to look beyond the SM.

Among many BSM physics models, we focus our study, primarily on models with neutrino mass generation mechanism and DM issue in this thesis. While we will not

discuss how these models address these issues, but we focus mostly on the possible collider signatures of such models, both in the context of the LHC and Future Leptonic Colliders (FLC) like the International Linear Collider(ILC) or Compact Linear Collider (CLIC). The study in general addresses identification of heavy charged and neutral fermions arising in different models. We limit our study to Type III seesaw model with heavy charged as well as neutral fermions, the Left Right Symmetric Model, where interesting collider phenomenology arise in the scalar sector, and one of the novel DM models with multiple DM candidates. In one of the projects under the thesis work, we search for the signature of heavy fermionic field arising in the Type III seesaw model including detailed background study. In the second work, search for doubly charged Higgs boson though leptonic channels arising in MLRSM is carried out in the context of LHC. In the third study, we consider collider study of charged fermion singlet arising in Multi Component Dark Matter Model.

1.4.1 Overview of Future Linear Colliders

The proposed two leading future electron-positron linear colliders are the ILC [37] and CLIC[38]. In this section we provide an overview of the two future colliders.

International Linear Collider:

The ILC would be the largest high luminosity linear collider across the globe in particle physics, intended to make it for precision measurement and studying the Higgs boson with a centre-of-mas energy of 250 GeV. The first stage of this collider will have a baseline center-of-mass energy of 250 GeV and the second stage will have a center-of-mass energy of 500 GeV which is planned with a possible upgradation upto 1 TeV. The length of the ILC will be 30 km to 50 km. Two detectors concept have been employed for the ILC: one is International Large Detector (ILD) [39] and other is Silicon Detector (SiD) [40]. The main prototypes of the ILC is shown in Table 1.2.

	250 GeV	500 GeV
Collision rate	5 Hz	5 Hz
Electron linac rate	10 Hz	5 Hz
Number of bunches	1312	1312
Bunch population	2×10^{10}	2×10^{10}
Bunch separation	554 ns	554 ns
Pulse current	5.8 mA	5.8 mA
Main linac average gradient	14.7 MVm^{-1}	31.5 MV m^{-1}
Average total beam power	5.9 MW	10.5 MW
Estimated AC power	122 MW	163 MW
Luminosity	0.75×10^{34} cm^{-2} s^{-1}	1×10^{34} cm^{-2} s^{-1}
Beam polarization (e^-)	80%	80%
Beam polarization (e^+)	30%	30%

Table 1.2: The parameters of ILC for 250 GeV and 500 GeV.

Compact Linear Collider:

The another proposed electron-positron linear particle collider is to build at CERN is CLIC [38] in order to better study the Higgs boson and top quark. There are three stages to be built for CLIC: the first stage is with center-of-mass energy of 380 GeV; the second stage is with a center-of-mass energy of 1.5 TeV and the final stage is with a center of mass energy of 3 TeV. The main parameters of the CLIC is listed in Table 1.3.

Parameters	Symbol	Unit	Stage 1	Stage 2	Stage 3
Center-of-mass energy	$\sqrt{s}$	GeV	380	1500	3000
Repetition frequency	f_{rep}	Hz	50	50	50
Number of bunches per train	n_b		352	312	312
Bunch separation	Δt	ns	0.5	0.5	0.5
Total luminosity	$\mathcal{L}$	10^{34} cm^{-2} s^{-1}	1.5	3.7	5.9
Total integrated luminosity per year	$\mathcal{L}_{int}$	fb^{-1}	180	444	708
Main Linac tunnel length	km		11.4	29.0	50.1
Number of particles per bunch	N	10^9	5.2	3.7	3.7
Bunch length	σ_z	μm	70	44	44

Table 1.3: The main parameters of CLIC energy stages.

Apart from these linear colliders, the Circular Electron Positron Collider (CEPC) [41–43], in a 100 km tunnel in China, which is aimed to study the Z, and W, and the Higgs boson, with centre-of-mass energies from 90 to 250 GeV. The Future Electron-positron

Circular Collider (FCC-ee) [44, 45] which will be built at CERN, for the study of the entire Electroweak sector (Z and W bosons, Higgs bosons and top quark) with centre -of-mass energies between 88 GeV and 365 GeV.

In the next section we explain the models considered for our study in some detail.

1.4.2 Structure of type III seesaw model

In this section we describe the features of the Type III seesaw model [46, 47] relevant to our study. The Lagrangian involving the $SU(2)_L$ triplet fermion field, denoted here as Σ, along with the SM part denoted by $\mathcal{L}_{SM}$ is given by $\mathcal{L} = \mathcal{L}_{SM} + \mathcal{L}_{\Sigma}$, with

$$\mathcal{L}_{\Sigma} = \mathrm{Tr}\big(\bar{\Sigma}\, i \not{D} \Sigma\big) - \frac{1}{2} M_{\Sigma}\, \mathrm{Tr}\left(\bar{\Sigma}\Sigma^c + \bar{\Sigma}^c\Sigma\right) - \sqrt{2}\, Y_{\Sigma\ell}\, \left(\tilde{\phi}^{\dagger}\bar{\Sigma}L - \bar{L}\Sigma\tilde{\phi}\right), \quad (1.33)$$

where M_{Σ} is the mass parameter of the triplet and $Y_{\Sigma\ell}$ is the Yukawa couplings corresponding to the lepton flavours $\ell = e,\ \mu,\ \tau$. The left-handed lepton doublets of the SM is denoted by $L \equiv (\nu, \ell)^T$, and the Higgs doublet by $\phi \equiv (\phi^+,\ \phi^0)^T \equiv (\phi^+,\ (v+H+i\eta)/\sqrt{2})^T$, with $\tilde{\phi} = i\tau_2\, \phi^*$. The fermion triplet Σ is explicitly given by

$$\Sigma = \begin{pmatrix} \Sigma^0/\sqrt{2} & \Sigma^+ \\ \Sigma^- & -\Sigma^0/\sqrt{2} \end{pmatrix}, \quad \Sigma^c = \begin{pmatrix} \Sigma^{0c}/\sqrt{2} & \Sigma^{-c} \\ \Sigma^{+c} & -\Sigma^{0c}/\sqrt{2} \end{pmatrix} \quad (1.34)$$

and $\Sigma^c \equiv C\bar{\Sigma}^T$ is the conjugate of Σ, where C is the charge conjugation operator. Since the triplets have zero hypercharge, covariant derivative takes the following form

$$D_{\mu} = \partial_{\mu} - i\sqrt{2}\, g \begin{pmatrix} W^3_{\mu}/\sqrt{2} & W^+_{\mu} \\ W^-_{\mu} & -W^3_{\mu}/\sqrt{2} \end{pmatrix}. \quad (1.35)$$

The two-component charged spinors are combined into Dirac spinor $\Psi \equiv \Sigma^{+c}_R + \Sigma^-_R$, with $\Psi_R \equiv \Sigma^-_R$, and $\Psi_L \equiv \Sigma^{+c}_R$, to conveniently express the mixing of the SM charged leptons with the triplets, whereas the neutral component, Σ^0_R is left as the two-component

Majorana fermion. The Lagrangian in the new set up is given by

$$\begin{aligned}\mathcal{L}_\Sigma &= \overline{\Psi} i \not{\partial}\Psi + \overline{\Sigma}^0_R i \not{\partial}\Sigma^0_R - g\, W^3_\mu\, \bar{\Psi}\gamma^\mu\Psi + g\left(W^+_\mu\, \bar{\Sigma}^0_R\gamma^\mu P_R\Psi + W^+_\mu\, \bar{\Sigma}^{0c}_R\gamma^\mu P_L\Psi + h.c.\right)\\ &\quad -M_\Sigma\bar{\Psi}\Psi - \left(\frac{1}{2}M_\Sigma\, \bar{\Sigma}^0_R\Sigma^{0c}_R + h.c\right)\\ &\quad -\sum_\ell Y_{\Sigma\ell}\left(\phi^0\bar{\Sigma}^0_R\, \nu_L + \phi^0\bar{\Sigma}^{0c}_R\, \nu^c_L + \sqrt{2}\phi^0\bar{\Psi}\ell_L + \phi^+\bar{\Sigma}^0_R\ell_L - \sqrt{2}\phi^+\bar{\nu}^c_\ell\Psi\right) + h.c.\end{aligned} \tag{1.36}$$

The first line of the $\mathcal{L}_\Sigma$ represents the kinetic terms and this gauge interaction terms; the second line of it gives the mass of the charged and neutral fermions and the last line represents the Yukawa coupling terms of charged and neutral fermions with Higgs field.

The explicit form of Lagrangian containing Dirac mass term for the charged sector of the model is given by

$$\mathcal{L} \ni -\begin{pmatrix}\overline{\ell}_R & \overline{\Psi}_R\end{pmatrix}\begin{pmatrix} m_\ell & 0 \\ vY_{\Sigma\ell} & M_\Sigma\end{pmatrix}\begin{pmatrix}\ell_L \\ \Psi_L\end{pmatrix} - \begin{pmatrix}\overline{\ell}_L & \overline{\Psi}_L\end{pmatrix}\begin{pmatrix} m_\ell & vY^\dagger_{\Sigma\ell} \\ 0 & M_\Sigma\end{pmatrix}\begin{pmatrix}\ell_R \\ \Psi_R\end{pmatrix}, \tag{1.37}$$

where vacuum expectation value $v = \sqrt{2}\left\langle\phi^0\right\rangle = 246$ GeV. A similar form of Lagrangian for the mass term for neutral sector including neutrino and neutral component of the fermion is given by

$$\begin{aligned}\mathcal{L} \ni &-\begin{pmatrix}\overline{\nu}_L & \overline{\Sigma}^{0c}_R\end{pmatrix}\begin{pmatrix} 0 & vY^\dagger_{\Sigma\ell}/2\sqrt{2} \\ vY^\star_{\Sigma\ell}/2\sqrt{2} & M_\Sigma/2\end{pmatrix}\begin{pmatrix}\nu^c_L \\ \Sigma^0_R\end{pmatrix}\\ &-\begin{pmatrix}\overline{\nu}^c_L & \overline{\Sigma}^0_R\end{pmatrix}\begin{pmatrix} 0 & vY^T_{\Sigma\ell}/2\sqrt{2} \\ vY_{\Sigma\ell}/2\sqrt{2} & M_\Sigma/2\end{pmatrix}\begin{pmatrix}\nu_L \\ \Sigma^{0c}_R\end{pmatrix},\end{aligned} \tag{1.38}$$

where we consider a diagonal $Y_{\Sigma\ell} = \begin{pmatrix}Y_{\Sigma e} & Y_{\Sigma\mu} & Y_{\Sigma\tau}\end{pmatrix}$. After diagonalizing the mass matrix in Eq 1.38, we can write down the neutrino mass matrix in this model

$$m_\nu = -\frac{v^2}{2}Y^T_{\Sigma\ell}\frac{1}{M_\Sigma}Y_{\Sigma\ell}. \tag{1.39}$$

The Lagrangian after diagonalizing the mass matrices can be represented in terms of mass basis and they are listed in Appendix A.1.

1.4.3 Details of the minimal left right symmetric model

Left-Right Symmetric Models [22–31] are extensions of the SM, where the gauge symmetry group is enlarged to $SU(3)_c \times SU(2)_L \times SU(2)_R \times U(1)_{B-L}$. In Minimal Left-Right-Symmetric incarnations, the theory is additionally invariant under discrete left-right symmetry (or D-parity) transformations that relate the $SU(2)_L$ and $SU(2)_R$ sectors. The right-handed SM fermionic degrees of freedom are grouped into $SU(2)_R$ doublets, which renders the presence of right-handed neutrinos natural. Compared to the SM case, the Higgs sector is significantly enriched. The SM $SU(2)_L$ Higgs doublet is promoted to a $SU(2)_L \times SU(2)_R$ Higgs bidoublet Φ allowing to write gauge-invariant Yukawa interactions yielding Dirac mass terms for all fermions. The breaking of the gauge symmetry down to the electroweak symmetry further requires the presence of an $SU(2)_R$ scalars, which is considered as a triplet Δ_R in MLRSM. In order to maintain the theory D-parity symmetric, we include its $SU(2)_L$ counterpart Δ_L. The Lagrangian of the model [48, 49] is written as,

$$\mathcal{L}_{\text{MLRSM}} = \mathcal{L}_{\text{kinetic}} + \mathcal{L}_{\text{Yukawa}} - V_{\text{scalar}}, \tag{1.40}$$

where $\mathcal{L}_{\text{kinetic}}$ contains standard kinetic and gauge interaction terms for all fields. The Yukawa interactions read

$$\begin{aligned}\mathcal{L}_{\text{Yukawa}} = & -\Big[y_{ij}\bar{\ell}_{iL}\Phi\ell_{jR} + y'_{ij}\bar{\ell}_{iL}\tilde{\Phi}\ell_{jR} + Y_{ij}\bar{q}_{iL}\Phi q_{jR} + Y'_{ij}\bar{q}_{iL}\tilde{\Phi}q_{jR} \\ & + \frac{1}{2}f_{ij}\left(\bar{\ell}^c_{iR}\tilde{\Delta}_R\ell_{jR} + \bar{\ell}^c_{iL}\tilde{\Delta}_L\ell_{jL} + \text{h.c.}\right)\Big],\end{aligned} \tag{1.41}$$

where $\tilde{\Phi} = \sigma_2\Phi^*\sigma_2$ and $\tilde{\Delta}_{L,R} = i\sigma_2\Delta_{L,R}$. As a consequence of the built-in D-symmetry, both $SU(2)_L$ and $SU(2)_R$ neutrino couplings f_L and f_R are equal to a unique value f.

The scalar potential $V_{\rm scalar}$ is given by

$$\begin{aligned}
V_{\rm scalar} = &-\mu_1^2 {\rm Tr}\big[\Phi^\dagger\Phi\big] - \mu_2^2 {\rm Tr}\big[\Phi^\dagger\tilde{\Phi} + \tilde{\Phi}^\dagger\Phi\big] - \mu_3^2 {\rm Tr}\big[\Delta_L^\dagger\Delta_L + \Delta_R^\dagger\Delta_R\big] + \lambda_1\Big({\rm Tr}\big[\Phi^\dagger\Phi\big]\Big)^2 \\
&+ \lambda_2\Big\{\Big({\rm Tr}\big[\Phi^\dagger\tilde{\Phi}\big]\Big)^2 + \Big({\rm Tr}\big[\tilde{\Phi}^\dagger\Phi\big]\Big)^2\Big\} + \lambda_3 {\rm Tr}\big[\Phi^\dagger\tilde{\Phi}\big]{\rm Tr}\big[\tilde{\Phi}^\dagger\Phi\big] \\
&+ \lambda_4 {\rm Tr}\big[\Phi^\dagger\Phi\big]{\rm Tr}\big[\Phi^\dagger\tilde{\Phi} + \tilde{\Phi}^\dagger\Phi\big] + \rho_1\Big\{\Big({\rm Tr}\big[\Delta_L^\dagger\Delta_L\big]\Big)^2 + \Big({\rm Tr}\big[\Delta_R^\dagger\Delta_R\big]\Big)^2\Big\} \\
&+ \rho_2\Big\{{\rm Tr}\big[\Delta_L\Delta_L\big]{\rm Tr}\big[\Delta_L^\dagger\Delta_L^\dagger\big] + {\rm Tr}\big[\Delta_R\Delta_R\big]{\rm Tr}\big[\Delta_R^\dagger\Delta_R^\dagger\big]\Big\} + \rho_3 {\rm Tr}\big[\Delta_L^\dagger\Delta_L\big]{\rm Tr}\big[\Delta_R^\dagger\Delta_R\big] \\
&+ \rho_4\Big\{{\rm Tr}\big[\Delta_L\Delta_L\big]{\rm Tr}\big[\Delta_R^\dagger\Delta_R^\dagger\big] + {\rm Tr}\big[\Delta_L^\dagger\Delta_L^\dagger\big]{\rm Tr}\big[\Delta_R\Delta_R\big]\Big\} \\
&+ \alpha_1 {\rm Tr}\big[\Phi^\dagger\Phi\big]{\rm Tr}\big[\Delta_L^\dagger\Delta_L + \Delta_R^\dagger\Delta_R\big] \\
&+ \Big\{\alpha_2\Big({\rm Tr}\big[\Phi^\dagger\tilde{\Phi}\big]{\rm Tr}\big[\Delta_L^\dagger\Delta_L\big] + {\rm Tr}\big[\tilde{\Phi}^\dagger\Phi\big]{\rm Tr}\big[\Delta_R^\dagger\Delta_R\big]\Big) + {\rm h.c.}\Big\} \\
&+ \alpha_3 {\rm Tr}\big[\Phi\Phi^\dagger\Delta_L\Delta_L^\dagger + \Phi^\dagger\Phi\Delta_R\Delta_R^\dagger\big] + \beta_1 {\rm Tr}\big[\Phi^\dagger\Delta_L^\dagger\Phi\Delta_R + \Delta_R^\dagger\Phi^\dagger\Delta_L\Phi\big] \\
&+ \beta_2 {\rm Tr}\big[\Phi^\dagger\Delta_L^\dagger\tilde{\Phi}\Delta_R + \Delta_R^\dagger\tilde{\Phi}^\dagger\Delta_L\Phi\big] + \beta_3 {\rm Tr}\big[\tilde{\Phi}^\dagger\Delta_L^\dagger\Phi\Delta_R + \Delta_R^\dagger\Phi^\dagger\Delta_L\tilde{\Phi}\big],
\end{aligned} \tag{1.42}$$

where we have introduced scalar mass parameters μ_i and quartic scalar interaction strengths λ_i, ρ_i, α_i and β_i.

The symmetry-breaking pattern of this model is splitted into two steps,

$$SU(2)_L \times SU(2)_R \times U(1)_{B-L} \xrightarrow{\langle\Delta_R\rangle} SU(2)_L \times U(1)_Y \xrightarrow{\langle\Phi\rangle} U(1)_{\rm e.m.}\,. \tag{1.43}$$

At high energy, the $SU(2)_L \times SU(2)_R \times U(1)_{B-L}$ symmetry group is first spontaneously broken down to the electroweak symmetry group, and at a lower energy scale, the electroweak symmetry is further broken down to electromagnetism. The first breaking step results from the non-vanishing VEV acquired by the neutral component of the Δ_R field at the minimum of the scalar potential, whilst electroweak symmetry breaking is induced by the VEV of the neutral components of the Higgs bidoublet. Introducing the notations

$$\langle\phi^0_{1,2}\rangle = \frac{k_{1,2}}{\sqrt{2}} \qquad \text{and} \qquad \langle\Delta^0_{L,R}\rangle = \frac{v_{L,R}}{\sqrt{2}}\,, \tag{1.44}$$

the Standard Model VEV is given by $v_{\rm SM} = \sqrt{k_1^2 + k_2^2} \approx 246$ GeV. Without any loss of generality, we make use of a rotation in the $SU(2)_L \times SU(2)_R$ space so that only one of the

neutral components of the Higgs bidoublet acquires a large VEV, $k_1 \approx v_{\rm SM}$ and $k_2 \approx 0$. In addition, electroweak precision tests constrain v_L to be smaller than 2 GeV [50], and the breaking pattern of Eq. (1.43) enforces v_R to be much greater than k_1. D-parity invariance moreover imposes the g_L and g_R gauge couplings to be equal to a common value g.

1.4.4 Concept of Inert Higgs Doublet Model

In the brief description of the IHDM in the previous section, we stated that there are two Higgs doublets available in this model which undergoes the same symmetry group as SM. The second Higgs doublet Φ_2 is imposed with an additional Z_2 odd symmetry while all other SM fields are even under this additional symmetry. One of the main motivation to impose this new symmetry is to prohibit the Yukawa coupling of Φ_2 with SM fields, though direct interaction with gauge fields are preserved. Another main implication of the model is to provide the lightest neutral particle belonging to Inert doublet which can be considered as the DM candidate. We can write down the potential of the model considering Φ_1 as the SM Higgs doublet field

$$\begin{aligned} V(\Phi_1,\Phi_2) &= \mu_1^2|\Phi_1|^2 + \mu_2^2|\Phi_2|^2 + \frac{\lambda_1}{2}|\Phi_1|^4 + \frac{\lambda_2}{2}|\Phi_2|^4 + \lambda_3^2|\Phi_1|^2|\Phi_2|^2 \\ &\quad + \lambda_4^2|\Phi_1^\dagger\Phi_2|^2 + \left(\frac{\lambda_5}{2}(\Phi_1^\dagger\Phi_2)^2 + h.c.\right), \end{aligned} \tag{1.45}$$

where μ_1 and μ_2 are the mass of the Φ_1 and Φ_2 fields, and λ_i (i = 1, 2, 3, 4, 5) are mass dimensionless couplings, and considered to be real parameters. Because of the presence of Z_2 odd symmetry, Φ_2 does not get VEV and only Φ_1 acquires VEV of 246 GeV through EWSB. After the symmetry breaking, we can write down the two Higgs fields in the form of unitary gauge,

$$\Phi_1 = \begin{pmatrix} 0 \\ \frac{v+h}{\sqrt{2}} \end{pmatrix}, \quad \Phi_2 = \begin{pmatrix} H^+ \\ \frac{H^0+iA}{\sqrt{2}} \end{pmatrix}. \tag{1.46}$$

Here h is the SM like Higgs, H^0 is the lightest neutral Higgs, A is the neutral pseudo scalar. Apart from these neutral scalars two charged Higgs bosons $H^\pm$ are obtained from the Φ_2 field.

In the third study of our thesis, we modify IHDM with charged fermion singlet for the study of the Multi Component Dark Matter scenario. We discuss the detailed description of the model in the working chapter 4.

1.5 Chapter outline

In this section we present the brief description of different chapters of the thesis.

Chapter 2:

The signatures of heavy fermionic isotriplets (Σ) arising in Type III seesaw model are probed through their direct production and subsequent decay at high energy electron-positron colliders. Unlike the case of LHC, the production process has strong dependence on the mixing of Σ with electron (V_e), making the leptonic collider unique to fingerprint the presence of such mixing. We establish that pair production considered at $\sqrt{s} = 2$ TeV can be employed to study both the cases of $V_e = 0$ and $V_e \neq 0$ with $\sim 100\ fb^{-1}$ luminosity, while the single production can probe the latter case with a few inverse femto barn luminosity at $\sqrt{s} = 1$ TeV. Exploring the mass reach, both the single and pair productions are capable of probing Σ of mass close to the kinematic limits through selected channels. Investigating simultaneous limits on $M_\Sigma - V_e$ parameter space, we identify suitable final states and their 3σ reach on V_e and M_Σ at 300 (100) fb^{-1} luminosity in the case of pair (single) Σ production.

Chapter 3:

We investigate the potential collider signatures of singly-charged and doubly-charged Higgs bosons such as those arising in MLRSM. Focusing on multi-leptonic probes in the context of the High-Luminosity (HL) run of the LHC, we separately assess the advantages of the four-leptonic and trileptonic final states for a representative benchmark setup designed by considering a large set of experimental constraints. Our study establishes possibilities of identifying singly-charged and doubly-charged scalars at the LHC with a large significance, for luminosity goals expected to be reached during the HL phase of the

LHC. We generalise our results and demonstrate that existing limits can in principle be pushed much further in the heavy mass regime.

Chapter 4:

We study the presence of heavy fermions appearing in many extensions of the SM, including models explaining DM issues, in the context of the proposed 250 GeV ILC. In particular we consider the pair production of such heavy fermions and their subsequent decay to τ leptons. Keeping in mind the DM models, we consider the final state involving a pair of τ leptons and large missing energy. We perform a detector level analysis for this final state with ILCSoft. A complete background study is performed considering SM processes having similar final state available with the ILC repository. Our study shows that exotic fermions of this type with mass around 120 GeV can be easily identified with very small luminosity. Further we have carried out possibilities at higher energies of 350 and 500 GeV at ILC, respectively.

Chapter 5:

We summarize the studies carried out in the thesis and conclude with future prospect of the research.

Chapter 2

Direct searches of triplet fermions at high energy e^+e^- collider

This chapter is devoted to the collider study of triplet fermions arising in the Type III seesaw model at high energy e^+e^- collider. We investigate the production and decay of charged as well neutral fermions resulting in all possible final states. We perform a detector level analysis with SM backgrounds. This work is published in Eur. Phys. J. C78 (2018) no.1, 42.

2.1 Introduction

It is now established beyond doubt by different experiments that neutrinos posses mass albeit very small. The well known seesaw mechanism has emerged as the most popular and perhaps the most viable way of generating tiny mass of the observed light neutrinos of three different flavours. The seesaw mechanism effectively exploits the idea by introducing a lepton number violating Majorana mass term, either directly or generated dynamically. The tininess of the neutrino mass [51] in this case is achieved with the help of a large mass scale present in the scenario, usually brought in as the mass of a heavy partner.

Some details of the seesaw mechanism is presented in Chapter 1, Subsection 1.3.1. One of the variants of the seesaw mechanisms, known as Type III seesaw model [21] introduced with fermionic triplet fields with hypercharge $Y = 0$, has additional fermions with masses in the range of TeV, and thus could possibly be searched for at the LHC and at the proposed high energy leptonic colliders like the ILC [52–61] or the CLIC [62–65]. Generically, we refer these high energy leptonic collider facilities as the FLC. The phenomenology of Type III seesaw model in the context of LHC has been carried out in some detail by many authors [66–73]. Experimental searches for the additional charged, as well as neutral heavy fermions arising in this model are performed by both CMS and ATLAS. Considering data from $\sqrt{s} = 13$ TeV run, CMS [74] has set a lower limit of 430 GeV on the triplet mass, while this study was carried out. The ATLAS results [75] rule out masses in the range below 560 GeV under specific scenarios considered. CMS had an update on their earlier study quoting mass limits of 390-930 GeV depending on different choice of mixings [76]. However, they have not considered electron or muon type couplings independently, as we consider in this study. We consider the mass of fermion as 500 GeV for our study. At the same time, we also discuss the mass reach possible through the process considered in this study, which can very well probe masses close to a TeV. The larger value corresponds to the assumption of decay of the heavy neutral fermion exclusively to $W\ell$, and the heavy charged fermion to $W\nu$. Single production of the charged and neutral heavy fermions in the electron-proton collider (LHeC) is studied in Ref. [77]. While there are studies of indirect influence of the presence of triplet fermions in the context of Higgs pair production at the ILC [78], the direct production is not explored to the best of our knowledge. The advantages of the leptonic colliders, being sensitive to the mixing of the heavy fermions with electron at the production level, as well as their clean environment, are exploited in the present study in which we investigate the possible reach of high energy e^+e^- collider in searching for heavy fermions, and discuss the sensitivity to the mixing. Here we envisage a scenario with sufficiently large mixing between the heavy leptons and the SM leptons. However, the compatibility of large mixing scenario will be in conflict with generating small neutrino mass in pure Type III seesaw model. We anticipate extended versions of the seesaw mechanism like for example the inverse seesaw mechanism [79] to invoke small neutrino mass, at the same time allowing to have

large Yukawa couplings, and consequently large mixing. In such extended scenarios, the low energy (TeV scale) spectrum is assumed to be that of the simple Type III seesaw mechanism, with all other particles beyond the kinematic reach of the colliders being considered here. From this point of view, although the study is made in the context of the Type III seesaw model, the conclusions can be easily adapted to any model in which such triplet fermions are present with sufficiently large mixing with the SM leptons.

We focus our attention on the production of both charged as well as neutral fermion triplets at the FLC and explore the identification of these triplets over the SM backgrounds in different channels. In particular, we discuss how the mixing can be probed through the processes we study here. We may note that, in a realistic seesaw model we need at least two triplet fields in order to accommodate the observed mass splittings of the three neutrino flavours. However, in this study, for simplicity, we consider a single family of triplet fermion field in addition to the SM fields. In a more realistic case, this is equivalent to the case when the other fermions are much heavier, and therefore not relevant to the phenomenology at the energies considered.

We organise this chapter as follows. In Section 2.2 we discuss the present theoretical and experimental constraints available on the Type III seesaw model parameters. In Section 2.3 we describe the processes under study, and discuss the results. In Section 2.4 we explain the dependence of the mixing in detail. Finally, we conclude in Section 2.5.

2.2 Present constraints on the model parameters

We have discussed the Type III seesaw model briefly in Chapter 1. In this section we describe the constraints arising from the different theoretical and experimental results related to the Type III seesaw model relevant to our discussion.

We present an expanded form of the Lagrangian in the mass basis in Appendix A.1, which provides various couplings explicitly. The Yukawa interaction term leading to the off-diagonal mass matrix for the neutral fermions causes mixing in the charged lepton sector. Mixing between the heavy fermion, Σ and the SM leptons ($\ell = e,\ \mu,\ \tau$) are

denoted by $V_\ell = \frac{v}{\sqrt{2}M_\Sigma} Y_{\Sigma\ell}$. Search for flavour changing rare decays, $\mu \to e\gamma$, $\tau \to \mu\gamma$ and $\tau \to e\gamma$ impose stringent constraints on the couplings when two of them are simultaneously present, with the latest limits given by [46, 47, 80, 81]

$$|V_e V_\mu| < 1.7 \cdot 10^{-7}, \quad |V_e V_\tau| < 4.2 \cdot 10^{-4}, \quad |V_\mu V_\tau| < 4.9 \cdot 10^{-4}. \tag{2.1}$$

However, these constraints will not be applicable if only one type of mixing is assumed to be present. In that case, the single parameter bounds obtained from Electroweak Precision Measurements are much weaker with the latest limits given by [81]

$$|V_e| < 0.055, \quad |V_\mu| < 0.063, \quad |V_\tau| < 0.63. \tag{2.2}$$

The presence of mixing allow the triplet fermions to decay to the SM final states involving leptons, gauge bosons and the Higgs boson, through the off-diagonal charged-current and neutral current interactions. The decay widths of different channels depend on the masses and mixings as given below

$$\begin{aligned}
\Gamma(\Sigma^0 \to \ell^\pm W^\mp) &= \frac{g^2}{64\pi}|V_\ell|^2 \frac{M_\Sigma^3}{M_W^2}\left(1-\frac{M_W^2}{M_\Sigma^2}\right)^2\left(1+2\frac{M_W^2}{M_\Sigma^2}\right) \\
\Gamma(\Sigma^0 \to \sum_\ell \nu_\ell Z) &= \frac{g^2}{64\pi\cos^2\theta_W}\sum_\ell |V_\ell|^2 \frac{M_\Sigma^3}{M_Z^2}\left(1-\frac{M_Z^2}{M_\Sigma^2}\right)^2\left(1+2\frac{M_Z^2}{M_\Sigma^2}\right) \\
\Gamma(\Sigma^0 \to \sum_\ell \nu_\ell H) &= \frac{g^2}{64\pi}\sum_\ell |V_\ell|^2 \frac{M_\Sigma^3}{M_W^2}\left(1-\frac{M_H^2}{M_\Sigma^2}\right)^2 \\
\Gamma(\Sigma^\pm \to \sum_\ell \nu_\ell W^\pm) &= \frac{g^2}{32\pi}\sum_\ell |V_\ell|^2 \frac{M_\Sigma^3}{M_W^2}\left(1-\frac{M_W^2}{M_\Sigma^2}\right)^2\left(1+2\frac{M_W^2}{M_\Sigma^2}\right) \\
\Gamma(\Sigma^\pm \to \ell^\pm Z) &= \frac{g^2}{64\pi\cos^2\theta_W}|V_\ell|^2 \frac{M_\Sigma^3}{M_Z^2}\left(1-\frac{M_Z^2}{M_\Sigma^2}\right)^2\left(1+2\frac{M_Z^2}{M_\Sigma^2}\right) \\
\Gamma(\Sigma^\pm \to \ell^\pm H) &= \frac{g^2}{64\pi}|V_\ell|^2 \frac{M_\Sigma^3}{M_W^2}\left(1-\frac{M_H^2}{M_\Sigma^2}\right)^2 .
\end{aligned} \tag{2.3}$$

Here g is the $SU(2)_L$ gauge coupling, θ_W is the weak mixing angle, and M_W, M_Z and M_H are the masses of the gauge bosons and the Higgs boson, respectively and we agree with the expression in Ref [67]. The individual decay widths, and thus the total width has the usual strong dependence on the mass of the decaying Σ. However, this strong

dependence cancels away in the branching ratio (BR), leaving it practically independent of the mass for heavy fermions of mass beyond 500 GeV. This is especially facilitated with

Decay $\Sigma^{\pm}$	Decay Σ^{0}	BR in %
$\Sigma^{\pm} \to W^{\pm}\nu$	$\Sigma^{0} \to W\ell$	51
$\Sigma^{\pm} \to Z\ell^{\pm}$	$\Sigma^{0} \to Z\nu$	26
$\Sigma^{\pm} \to H\ell^{\pm}$	$\Sigma^{0} \to H\nu$	23

Table 2.1: *Branching ratio of the charged and neutral triplet fermion with mass, $M_\Sigma \geq 500$ GeV, with only one of V_ℓ is considered to be present, setting the other two to zero.*

the fact that the masses of the gauge bosons and the Higgs boson are all approximately around 100 GeV. From Eq. 2.3 it may also be noted that when only one mixing is present we have $\Gamma(\Sigma^0 \to \sum_\ell \ell^{\pm}W^{\mp}) = \Gamma(\Sigma^{\pm} \to \sum_\ell \nu_\ell W^{\pm})$, $\Gamma(\Sigma^0 \to \sum_\ell \nu_\ell Z) = \Gamma(\Sigma^{\pm} \to \ell^{\pm}Z)$ and $\Gamma(\Sigma^0 \to \sum_\ell \nu_\ell H) = \Gamma(\Sigma^{\pm} \to \sum_\ell \nu_\ell W^{\pm})$, thus resulting in the same BR's to the respective channels in both the cases, as presented in Table 2.1 for $M_\Sigma \geq 500$ GeV. This is naturally expected, as all the decays are facilitated by the same Yukawa interaction term inducing mixing between the heavy fermions and the SM leptons, and the topology of the two body decays keep the phase space factor the same. Of the charged (neutral) triplets, about 51 percent decay to $W\nu$ ($W\ell$), and 26 percent to $Z\ell$ ($Z\nu$), with 23 percent decaying to $H\ell$ ($H\nu$).

Direct production of Σ at the LHC goes through the single production process, $pp \to \ell\Sigma^{0,\pm}$, $\nu\Sigma^{0,\pm}$ with s-channel quark annihilation mediated by Z or W, and the pair production, $pp \to \Sigma^{0,+}\Sigma^{0,-}$ mediated by the Z or γ. The production cross sections (the expression for invariant amplitude is given in the Appendix A.2) for the best case scenario of $M_\Sigma = 500$ GeV and $V_e = 0.05$ is presented in Table 2.2 (right). While considering the present best case scenario, we are aware of the LHC future run projections, where possibly regions up to $M_\Sigma \sim 1$ TeV can be explored with moderate luminosity of 300 fb^{-1}, which can go even up to 1.5 TeV with its HL option [73]. However, these conclusions are sensitive to the inherent uncertainties and assumptions that require in the case of a hadronic machine like the LHC. In this study, we go further to find the reach of high energy electron-positron colliders on the mass, and find that it is mostly limited by

Process	cross section (fb)
$pp \to \Sigma^+\Sigma^-$	17.9
$pp \to \Sigma^0\Sigma^0$	4.57×10^{-6}
$pp \to \Sigma^\mp \ell^\pm$	0.1143
$pp \to \Sigma^0 \ell^\pm$	0.1092
$pp \to \Sigma^0 \nu$	0.062
$pp \to \Sigma^\pm \nu$	0.2329

Process	cross section(fb)		
	$V_e = 0.05$ $V_\mu = 0$	$V_e = 0$ $V_\mu = 0.05$	$V_e = 0$ $V_\mu = 0$
$e^+e^- \to \Sigma^+\Sigma^-$	42.8	55.67	55.81
$e^+e^- \to \Sigma^0\Sigma^0$	0.48	2.47×10^{-5}	0
$e^+e^- \to \Sigma^\mp e^\pm$	19.13	0	0
$e^+e^- \to \Sigma^\mp \mu^\pm$	0	0.054	0
$e^+e^- \to \Sigma^0\nu$	246.2	0.027	0

Table 2.2: *Cross sections for different production processes at 14 TeV LHC and 2 TeV e^+e^- colliders. In the case of LHC, $\ell = e,\ \mu$ corresponding to the two combinations of $(V_e = 0.05,\ V_\mu = 0)$ or $(V_\mu = 0.05,\ V_e = 0)$, respectively. Both the above mixing scenarios give identical results in the case of LHC processes with ν in the final state, whereas the pair production processes are independent of the mixing. The mixing in the case of e^+e^- collider is as explicitly mentioned. Mass of the fermion is taken to be $M_\Sigma \geq 500$ GeV.*

the kinematics, and thus can reach close to $M_\Sigma = \sqrt{s}$ in the case of single production, and $M_\Sigma = \frac{\sqrt{s}}{2}$ in the case of pair production. A similar reach on the mixing parameter is also obtained. The pair production mechanism being independent of the mixing, it is hard to obtain information regarding mixing parameters at LHC. Firstly, the pair production mechanisms involve gauge couplings of the triplets, and therefore the dependence on mixing is not significant. The decay widths, on the other hand have strong dependence on the mixings. However, in the total cross section, which is a product of production cross section and branching ratio of the decay channel considered, this dependence is cancelled, as long as the heavy flavour mixes with one flavour of the SM leptons. The single production processes have very small cross section to be of significance even in the best case scenario.

The e^+e^- colliders on the other hand has the advantage that the production mechanism itself could depend on the electron-triplet mixing parametrised by V_e, directly through the couplings of the form $e\Sigma V$, where $V = W,\ Z$, in the case of both pair production as well as the single production of the heavy fermions. To illustrate this the cross sections of different processes are given in Table 2.2 (right), for the case of $M_\Sigma = 500$ GeV and different combinations of V_ℓ. Details including the relevant Feynman diagrams is given in the next section.

2.3 Direct production of the triplets

In this section we discuss details of the single as well as pair production of both the neutral and charged triplet fermions at the high energy e^+e^- colliders.

2.3.1 Single production of Σ^0 and $\Sigma^\pm$

The single production of neutral and charged components of the fermion triplet along with a neutrino or lepton, respectively, are sensitive to the mixing of these heavy fermions with the SM leptons at the production level. The Feynman diagrams involve an s-channel exchange of gauge bosons. In addition, when $V_e \neq 0$ the process receives a t-channel contribution, as shown in Fig. 2.1. The Higgs mediated diagram is not included as the contributions from this is negligible in the high energy lepton colliders, where the electrons can be considered practically massless.

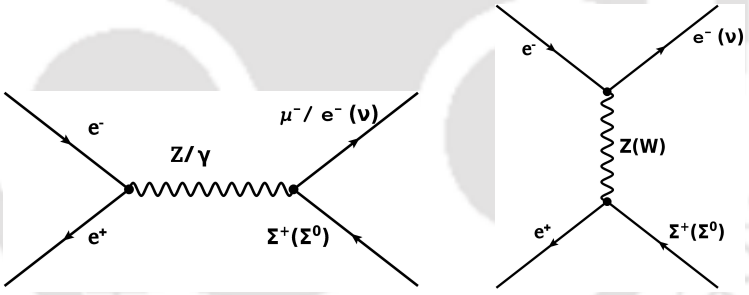

Figure 2.1: *Feynman diagrams contributing to the process $e^+e^- \to \Sigma^+\ell^-$ ($\Sigma^0\nu$). Note that $\Sigma^0\nu$ production does not have a photon mediated s-channel contribution.*

The expressions for cross sections of different cases are given in Appendix A.1. From the Feynman diagrams, it is clear that the cross section is proportional to $\sum_\ell |V_\ell|^2$ in case of neutral triplet production, and to the individual $|V_\ell|^2$ in the case of charged triplet production. It is expected that the s-channel contribution falls off with increasing $\sqrt{s}$, and thus become negligible at high energies considered here. On the other hand, the t-channel contribution and the interference between the t- and the s-channel give substantial contributions when $V_e \neq 0$. We consider two different cases of (i) $V_e \neq 0$, $V_\mu = 0$, and (ii) $V_e = 0$, $V_\mu \neq 0$, with $V_\tau = 0$ in both cases. The first case leads to $e^+e^- \to e^\mp\Sigma^\pm$, $\Sigma^0\nu$ through both the s- and t-channels, whereas the second case leads to $e^+e^- \to \mu^\mp\Sigma^\pm$, $\Sigma^0\nu$

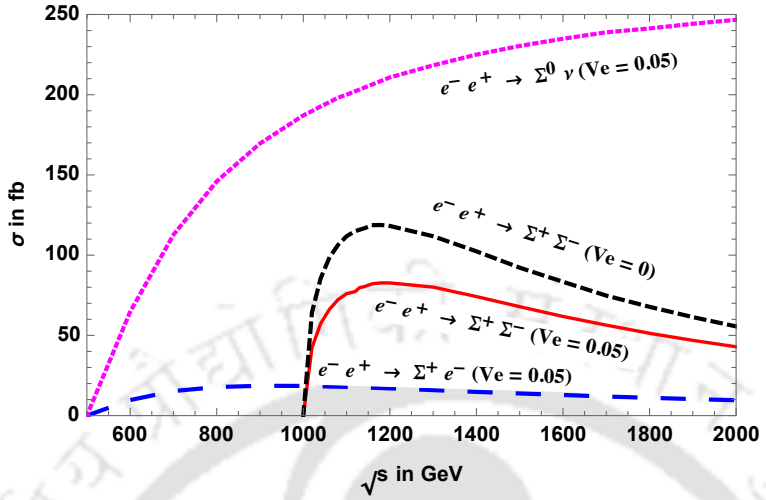

Figure 2.2: *Cross section for $e^+e^- \to \Sigma^0\nu$, $\Sigma^\pm e^\mp$, $\Sigma^+\Sigma^-$ against the centre of mass energy, with $M_\Sigma = 500$ GeV.*

through purely s-channel process. As quoted in Table 2.2 the cross sections for the latter case are very small, and therefore we consider the first case only in our analysis. Figure 2.2 shows the cross section against the centre of mass energy, with the cross section for $\Sigma^0\nu$ grows to a saturation of 250 fb at around 2 TeV, while $e^\mp\Sigma^\pm$ production cross section saturates at 18 fb around 1 TeV centre of mass energy. For our numerical analysis we fix the centre of mass energy at 1 TeV, where the cross section for neutral single production is sizeable, with 187 fb. While one of the expected design centre-of-mass energy of CLIC is 1.5 TeV, we have not made specific attempt to tune to this energy. The results of the analyses and the conclusions are expected to be applicable at this energy as well.

The heavy fermions further decay as per Eq. 2.3, leading to $W\ell\nu$, $Z\nu\nu$ and $H\nu\nu$ final states in the case of Σ^0, and $W\ell\nu$, $Z\ell\ell$ and $H\ell\ell$ final states in the case of $\Sigma^\pm$ productions. With further decay of W, Z and H, this leads to the detector level final states of $2j + \not{E}$, $2b + \not{E}$ (arising only from Σ^0 production), $2b + 2\ell$, $2j + 2\ell$, $2\ell^+ + 2\ell^-$ (arising only from $\Sigma^\pm$ production), and $2j + \ell + \not{E}$ and $2\ell + \not{E}$ (arising from both Σ^0 and $\Sigma^\pm$ productions). The lepton flavour depends on the scenarios (i) $V_e \neq 0$ or (ii) $V_\mu \neq 0$ considered, as well as on the W decay channel. Scenario (i) can lead to single flavour final states, having only electrons present, listed in Table 2.3 with the cross sections corresponding to these final states, along with the SM backgrounds. The cross sections quoted are the fiducial cross sections including the respective branching fractions obtained from Madgraph5 [82] with

basic generation level cuts on the transverse momenta of the jets and leptons, $p_T(j) \leq 20$ GeV, $p_T(\ell) \leq 10$ GeV, and pseudorapidity of $|\eta| \leq 2.5$ employed. In addition, this scenario can lead to mixed flavour cases of $e\mu\not{E}$, $e^+e^-\mu^+\mu^-\not{E}$ with cross sections very close to those of $e^+e^-\not{E}$, $2e^+2e^-\ \not{E}$ cases, respectively. Scenario (ii) will also lead to mixed flavour case of $e\mu\not{E}$ along with $\mu\ 2j\ \not{E}$ and $\mu^+\mu^-\not{E}$ final states. In the following we restrict to the single flavour case with only electrons and jets appearing in the final state. Coming to the backgrounds, the $2j + \not{E}$ coming from neutral triplet has large continuum QCD background. Similarly, the purely leptonic channel, $2e^+2e^-$ has small cross section. We therefore focus on the other cases of purely leptonic and semi-leptonic final states, as well as the $b\bar{b} + \not{E}$, where the $b-$quark pair arises from the H decay.

Final State	Process ($e^+e^- \to \Sigma^\pm e^\mp,\quad \Sigma^0\nu$)	$\sigma\times$ BR in fb	
		Signal	Background
$2j + e^- + \not{E}$	$\Sigma^+e^- \to W^+e^-\ \nu$	32.7	WWZ(0.5), WW(74.5),
	$\Sigma^0\nu \to W^+e^-\nu$		$t\tilde{t}$(1.68), ZZ(2.17), Zjj(2.77)
$2j + e^-\ e^+$	$(\Sigma^+e^- + \Sigma^-e^+) \to Ze^+e^-$	4.2	eejj(34.5)
$e^-e^+ + \not{E}$	$(\Sigma^+e^- + \Sigma^-e^+) \to W^\pm e^\mp\nu,\ \ Ze^-e^+$	14.8	WW(14.09), WWZ(0.036)
	$\Sigma^0\nu \to W^\pm e^\mp\nu,\ \ Z\nu\nu$		ZZ(0.35), $t\tilde{t}$(1.6)
$2e^- + 2e^+$	$(\Sigma^+e^- + \Sigma^-e^+) \to$ Z e^+e^-	0.3	ZZ(0.065), $eeee$(3.6)
$b\bar{b} + e^+e^-$	$(\Sigma^+e^- + \Sigma^-e^+) \to H\ e^+e^-$	7.2	HZ(0.27), ZZ(0.78)
$b\bar{b} + \not{E}$	$\Sigma^0\nu \to H\ \nu\nu$	37.6	HZ(2.1), ZZ(8.9)
$2j + \not{E}$	$\Sigma^0\nu \to Z\ \nu\nu$	22.3	$q\bar{q}$ (440.1)

Table 2.3: *Fiducial ross sections of signal and SM backgrounds corresponding to different final states arising from the process $e^-e^+ \to \Sigma^\pm e^\mp$ and $e^+e^- \to \Sigma^0\nu$, with $p_T(j) \geq 20$ GeV, $p_T(\ell) \geq 10$ GeV, and pseudo rapidity $|\eta| \leq 2.5$ for jets and leptons. Centre of mass energy of $\sqrt{s} = 1$ TeV and $M_\Sigma = 500$ GeV are considered with the assumed mixing of $V_e = 0.05,\ \ V_\mu = V_\tau = 0$.*

We have used the FeynRules implementation of the model as explained in the reference [46]. To analyse these selected final states, we generated 50000 events in each case using Madgraph5 with the in-built Pythia6 [83] used for ISR, FSR, showering and hadronization. The basic generation level cuts are those quoted above, with $p_T(j) \geq 20$ GeV, $p_T(\ell) \geq 10$ GeV, and $|\eta| \leq 2.5$ for the jets as well as leptons. These events are then passed on to Madanalysis5[82] to analyse and optimise the final selection criteria. Fastjet [84] is used for jet reconstruction with anti-k_T algorithm and jet radius of $R = 0.4$. For the detector

simulation, Delphes3 [85] with standard ILD card is used. Before applying any selection cuts, proximity check for leptons are done with leptons closer than $\Delta R_{j\ell} = 0.4$ ignored. Further selection was based on the required number of final state leptons and jets, and considering the distinguishability of the kinematic distributions. In Table 2.4 the cut-flow chart is presented along with the final significance that is expected at an integrated luminosity of 100 fb^{-1}. We briefly discuss the selection cuts of each of the final states below.

Final State	Selection cuts (All figures, except N are in GeV)	No. of events		$V_e = 0.05, V_{\mu,\tau} = 0$	
		Signal	Backgd	$\frac{S}{\sqrt{S+B}}$	$S_{\rm sys}$
$2j + e^- + \not{E}$	No cut	3273	8170		
	N(j) =2 ,N(e^-) = 1 ,N(b) = 0	2187	3871		
	$p(e^-) > 100$, $p(j_1) < 300$, $p(j_2) < 200$	1681	285	37.9	17.5
$2j + e^-e^+$	No cut	420	3450		
	N(e^+) = 1, N(e^-) = 1, N(j) = 2	273	1500		
	$p(e^-)$, $p(e^+) > 140$, M(e^+e^-) > 200	270	948		
	$\eta(e^+) < 1$, $\eta(e^-) > -1$	269	110	13.8	11.1
$e^-e^+ + \not{E}$	No cut	1489	1620		
	N($e^\pm$) = 1, N(b) = 0	1103	1036		
	$\Delta R(e^+, e^-) < 4$	1014	479	26.2	14.9
$b\bar{b} + e^-e^+$	No cut	718	105		
	N(e^+) = 1, N(e^-) = 1, N(b) = 2	180	14		
	M(e^+e^-) > 140	180	0	13.4	11.1
$b\bar{b} + \not{E}$	No cut	3760	1100		
	N(e^+) = 0, N(e^-) = 0, N(b) = 2	1243	221		
	$\Delta R(b, \bar{b}) > 0.6$	1194	140	32.7	17.0

Table 2.4: *The cut-flow and signal significance for different final states arising from the single production of Σ^0 and $\Sigma^\pm$ at $\sqrt{s} = 1$ TeV and 100 fb^{-1} luminosity for processes $e^-e^+ \to \Sigma^\pm\ell^\mp$ and $e^+e^- \to \Sigma^0\nu$, with $M_\Sigma = 500$ GeV and $V_e = 0.05$, $V_\mu = V_\tau = 0$.*

1. $2j + e^- + \not{E}$

   The signal and background events after the basic generation level cuts are 3273 and 8170, respectively. After demanding that the event should contain two jets and one electron, and veto-ing the presence of b-jet, the number of events reduce to 2187 and

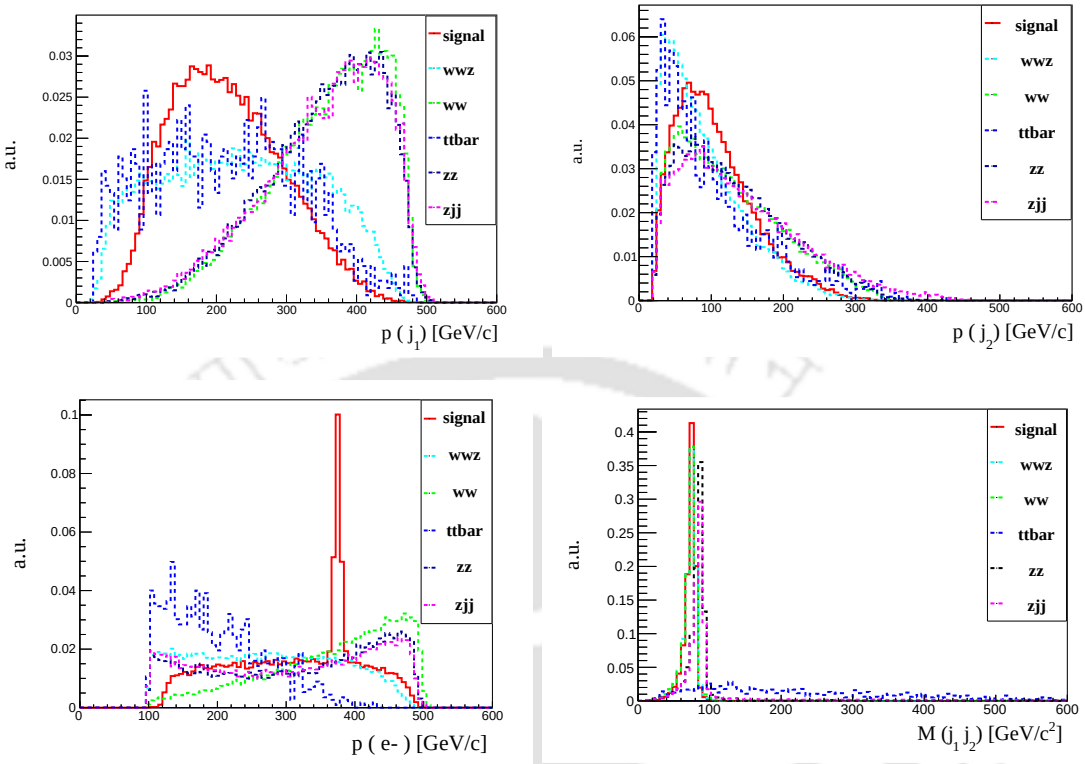

Figure 2.3: *Kinematic distributions for the final state* $2j + e^- \not{E}$ *with* $p_T(j) \geq 20$ *GeV,* $p_T(\ell) \geq 10$ *GeV, and pseudo rapidity* $|\eta| \leq 2.5$ *for jets and leptons. Center of mass enregy of 1 TeV and integrated luminosity of 100* fb^{-1} *is considered.*

3871 for the signal and background, respectively. The b-jet veto is used to reduce the $t\bar{t}$ background events. A set of kinematic distributions are shown in Fig 2.3 before applying further selections. This is followed by the selection of events with 100 GeV $\leq p(e^-)$, $p(j_1) \leq 300$ GeV and $p(j_2) \leq 200$ GeV which reduces the background events to about 7%, at the same time keeping about 77% of the signal events. This leaves 285 background events against a signal of 1681. Overall, about 51% of the original signal events are retained, against about 3.5% of the background events.

Assuming only statistical uncertainty, signal significance computed with formula, $\frac{S}{\sqrt{S+B}}$, where S is the number of signal events and B is the number of background events, is 37.9 at the luminosity of 100 fb^{-1} considered. In order to accommodate the systematic uncertainties, we have considered the following formula,

$$S_{\text{sys}} = \frac{S}{\sqrt{S + B + \alpha^2\ B^2 + \beta^2\ S^2}}, \tag{2.4}$$

where α and β are the systematic uncertainties in the background and signal events, respectively. Systematics at leptonic colliders like ILC are expected to be well under control. Assuming a very conservative value of 5% uncertainty in both the signal and background cases, we obtain a significance of 17.5 at the integrated luminosity of 100 fb^{-1}.

2. $\underline{2j + e^-e^+}$

In this case, $p(e^-) \geq 140$ GeV and $p(e^+) \geq 140$ GeV, and a selection of invariant mass of electron-positron pair, $M_{e^+e^-} > 200$ GeV, apart from demanding that there be one electron and one positron, and two jets are employed to reduce the background from 3450 to its 27.5%, while retaining 64.3 % of the signal events. The background is further reduced to 110 events by a selection of the pseudo rapidity of the leptons, $\eta(e^+) < 1$ and $\eta(e^-) > -1$, leaving the signal almost unaffected. A signal significance of 13.8 and 11.1 without and with assumed systematics as above could be achieved in this case.

3. $\underline{e^-e^+ + \not{E}}$

Here, electron-positron pairs are more back to back compared to those in the signal events. Demanding lepton separation, $\Delta R(e^+,\ e^-) < 4$ reduces the background to 479 from 1620, while keeping 1014 signal events starting from 1489 events. This leads to a signal significance of about 26.2 without any systematics, which goes down to 14.9 with the assumed systematic uncertainties.

4. $\underline{b\bar{b} + e^+e^-}$

A cut on the invariant mass of the lepton pair, $M_{e^+e^-} > 140$ GeV, apart from demanding two b-jets, one electron and one positron, takes away all the backgrounds, leaving 180 signal events with signal significance of 13.4 without systematics uncertainty and 11.1 with systematic uncertainty.

5. $\underline{b\bar{b} + \not{E}}$

In this case, $\Delta R(b, \bar{b}) > 0.6$ reduces the background events from 1100 to 140, while the signal is reduced from 3760 to 1194. The corresponding signal significance without systematics is 32.7, which is reduced to 17.0 with the assumed systematics.

Assuming that the kinematics of both the background and signal events remain more or less the same, we can scale the luminosity to the required value for signal significance of 5σ. In Table 2.5 we present the projected requirement of luminosity for this case assuming only statistical uncertainty, along with the expected number of signal and background events after the selection criteria adopted as in Table 2.4. The $2j + e^- + \not{E}$ final state gives the best case scenario with less than 2 fb^{-1} luminosity leading to 5σ sensitivity, whereas the $2b + \not{E}$ channel can be probed at 5σ level with a little more than 2 fb^{-1} luminosity. Purely leptonic channel of $e^+e^- + \not{E}$ also require only less than 4 fb^{-1} for this significance.

Final state	for $\frac{S}{\sqrt{S+B}} = 5\sigma$			for $S_{sys} = 5\sigma$		
	$\int \mathcal{L}$ (in fb^{-1})	S	B	$\int \mathcal{L}$ (in fb^{-1})	S	B
$2j + e^- + \not{E}$	1.7	29	5	1.9	31	5
$b\bar{b} + \not{E}$	2.3	28	3	2.5	30	4
$e^-e^+ + \not{E}$	3.6	37	17	3.9	40	19
$2j + e^-e^+$	13.1	35	14	14.1	38	16
$b\bar{b} + e^+e^-$	13.9	25	0	14.8	27	0

Table 2.5: *Luminosity requirement for signal significance of 5σ for different final states of the processes $e^-e^+ \to \Sigma^\pm e^\mp$ and $e^+e^- \to \Sigma^0\nu$ at $\sqrt{s} = 1$ TeV with $M_\Sigma = 500$ GeV, for the case of $V_e = 0.05$, $V_\mu = V_\tau = 0$, along with the signal (S) and background (B) events at the specified luminosities. S_{sys} is taken as defined in Eq. 2.4.*

2.3.2 Pair production of Σ

We next consider the pair production of the triplet fermions. The Feynman diagrams corresponding to the production of charged fermion pairs are shown in Fig.2.4. The neutral fermion pair production also goes through the same channels, except the one with the photon exchange. Notice that the t-channel contribution to the cross section here is proportional to the fourth power of the mixing parameter V_ℓ. Thus, it is expected that the s-channel dominates. Again, the s-channel for Σ^0 pair production is proportional to the square of the $Z\Sigma^0\Sigma^0$ vertex, which is proportional to the $|V_\ell|^2$. Thus, the cross section for neutral fermion pair production is very small. On the other hand, the $Z\Sigma^+\Sigma^-$ vertex is proportional to $\left(|V_\ell|^2 - 2\ \cos^2\theta_W\right) - |V_\ell|^2\,\gamma^5$, and therefore receives a sizeable contribution

even in the absence of mixing. In addition, the $V_e \neq 0$ case has a t-channel contribution with the initial electron (positron) converting to Σ^- (Σ^+). However, non-zero values of $V_{\mu,\tau}$ do not lead to such t-channel contribution. Thus the pair production process, while sensitive to V_e, is not sensitive to $V_{\mu,\tau}$. In our analyses we consider these two cases of (i) $V_e \neq 0$ and (ii) $V_e = 0$, with the former resulting in a slightly smaller cross section than the latter case, indicating destructive interference between the s- and the t-channel processes. We reiterate that this advantage of the FLC, where the production is sensitive to the mixing is absent at the LHC. The pair production of neutral fermions happens with very small cross section, and therefore difficult to probe with the expected luminosities. Therefore in the following we consider only the pair production of the charged fermions. The cross section against the centre of mass energy for the two cases considered is given in Fig. 2.2. The cross section peaks at about 1.2 TeV centre of mass energy with values of 83 fb and 119 fb corresponding to the cases of $V_e = 0.05$ and $V_e = 0$, respectively. At $\sqrt{s} = 2$ TeV, the cross section is reduced by a factor of two with 43 fb and 55.7 fb for the two cases.

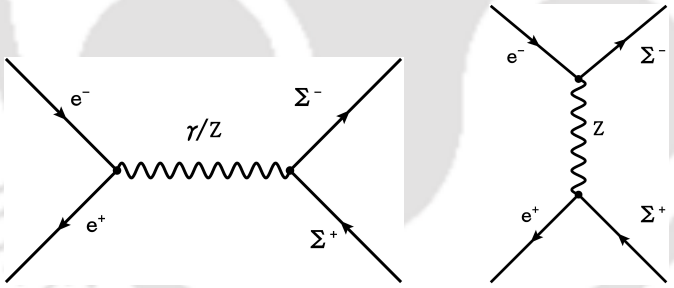

Figure 2.4: *Feynman diagrams contributing to the process $e^+e^- \to \Sigma^+\Sigma^-$ in isotriplet-electron mixing scenario.*

While the production is not sensitive to the presence or absence of V_μ of V_τ, the decay require one of these to be present for the second case considered above (viz $V_e = 0$). Thus in our further analysis, we consider the two cases as (i) $V_e = 0.05$, $V_\mu = V_\tau = 0$ and (ii) $V_\mu \neq 0$, $V_e = V_\tau = 0$. We would like to remind our reader that the mixing entering only through the decay, as in the second case here, is not sensitive to the value of the mixing as long as the mean life of the particle is so that it decays within the detector. The dependence will cancel in the BR when only one V_ℓ is non-zero. With the decay of $\Sigma^\pm$ to $W\nu$, $Z\ell$ or $H\ell$, and the subsequent decays of W, Z and H considered,

Final State	Process $(e^+e^- \to \Sigma^+\Sigma^-)$	$\sigma\times$ BR in fb		
		Signal		Background
		$V_e = 0.05$	$V_\mu \neq 0$	
$4j + \not{E}$	$W^+W^-\nu\nu$	1.3	2.0	WWZ (1.4), $WW\nu\nu$(16.6)
$4j + \ell + \not{E}$	$W^+Z\ell^-\nu$	0.6	0.8	$t\tilde{t}$(1.4), $WWjj$(0.5)
$4j + \ell\ell$	$ZZ\ell^+\ell^-$	0.3	0.4	WWZ(0.15), $ZZjj$(0.7)
$2j + 4\ell$	$ZZ\ell^+\ell^-$	0.02	0.03	ZZZ(0.0002)
$2j + 3\ell + \not{E}$	$W^+Z\ell^-\nu$	0.04	0.05	WWZ(0.03)
$2j + 2\ell + \not{E}$	$ZZ\ell^+\ell^-$, $W^+Z\ell^-\nu$	0.4	0.5	WWZ(0.12),$t\tilde{t}$(0.44)
$2j + \ell + \not{E}$	$W^+W^-\nu\nu$, $W^+Z\ell^-\nu$	0.8	1.0	WWZ(0.27),WW(12.2), t$\tilde{t}$(1.4), ZZ(0.27)
$2\ell + \not{E}$	$W^+W^-\nu\nu$	0.1	0.2	WW(3.4), $t\bar{t}$(0.43), $\ell\ell\nu\nu$(181.7)
$4b + 2\ell$	$HH\ell^+\ell^-$	1.7	2.2	$b\tilde{b}b\tilde{b}$ $\ell^+\ell^-$(0.006), $t\tilde{t}Z$(0.026), $t\tilde{t}H$(0.006)

Table 2.6: *Final state fiducial cross sections of the signal from $e^+e^- \to \Sigma^-\Sigma^+$, and the corresponding SM background processes, with the selection of $p_T(\ell) \geq 10$ GeV , pseudo rapidity of leptons $|\eta_\ell| \leq 2.5$ and the selection of $p_T(j) \geq 20$ GeV, $|\eta_j| \leq 2.5$. Centre of mass energy of $\sqrt{s} = 2$ TeV, and $M_\Sigma = 500$ GeV are considered. The lepton in the final state ℓ is e or μ for the cases of $V_e = 0.05$ and $V_\mu \neq 0$, respectively.*

we have the purely hadronic final states of $4j + \not{E}$, semi-leptonic final states of $4j + 2\ell$, $4j+\ell+\not{E}$, $2j+4\ell$, $2j+3\ell+\not{E}$, $2j+2\ell+\not{E}$, $2j+\ell+\not{E}$, $4b+2\ell$ and the purely leptonic case of $2\ell+\not{E}$. Here $\ell = e$ for the first scenario and $\ell = \mu$ for the second one. We have included only the case of Higgs decay to b-pair, as the other cases come with much smaller effective cross section. Again, Z to b-pair decay is not included, and Z decaying to charged leptons is not considered, as they have very small cross section. In Table 2.6 the cross sections of these final states arising from the signal for the two cases considered are given, along with the corresponding SM background cross sections. The cross sections are obtained from the MC simulation with Madgraph5 with Pythia6 used for hadronisation and showering. We have included the generation level basic cuts on the transverse momenta of jets and leptons of $p_T(j) > 20$ GeV and $p_T(\ell) > 10$ GeV, and considered jets and leptons with pseudo rapidity of $|\eta| < 2.5$. The final states with $2j + 4\ell$ and $2j + 3\ell + \not{E}$ have very small cross sections, and therefore require very large luminosities to probe these channels. The purely leptonic final state of $2\ell + \not{E}$ comes with large SM background of about three orders larger than the signal. Thus, in our further analysis we do not consider these three cases.

As in the case of single triplet production, the events generated are then passed on to

Final State	Selection cuts (All dimensional quan -tities are in GeV)	$V_e = 0.05$				$V_\mu \neq 0$			
		S	B	$\frac{S}{\sqrt{S+B}}$	$S_{\rm sys}$	S	B	$\frac{S}{\sqrt{S+B}}$	$S_{\rm sys}$
$4j + \not{E}$	$N(j) = 4$, $p(j_1) > 100$	147	1679	3.4	1.5	243	2164	5	2
	$N(j) \geq 3$, $p(j_1) > 100$	353	3914	5.4	1.7	503	3914	7.5	2.4
$4j + \ell^\pm + \not{E}$	$N(\ell^\pm) = 1$, $N(j) = 4$, $N(b) = 0$, $p(\ell^\pm) > 100$, $\not{E} > 100$	50	12	6.3	6	73	13	7.8	7.3
	$N(\ell^\pm) = 1$, $N(j) \geq 3$, $N(b) = 0$, $p(\ell^\pm) > 100$, $\not{E} > 100$	106	33	8.9	8.1	154	39	11.1	9.6
$4j + \ell^+\ell^-$	$N(\ell^\pm) = 1$, $N(j) = 4$, $p(\ell^\pm) > 100$, $\Delta R(\ell^+, \ell^-) \geq 2$	29	0	5.3	5.2	74	0	8.6	7.9
	$N(\ell^\pm) = 1$, $N(j) \geq 3$, $p(\ell^\pm) > 100$, $\Delta R(\ell^+, \ell^-) \geq 2$,	56	0	7.4	7	140	0	11.8	10.1
$2j + \ell^+\ell^- + \not{E}$	$N(\ell^+) = 1$, $N(\ell^-) = 1$, $N(j) = 2$, $N(b) = 0$, $p(\ell^-) > 100$	47	12	6.1	5.8	54	15	6.5	6.1
$2j + \ell^\pm + \not{E}$	$N(\ell^\pm) = 1$, $N(j) = 2$, $N(b) = 0$, $\lvert\eta(\ell)\rvert < 1$, $p(\ell) < 900$, $p(j_1) < 600$, $p(j_2) < 300$	87	365	4.0	3.0	121	10	10.5	9.3
$4b + \ell^+\ell^-$	$N(\ell^+) = 1$, $N(\ell^-) = 1$, $N(b) = 4$, $p(e^\pm) > 60$	24	0	4.9	4.7	34	0	5.8	5.5
	$N(\ell^+) = 1$, $N(\ell^-) = 1$, $N(b) \geq 3$, $p(e^\pm) > 60$	114	0	10.6	9.4	163	0	12.7	10.8

Table 2.7: *Number of surviving events, and signal significance for different final states arising from the pair production of $\Sigma^\pm\Sigma^\mp$ at $300fb^{-1}$ luminosity at $\sqrt{s} = 2$ TeV, and $M_\Sigma = 500$ GeV. $S_{\rm sys}$ corresponds to the signal significance with assumed systematics according to Eq. 2.4. S and B represent signal and background events, respectively.*

Madanalysis5, using Fastjet for jet reconstruction with anti-k_T algorithm and jet radius of $R = 0.4$. Detector simulation is carried out with the help of Delphes3 with standard ILD card. Before applying any selection cuts, proximity check for leptons were done with leptons closer than $\Delta R_{j\ell} = 0.4$ to the jets ignored. Further selection is based on the required number of final state leptons and jets, and considering the distinguishability of the kinematic distributions. In the $4j$ events, we consider two different situations with (i) setting the number of jets exactly equal to four, and (ii) demanding every event has three

jets or more. The second case provides marginal improvement in the significance, and about double the signal events in each case. In Table 2.7 the cut-flow chart is presented along with the final significance that is expected at an integrated luminosity of 300 fb^{-1}. We briefly discuss the cuts used to optimise the selection below.

1. $4j + \not{E}$

   With $p(j_1) > 100$ GeV, the two cases of $N(j) = 4$ and $N(j) \geq 3$ give significance of 3.4 and 5.4, respectively, for the scenario with $V_e = 0.05$ when only statistical errors are assumed. This is reduced to 1.5 and 1.7, respectively, with the assumed systematics of 5% on both the signal and background event determination. The scenario with $V_e = 0$ has the corresponding significances of 5 (2) and 7.5 (2.4) considering statistical (statistical plus systematic) uncertainty. Notice that this channel is purely hadronic, and does not leave any trace of the type of mixing involved.

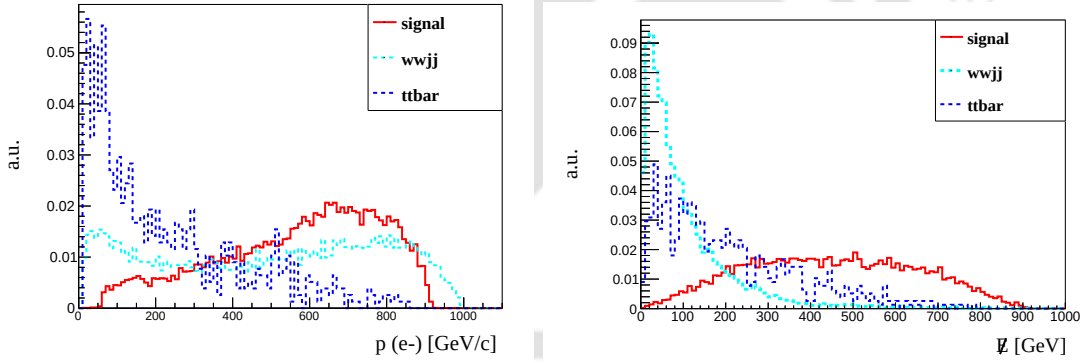

Figure 2.5: *Kinematic distributions for the final state $4j + \ell^{\pm} + \not{E}$ with $p_T(j) \geq 20$ GeV, $p_T(\ell) \geq 10$ GeV, and pseudo rapidity $|\eta| \leq 2.5$ for jets and leptons. Center of mass energy of 2 TeV and integrated luminosity of 300 fb^{-1} is considered for $V_e = 0.05$.*

2. $4j + \ell^{\pm} + \not{E}$

   Here ℓ is electron or muon depending on the case of $V_e \neq 0$ or $V_\mu \neq 0$. Unlike the case of $4j + \not{E}$, here the missing energy has a different topology (see in Fig 2.5 before applying selection cuts $p(\ell^{\pm}) > 100$, $\not{E} > 100$) in signal compared to that of the background (refer to Table 2.6 for the list of major backgrounds). A

cut of $p(\ell) > 100$ GeV and $\not{E} > 100$ GeV are used apart from demanding one lepton and $N(j) = 4$ or $N(j) \geq 3$, along with demanding $N(b) = 0$ to reduce the $t\bar{t}$ background. The significance for the case of electron are 6.3 (6) and 8.9 (8.1) without (with) systematics assumed, for the two cases of jet counting of $(i)N(j) = 4$ and $(ii)N(j) \geq 3$, respectively. In the case of muon, these are 7.9 (7.3) and 11.1 (9.6), respectively. Notice that the systematics have less pronounced effect here, as the events are small in number. We assume the charge of the lepton is identified, with both the cases giving similar results.

3. $\underline{4j + \ell^+\ell^-}$

In this final state, the oppositely charged dileptons originate at the production in signal, whereas they come from the decay of Z bosons in the case of the backgrounds. Therefore, the leptons are expected to be more energetic in the case of signal events. We employ a cut of $p(\ell^\pm) > 100$ GeV in both the cases of $N(j) = 4$ and $N(j) \geq 3$. In addition, we have assumed that the two leptons are separated with $\Delta R \geq 2$, as they are expected to be well separated in the case of signal events, whereas in the case of background events they will be more collimated as they originate from the Z boson in flight. With these selection cuts, the background is practically eliminated. The significance for the four and three jet-counting are 5.3 and 7.5 for electrons, and 8.6 and 11.8 respectively for the case of muons. As the events are not very large, the systematics do not have much effect here.

4. $\underline{2j + 2\ell + \not{E}}$

Coming to the $2j + \ell + \not{E}$ events, $p(\ell^-) > 100$ GeV is employed after demanding exactly two jets and two oppositely charged same-flavour leptons, leading to a significance of 6.1 and 6.5 for the case of electron and muon, respectively. Here again, the systematics have only a small role to play.

5. $\underline{2j + \ell^\pm + \not{E}}$

The major background here is the WW production with the semi-leptonic decay of the pair. The lepton coming from the W is expected to be very energetic, unlike

the case of the signal. A cut on the energy of the lepton, $p(\ell) < 900$ GeV is employed, along with a cut on the pseudo rapidity of lepton $|\eta(\ell)| < 1$, reduced the background considerably. Further cuts on the momenta of jets $p(j_1) < 600$ GeV and $p(j_2) < 300$ GeV are considered to reach an expected significance of 4(3) for electron without(with) systematics considered. The case of muons presents a much better scenario with expected significance of 10.6 (9.3).

6. $4b + 2\ell$

The background for the $4b$ events is quite suppressed. We have considered identifying two oppositely charged leptons, and the cases of $N(b) = 4$ and $N(b) \geq 3$, along with demanding $p(e^{\pm}) > 60$ GeV. The number of events surviving in the case of electron mixing are 24 and 114 respectively, with vanishing backgrounds in both cases. In the case of muon mixing, the significance is improved with the surviving number of events of 34 and 163, respectively.

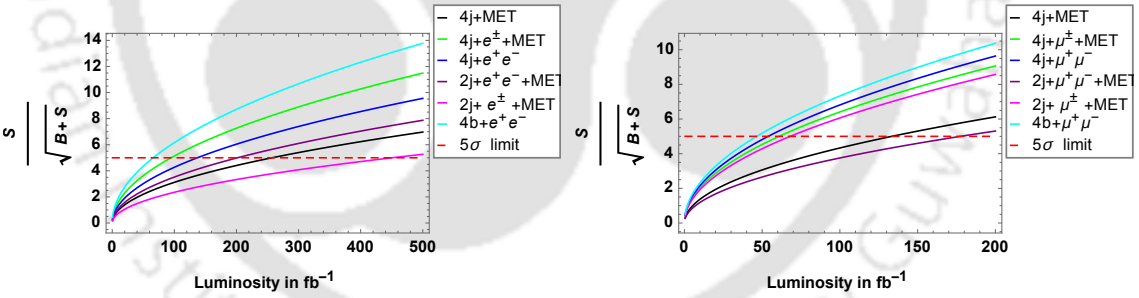

Figure 2.6: *Signal significance of different final states from pair production of $\Sigma^{\pm}$ against integrated luminosity at $\sqrt{s} = 2$ TeV. Mass of triplet fermion, $M_{\Sigma} = 500$ GeV and mixing parameters of $V_e = 0.05$ (left) and $V_{\mu} \neq 0$ (right) are considered with other mixings set to zero.*

Summarising, $4j + 2\ell$ and $4b + 2\ell$ provides the best case scenarios, where practically no background events are present. Both of these cases could also distinguish the mixing scenarios from the flavour of the leptons produced. The single lepton events with missing energy accompanied by either four jets or two jets also provide very promising scenarios. Here the four jet case can distinguish the two mixing scenarios with the flavour identification, whereas the two jet case has the leptons arising also from the W decay, and therefore, it will give a mixed signal.

All the final states in both the cases with two different mixing scenarios are used to indicate the projected luminosity required for 5σ significance in Fig. 2.6. Luminosity of less than 300 fb^{-1} is sufficient to probe all the channels with electron in the final state (except $2j + e^{\pm} + \not{E}$) at 5σ level . On the other hand, $4j + \not{E}$ and $2j + \mu^+\mu^- + \not{E}$ require about 130 and 180 fb^{-1} luminosity, whereas all other channels with μ in the final state can be explored at 5σ level with less than 100 fb^{-1} luminosity.

2.3.3 Dependence on the mass of Σ

So far in the analysis we fix the mass of the heavy fermion to $M_\Sigma = 500$ GeV. In this section, we explore the mass dependence for a specific choice of mixing at a given centre of mass energy. The cross sections for single and pair productions considered at the centre of mass energies of 1 and 2 TeV's, respectively, are presented in Fig. 2.7 against M_Σ. The near threshold behaviour of the pair production with $V_e = 0$ is distinctly different from the case with $V_e \neq 0$. This may be attributed to the fact that while the former case is a purely s-channel process, the latter has a contribution from the t-channel as well, facilitated by the presence of $Z\Sigma e$ coupling. The single production cases are presented only for $V_e \neq 0$ case, as the Σe production is not possible with $V_e = 0$, while $\Sigma\nu$ production is very small in the case of $V_\mu \neq 0$. The mass dependence seems to follow the same pattern in the two cases of neutral as well as the charged fermion single production considered here. We shall now demonstrate that with 300 fb^{-1} integrated luminosity, the reach of ILC is close to $M_\Sigma = 1$ TeV.

Let us consider the case of $4b + 2\ell$ final state in the $\Sigma^+\Sigma^-$ pair production with a cross section of 43 fb at $\sqrt{s} = 2$ TeV with an assumed mixing of $V_e = 0.05$ and mass of $M_\Sigma = 500$ GeV. The selection criteria considered in this study leaves 114 signal events with an integrated luminosity of 300 fb^{-1}. This corresponds to an effective cross section times branching ratio of 0.38 fb. The selection cuts have eliminated the background, and thus number of signal events required for 3σ signal significance is about 9, corresponding to a cross section times branching ratio of $\frac{9}{300} = 0.03$. Assuming that the selection cuts behave the same way, the production cross section required to get this significance is $\frac{43}{0.38} \times 0.03 = 3.39$ fb. At $\sqrt{s} = 2$ TeV, keeping $V_e = 0.05$, this cross section corresponds

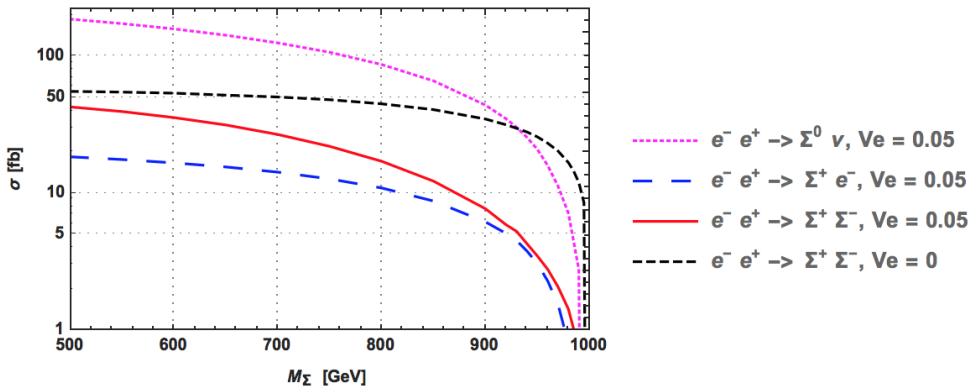

Figure 2.7: *Dependence of cross-section on the mass of fermions for pair and single production. Single production is considered at $\sqrt{s} = 1$ TeV, whereas $\sqrt{s} = 2$ TeV is considered for pair production process. Mixing is considered as indicated, with $V_\mu = V_\tau = 0$ in all cases.*

Final State	$V_e = 0.05$				$V_\mu \neq 0$			
	S	B	$\sigma(\Sigma^+\Sigma^-)$ in fb	M_Σ in GeV	S	B	$\sigma(\Sigma^+\Sigma^-)$ in fb	M_Σ in GeV
$4b + 2\ell$	9	0	3.4	945	9	0	3.0	997
$4j + 2\ell$	9	0	6.9	910	9.2	0.17	3.6	995
$4j + \ell^\pm + \not{E}$	16	33.3	9.1	885	23.7	38.5	8.5	990
$2j + \ell^\pm + \not{E}$	62	365	30.7	660	15	9.7	6.9	992

Table 2.8: *The Mass reach at 2 TeV with integrated luminosity of 300 fb^{-1} from selected channels of pair production of charged fermions, giving 3σ sensitivity. The corresponding production cross sections $\sigma(\Sigma^+\Sigma^-)$, and the number of signal (S) and background (B) events after employing the selection criteria are also given. Only single flavour with $\ell = e,\ \mu$ is considered for the cases of $V_e = 0.05$ and $V_\mu \neq 0$, respectively.*

to a mass of $M_\Sigma = 950$ GeV. A similar study of the $4j + 2\ell$ and $4j + \ell^\pm + \not{E}$ final states show that about 3σ significance is reached with a pair production cross section of 6.9 and 9.1 fb, respectively. These correspond to mass reaches of about 910 and 885 GeV, respectively. Considering the μ channels with $V_\mu \neq 0$ (as explained earlier, the results do not depend on the value of V_μ), the situation gets some what better with the addition of $2j + \ell^\pm + \not{E}$ also able to probe the model with M_Σ very close to the kinematic limit of 1000 GeV. Table 2.8 summarises the mass reach at a 2 TeV ILC with an integrated luminosity of 300 fb^{-1}.

The mass reach estimated to be achieved through the single production process at

$\sqrt{s} = 1$ TeV with an integrated luminosity of 100 fb^{-1} for selected final states (arising through single production channel) is given in Table 2.9. With the two selected channels of $2j + e^+e^-$ and $2b + e^+e^-$ arising from $\Sigma^{\pm}e^{\mp}$ production, and the final state $2b + \not{E}$ arising from $\Sigma^0\nu$ could probe the model with M_Σ close to 1 TeV, assuming $V_e = 0.05$.

Final State	S	B	$\sigma(\Sigma^+e^-)$ in fb	M_Σ in GeV	Final state	S	B	$\sigma(\Sigma^0\nu)$ in fb	M_Σ in GeV
$2j + e^-e^+$	37	110	2.5	956	$b\bar{b} + \not{E}$	40.4	140.3	6.3	982
$b\bar{b} + e^-e^+$	9	0	0.92	978					

Table 2.9: *The Mass reach at 1 TeV with integrated luminosity of 100 fb^{-1} from selected channels of single production of charged and neutral fermions, giving 3σ sensitivity. The corresponding production cross sections $\sigma(\Sigma^{\pm}e^{\mp})$, $\sigma(\Sigma^0\nu)$ and the number of signal (S) and background (B) events after employing the selection criteria are also given.*

2.4 Dependence on the mixing

The limiting cross sections required for 3σ significance listed in Tables 2.8 and 2.9 are exploited to extract the two-parameter contours in the $V_e - M_\Sigma$ plane. As mentioned

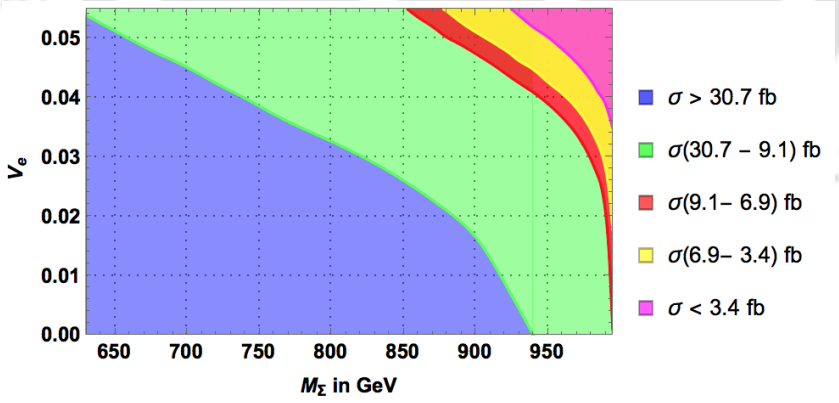

Figure 2.8: *Regions of $M_\Sigma - V_e$ plane with different ranges of cross section values for pair production at 2 TeV centre of mass energy as indicated. The ranges of cross sections are the 3σ limiting values given in Table 2.8.*

earlier, in the case when only V_μ is non-zero, the process including the decay rates does not depend on the value of the mixing. On the other hand, both the single and pair productions are sensitive to the value of V_e. Table 2.8 lists the limiting cross sections for 3σ significance in the case of different final states arising from the pair production. It may

be noted that the pair production process has a large contribution from the gauge coupling, and the presence of non-zero mixing results in a destructive interference, thus reducing the cross section from its value when $V_e = 0$. In Fig. 2.8 regions of production cross section, $\sigma > 30.7$ fb is indicated in blue colour. The $M_\Sigma - V_e$ two-parameter limits obtainable from the final state $2j + e + \not{E}$ is indicated by the boundary of this blue region. Similarly, the 3σ limits of $M_\Sigma - V_e$ obtained from $4j + e + \not{E}$ final state are indicated by the boundary between the green and red regions, and that from $4j + e^+e^-$ and $4b + e^+e^-$ are given by the boundaries of red and yellow regions, and yellow and pink regions, respectively. $2j + e + \not{E}$ channel is capable of probing the entire range of presently allowed values of V_e for varying value of M_Σ. On the other hand, the other channels, $4j + e + \not{E}$, $4j + e^+e^-$ and $4b + e^+e^-$ are not able to probe below $M_\Sigma \sim 850,\ 875,\ 925$ GeV's.

Coming to the single production of Σ, the cross section vanishes in the absence of V_ℓ. In Fig. 2.9 regions of different cross section values corresponding to the limiting cases of 3σ limits obtainable from different final states are indicated in the $M_\Sigma - V_e$ plane. Case

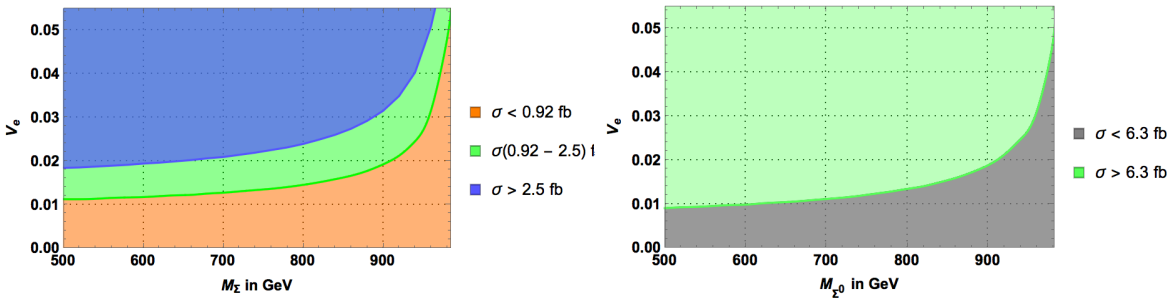

Figure 2.9: *Regions of $M_\Sigma - V_e$ plane with different ranges of cross section values for single production at 1 TeV centre of mass energy as indicated. Figure on the left corresponds to $\Sigma^\pm e^\mp$ production, and that on the right corresponds to $\Sigma^0\nu$ production. The ranges of cross sections are the 3σ limiting values given in Table 2.9.*

of Σe production is shown in the left figure, with the boundary between blue and green regions showing the two-parameter limits obtainable from $2j + e^+e^-$ channel, whereas the boundary between green and orange regions indicating the limits from $2b + e^+e^-$ final state. In the figure on the right the two-parameter limits from $2b + \not{E}$ resulting from $\Sigma^0\nu$ is indicated by the boundary of the green and grey regions. Channels of $2b + e^+e^-$ and $2b + \not{E}$ can probe V_e to 0.04 to 0.01, depending on the value of M_Σ, whereas the final state, $2j + e^+e^-$ is slightly less sensitive.

2.5 Conclusions

Type III seesaw mechanism proposed to generate tiny neutrino mass provides an example of BSM scenario with heavy leptons. We study the direct production of heavy leptons at high energy e^+e^- collider through possible final states arising from their subsequent decays. Present direct searches at the LHC limits the masses of such heavy fermions in the range of 500 GeV or above. While the LHC is capable of discovering the presence of heavy leptons in the TeV mass range, it is hard to probe the details of the couplings involving mixing with the SM leptons. On the other hand, high energy e^+e^- colliders like the ILC or CLIC with electrons in the initial state are suitable for this purpose, where the production process itself is sensitive to the mixing. While the simple Type III seesaw models require small Yukawa couplings, and consequently small mixing, we imagine a broader scenario with additional mechanism to generate small neutrino mass despite the presence of large mixing, and explore the collider consequence that may follow. Thus the conclusions drawn in this work are applicable to any scenario where there exists a heavy lepton which mixes with the SM leptons, as long as any additional spectrum arising in such scenario do not affect the decay branching ratio of the heavy leptons, possibly because such resonances are heavier, and thus beyond the reach of TeV energy colliders.

Investigating the single and pair production of the neutral as well as charged leptons at e^+e^- collider at centre of mass energies of 1 TeV and 2 TeV, respectively, we perform detailed detector-level analyses to identify interesting final states, and the achievable significance for selected parameter choices.

Single charged (neutral) triplet fermions are produced in association with a charged (neutral) SM leptons or a neutrino. Consequently these processes are absent in the case when Σ do not have any mixing with the SM leptons. In order to avoid FCNC constraints, in our study we assume that the triplets mix with either electron (V_e) or muon (V_μ), and not to both. The case of mixing with tau lepton in not considered in this work as we focus on final states involving only electrons, muons and jets. Study of $\Sigma^\pm\ell^\mp$ and $\Sigma^0\nu$ production show that the cross sections in the case of $V_\mu \neq 0$ is negligibly small. Focusing on the triplet-electron mixing scenario, we first study the most optimistic case

of $V_e = 0.05$ and $M_\Sigma = 500$ GeV, fixing these parameters at their present experimental limits. Performing a full detector simulation, considering all the SM backgrounds for various detector level final states arising from Σe and $\Sigma\nu$, we find that $2j + e^- + \not{E}$, $2b + \not{E}$ and $e^+e^- + \not{E}$ could be probed at 5σ significance (assuming only statistical uncertainty) with 2 to 4 fb^{-1} luminosity. Among the other final states, $2j + e^+e^-$ and $2b + e^+e^-$ channels require about 14 to 15 fb^{-1} luminosity for 5σ significance. Extrapolating this result to higher values of M_Σ, we find that a 1 TeV e^+e^- collider with 100 fb^{-1} luminosity could probe the mass very close to the kinematic limit of about 950 to 980 GeV, assuming $V_e = 0.05$.

Coming to the pair production, the cross section for Σ^0 pair production turns out to be negligibly small. On the other hand, the $\Sigma^+\Sigma^-$ production process is present even in the absence of mixing, as the gauge coupling dictates the strength of $Z\Sigma^+\Sigma^-$ coupling, leading to the pair production through s-channel process. The presence of mixing provides only a very negligible addition to this in the s-channel. The production is practically insensitive to the triplet mixing with muon or tau lepton. In the scenario with $V_e \neq 0$ additional t-channel opens the avenue to discriminate this case with the case of $V_e = 0$. In the latter case, we consider $V_\mu \neq 0$ so as to facilitate the decay of the triplet to the SM leptons. However, the dependence on V_μ, when present alone, is cancelled out in the BR. Thus we carry out our analysis in the two scenarios of (i) $V_e = 0,\ V_\mu \neq 0$ and (ii) $V_e \neq 0,\ V_\mu = 0$. We perform the analysis with all possible detector level final states arising from the pair production and subsequent decays. Cross sections of multi-lepton channels with more than two leptons in the final state, and the purely leptonic channel of $2\ell + \not{E}$ are very small, and therefore is not considered in this analysis. Among the other channels, the best case scenario is given by the $4b + 2\ell$ channels coming from the $H\ell$ decay of Σ, requiring about 50 fb^{-1} luminosity for 5σ significance in both the scenarios considered. In all cases, the first scenario with triplet-muon mixing provides better sensitivity, mostly because of the larger cross section available. The final states of $4j + \mu^+\mu^-$, $4j + \mu + \not{E}$ and $2j + \mu + \not{E}$ can be probed at 5σ level with luminosities of 50, 60 and 70 fb^{-1}, respectively, whereas their counterparts in the $V_e \neq 0$ case replacing μ with electron require luminosities of 140, 100 and 460 fb^{-1}, respectively. The difference between the two scenarios can be attributed to the distinctions in muon and electron identification and efficiencies, as well

as to the slightly different kinematic distributions in the two cases. $2j+\ell\ell+\not{E}$ final state, on the other hand, does not seem to favour any scenario, requiring moderate luminosities of about 200 fb^{-1} in the case of $V_e \neq 0$, and 175 fb^{-1} in the case of $V_\mu \neq 0$. This may be due, again, to the fact that the cross sections are almost the same in the two cases. The purely hadronic case of $4j+\not{E}$ has a much better background compared to other channels (except the $4b+2\ell$ case), but suffers from efficiencies involved in the jet formation and identification, thus requiring slightly larger luminosities of 260 and 130 in the cases of $V_e \neq 0$ and $V_\mu \neq 0$, respectively. Coming to the reach of M_Σ through the pair production, the two channels, $4b+e^+e^-$ and $4j+e^+e^-$ could probe beyond 900 GeV with 300 fb^{-1} luminosity, whereas all the channels with muonic final states could probe very close to the kinematic reach, going above 990 GeV.

Probing the sensitivity to the mixing parameter, V_e, we obtain two-parameter limits achievable by different final states from single and pair productions. The single production channels are capable of probing low mass regions for small mixing values, going up to 0.01 for triplet-electron mixing parameter in the case of masses close to 500 GeV with $2b+e^+e^-$ and $2b+\not{E}$ arising from Σe and $\Sigma^0\nu$, respectively. The pair production, on the other hand can probe smaller values of mixings for larger $M-\Sigma$ values, where the best suitable final state is $2j+e+\not{E}$.

The study clearly demonstrates the potential of high energy e^+e^- collider to probe the presence of heavy leptons, and the details of their couplings with the SM particles, thus supporting the case for such leptonic collider even with successful running of the LHC. Considering the nature of the process, with the presence of t-channel production in some of the mixing scenarios, we anticipate that beam polarisation could be utilised to enhance the sensitivity.

Chapter 3

Investigating the scalar sector of left-right symmetric models with leptonic probes

In this chapter, we study the multi-leptonic channels to probe the heavy Higgs bosons in the context of Minimal Left Right Symmetric Model at 14 TeV LHC. We perform a detailed signal versus SM background analysis which indicates that the channels we study have the potential to probe heavier mass of doubly charged Higgs bosons with a High-Luminosity LHC. This work is published in Phys. Rev. D98 (2018) no.3, 035008.

3.1 Introduction

As we have discussed earlier in the previous chapters, the SM cannot provide any explanation for the observed non-zero neutrino masses and mixings [50]. In the SM, the Higgs field is responsible for the generation of the masses of all known fundamental particles, but it

cannot accommodate the tiny observed neutrino masses within only renormalizable interactions. The situation nonetheless changes at the non-renormalizable level since neutrino masses can be generated through the dimension-five Weinberg operator [86] that generally arises, within a renormalisable ultraviolet-complete theory where new heavy fields are introduced, through a seesaw mechanism. As mentioned in Chapter 1, the different realisations of such a mechanism can be broadly classified into three categories named Type I [13–15, 17, 87] (that relies only on right-handed neutrinos coupling to the Higgs field), Type II [16, 19, 20, 88] (that makes use of a new scalar field lying in the adjoint representation of $SU(2)_L$) and Type III [21] (where at least two extra fermionic fields lying in the adjoint representation of $SU(2)_L$ are included) seesaws. In most common seesaw implementations, heavy fields are supplemented to the SM in an *ad-hoc* fashion so that the desired neutrino properties are reproduced after the breaking of the electroweak symmetry. Seesaw options where the symmetries of the SM are extended also exist, like in Left-Right Symmetric theories [22–33] where minimal and non-minimal realisations naturally feature Type I/II and Type III seesaw mechanisms respectively. In their most minimalistic form, Left-Right Symmetric theories are symmetric under parity transformations in the ultraviolet regime, although low-energy parity violation arises after the spontaneous breaking of the Left-Right Symmetry at a high energy scale. Finally, such theories can also be embedded within an $SO(10)$ grand unified context and feature gauge coupling unification.

With a particle content exhibiting three extra vector bosons, three right-handed neutrinos and several new scalar (Higgs) fields whose components possess either a double, a single or a vanishing electric charge, MLRSM feature various collider signatures that can be used as probes for new physics [22–31, 33]. The Higgs sector of the model has in particular been recently investigated [89–101]. In the present work, we study several Higgs processes giving rise to the production of four-lepton and three-lepton systems and focus on setups where these final states are stemming from the production and decay of either a pair of doubly-charged Higgs bosons, or of an associated pair comprised of a doubly-charged Higgs boson and a singly-charged Higgs or vector boson. Unlike most earlier studies, we consider a framework where both Type I and Type II seesaw mechanisms are implemented and contribute to neutrino mass generation. Equivalently, the

neutral component of the left-handed (Δ_L) and right-handed (Δ_R) Higgs triplets both acquire non-vanishing vacuum expectation values $v_{L,R} \neq 0$. This opens up certain decay modes that are forbidden when $v_L = 0$ (as for a Type I seesaw mechanism) and that could be used as handles on distinguishing a $v_L = 0$ from a $v_L \neq 0$ scenario. While the phenomenology corresponding to the $v_L \neq 0$ case has been widely studied in a pure Type II seesaw context [68, 102–108], the one connected to a mixed Type I/II seesaw model still remains to be comprehensively explored. Several processes become open only by virtue of the non-zero v_L value, but still remain suppressed as v_L is bound to be small. This non-vanishing v_L value nevertheless allows us to weaken the constraints on the charged scalar particles stemming from flavour data.

Unlike in earlier MLRSM studies, we consider a high integrated luminosity of LHC collisions at a centre-of-mass energy of 14 TeV. We adopt a scenario motivated by current experimental constraints (in particular on the doubly-charged Higgs bosons) and perform a systematic comparison of expected new physics signals and SM background including the simulation of the detector effects. The rest of this chapter is organised as follows. In section 3.2, we discuss the MLRSM theoretical framework and its particle content, before designing a representative benchmark scenario that could be probed by multi-leptonic probes. In section 3.3, we study the collider phenomenology of this setup and quantitatively estimate how it could be discovered or constrained at the High-Luminosity run of the LHC. We then generalise our findings as a function of the mass scale of the model, before concluding in section 3.4.

3.2 The minimal left-right symmetric model

3.2.1 Theoretical framework

We have briefly discussed the Minimal Left Right Symmetric Model in Chapter 1. The scalar potential of the model is given in Eq.1.42. In this same notation, all field transformations under a D-parity symmetry operation can be written as [101]

$$\begin{cases} q_L \leftrightarrow q_R \\ \ell_L \leftrightarrow \ell_R \\ \Delta_L \leftrightarrow \Delta_R \\ \Phi \leftrightarrow \Phi^\dagger \end{cases} \quad \text{or} \quad \begin{cases} q_L \leftrightarrow q_R^c \\ \ell_L \leftrightarrow \ell_R^c \\ \Delta_L \leftrightarrow \Delta_R^* \\ \Phi \leftrightarrow \Phi^t \end{cases} , \tag{3.1}$$

depending whether D-parity symmetry is seen as a generalised parity or charge conjugation. The minimal model field content is shown in Table 3.1.

Field	$SU(3)$	$SU(2)_L$	$SU(2)_R$	$U(1)_{B-L}$
$q_L = \begin{pmatrix} u_L \\ d_L \end{pmatrix}$	**3**	**2**	**1**	$\frac{1}{3}$
$q_R = \begin{pmatrix} u_R \\ d_R \end{pmatrix}$	**3**	**1**	**2**	$\frac{1}{3}$
$\ell_L = \begin{pmatrix} \nu_L \\ e_L \end{pmatrix}$	**1**	**2**	**1**	-1
$\ell_R = \begin{pmatrix} \nu_R \\ e_R \end{pmatrix}$	**1**	**1**	**2**	-1
$\Phi = \begin{pmatrix} \phi_1^0 & \phi_1^+ \\ \phi_2^- & \phi_2^0 \end{pmatrix}$	**1**	**2**	**2**	0
$\Delta_L = \begin{pmatrix} \Delta_L^+/\sqrt{2} & \Delta_L^{++} \\ \Delta_L^0 & -\Delta_L^+/\sqrt{2} \end{pmatrix}$	**1**	**3**	**1**	2
$\Delta_R = \begin{pmatrix} \Delta_R^+/\sqrt{2} & \Delta_R^{++} \\ \Delta_R^0 & -\Delta_R^+/\sqrt{2} \end{pmatrix}$	**1**	**1**	**3**	2

Table 3.1: *MLRSM field content, presented together with the representations under* $SU(3)_c \times SU(2)_L \times SU(2)_R \times U(1)_{B-L}$.

Under those assumptions mentioned in model description in Chapter 1, we neglect all contributions to the gauge boson masses that are proportional to v_L, so that these masses approximatively read

$$M_W^2 = \frac{g^2}{4}k_1^2 , \qquad M_{W_R}^2 = \frac{g^2}{2}v_R^2 , \qquad M_Z^2 = \frac{g^2 k_1^2}{4\cos^2\theta_W}\left(1 - \frac{\cos^2 2\theta_W}{2\cos^4\theta_W}\frac{k_1^2}{v_R^2}\right) , \qquad M_{Z_R}^2 = \frac{g^2 v_R^2 \cos^2\theta_W}{\cos 2\theta_W} , \tag{3.2}$$

with θ_W indicating the weak mixing angle.

After symmetry breaking, the Higgs sector is left with four neutral scalar fields H_0^0, H_1^0, H_2^0 and H_3^0, two neutral pseudoscalar fields A_1^0 and A_2^0 (as well as two neutral Goldstone bosons eaten by the Z and Z_R bosons), two singly-charged Higgs bosons $H_1^\pm$ and $H_2^\pm$ (as well as four charged Goldstone bosons eaten by the $W^\pm$ and $W_R^\pm$ bosons) and two doubly-charged scalar bosons $H_L^{\pm\pm}$ and $H_R^{\pm\pm}$. Within the above-mentioned approximations, the scalar masses are given by

$$\begin{aligned} M^2_{H_0^0} &= 2\lambda_1 k_1^2 \ , \qquad M^2_{H_1^0} = \frac{1}{2}\alpha_3 v_R^2 \ , \qquad M^2_{H_2^0} = 2\rho_1 v_R^2 \ , \qquad M^2_{H_3^0} = \frac{1}{2}(\rho_3 - 2\rho_1) v_R^2 \ , \\ M^2_{A_1^0} &= \frac{1}{2}\alpha_3 v_R^2 - 2(2\lambda_2 - \lambda_3) k_1^2 \ , \qquad M^2_{A_2^0} = \frac{1}{2} v_R^2 (\rho_3 - 2\rho_1) \ , \\ M^2_{H_1^\pm} &= \frac{1}{2}(\rho_3 - 2\rho_1) v_R^2 + \frac{1}{4}\alpha_3 k_1^2 \ , \qquad M^2_{H_2^\pm} = \frac{1}{2}\alpha_3 v_R^2 + \frac{1}{4}\alpha_3 k_1^2 \ , \\ M^2_{H_L^{\pm\pm}} &= \frac{1}{2}(\rho_3 - 2\rho_1) v_R^2 + \frac{1}{2}\alpha_3 k_1^2 \ , \qquad M^2_{H_R^{\pm\pm}} = 2\rho_2 v_R^2 + \frac{1}{2}\alpha_3 k_1^2 \ . \end{aligned} \tag{3.3}$$

Here we neglected the left-right triplet mixing induced by the β_i potential terms as they are suppressed by the k_1^2/v_R^2 ratio. Notice that the different states are not necessarily mass-ordered.

Turning to the neutrino sector, the f_{ij} Yukawa couplings of Eq. (1.41) give rise to neutrino Majorana masses after symmetry breaking, as the neutral component of the Δ_L Higgs field acquires a non-zero vacuum expectation value [31],

$$v_L = \frac{\beta_2 k_1^2}{(2\rho_1 - \rho_3) v_R} \ . \tag{3.4}$$

Hierarchy of the vacuum expectation values expected in this case is $|v_L| \ll v_{\rm SM} \ll |v_R|$. The 6×6 neutrino mass matrix is then given, in the (ν_L, ν_R) gauge eigenbasis, by

$$M = \begin{pmatrix} \sqrt{2} f v_L & M_D \\ M_D^T & M_R \end{pmatrix} \ , \tag{3.5}$$

where M_D, M_R and f are 3×3 matrix with elements $(M_D)_{ij} = \frac{1}{\sqrt{2}} y_{ij} k_1$, $(M_R)_{ij} = \sqrt{2} f_{ij} v_R$ and f_{ij} are the Yukawa couplings.

The light and heavy neutrino sectors are decoupled in the absence of any left-right

mixing potentially induced by a non-vanishing Dirac mass matrix M_D, and the light and heavy masses are in this case respectively governed by the f_{ij} and $M_{R_{ij}}$ parameters. In contrast, non-zero Dirac masses give rise to neutrino mixings parameterised by a mixing matrix R^ν,

$$R^\nu = \begin{pmatrix} U & S \\ T & V \end{pmatrix} = \begin{pmatrix} 1 - \frac{1}{2}RR^\dagger & R \\ -R^\dagger & 1 - \frac{1}{2}R^\dagger R \end{pmatrix} \begin{pmatrix} U_L & 0 \\ 0 & U_R \end{pmatrix} . \tag{3.6}$$

In this expression, $R = M_D M_R^{-1}$, whilst U_L and U_R are respectively the two matrices diagonalising the light and heavy neutrino mass matrices M_ν and M_R, with

$$(M_\nu)_{ij} = \sqrt{2} f_{ij} v_L - (M_D)_{ik} (M_R)^{-1}_{kl} (M_D^T)_{lj}. \tag{3.7}$$

This shows that light neutrino masses arise from a combination of Type-I and Type-II seesaw contributions and are derived from the diagonalisation of the upper-left block of the mass matrix M by a U_L rotation, U_L being the usual Pontecorvo-Maki-Nakagawa-Sakata (PMNS) matrix.

3.2.2 Constraints and MLRSM benchmark scenarios with light doubly-charged Higgs bosons

In order to design simplified phenomenologically viable benchmark scenarios for the collider studies performed in the next section, we account for various constraints arising from current data.

The scalar sector of the theory must include a neutral scalar boson that is consistent with the observation of a SM-like Higgs boson with a mass of about 125 GeV. We enforce the H_0^0 boson to be such a boson, its mass being set to

$$M_{H_0^0} = 125 \text{ GeV}. \tag{3.8}$$

The extra neutral scalar bosons, in particular those with a large bidoublet component (*i.e.*, H_1^0 and A_1^0), generally mediate tree-level flavor-changing neutral current interactions. Consequently, their mass is constrained to be above about 10 TeV [109–113] from experimental kaon mixing data [114]. On the other hand, the scalar potential perturbativity and unitarity further push these Higgs bosons to be heavier than 18 TeV. The minimum mass configuration is realised for a W_R boson satisfying $M_{W_R} > 8$ TeV [115], a constraint that is by far compatible with the most stringent LHC bounds regardless of the details of the right-handed neutrino sector [116–120]. Consequently, we impose

$$M_{H_1^0} = M_{A_1^0} = 20 \text{ TeV}, \qquad M_{W_R} = 10 \text{ TeV} \quad \Leftrightarrow \quad v_R = 21639.39 \text{ GeV}. \tag{3.9}$$

Saturating the present limits on the $SU(2)_L$ triplet VEV arising from the ρ-paramater [50],

$$v_L = 2 \text{ GeV}, \tag{3.10}$$

and recalling that we have chosen

$$k_1 \approx v_{\text{SM}} = 246 \text{ GeV} \qquad \text{and} \qquad k_2 \approx 0, \tag{3.11}$$

we make use of Eq. (3.3) together with the setup of Eq. (3.8) through Eq. (3.9) to numerically derive the (tree-level) parameters of the scalar potential,

$$\lambda_1 = 0.129 \ , \qquad \alpha_3 = 1.708 \ , \qquad 2\lambda_2 - \lambda_3 = 0. \tag{3.12}$$

On the basis of the results of the ATLAS searches for same-sign dileptonic new physics signals [121], we moreover impose a lower bound on the masses of the doubly-charged scalars $H_L^{\pm\pm}$ and $H_R^{\pm\pm}$. Assuming that the branching ratios into electronic and muonic final states are both equal to 50%, the $SU(2)_L$ and $SU(2)_R$ doubly-charged Higgs-boson masses have to be larger than 785 GeV and 675 GeV respectively. We adopt an optimistic scenario and take their masses close to the experimental limits,

$$M_{H^{++}} \equiv M_{H_L^{++}} = M_{H_R^{++}} = 800 \text{ GeV}. \tag{3.13}$$

This leads to

$$\rho_2 = 6.2817 \times 10^{-4} \ , \qquad \rho_3 - 2\rho_1 = 0.0025 \ , \tag{3.14}$$

with the other gauge and scalar boson masses being, therefore,

$$M_{Z_R} = 16754 \text{ GeV}, \quad M_{H_2^0} = 6756 \text{ GeV}, \quad M_{H_3^0} = M_{A_2^0} = 767 \text{ GeV},$$

$$M_{H_1^+} = 784 \text{ GeV}, \quad M_{H_2^+} = 20 \text{ TeV}. \tag{3.15}$$

The parameters related to the neutrino masses and mixings can be constrained by LHC searches in the same-sign dilepton plus dijet channel, such a signature being relevant for probing right-handed neutrino production via an s-channel W_R exchange [122]. A wide fraction of the parameter space turns out to be excluded by 8 TeV and 13 TeV LHC data due to the non-observation of any such signal [123, 124]. For the choice of Eq. (3.9), right-handed neutrinos have to be heavy. The neutrino sector can also undergo several low energy tests from intensity frontier experiments looking for lepton-number violation (such as neutrinoless double-beta decays) or for lepton-flavor violation (like rare muonic decays into electrons such as $\mu \to e\gamma$ or $\mu \to 3e$). The associated combined limits induce a hierarchy between the mass of the $SU(2)_R$ scalar bosons and the mass of the heaviest right-handed neutrino that must be 2 to 10 times smaller [125, 126] for $M_{W_R} = 3.5$ TeV. These bounds are however derived under the assumption that either a Type I or a Type II seesaw mechanism is implemented. Considering a model featuring a combination of Type I and Type II seesaw mechanisms (as in this work) enables us to evade those bounds [127, 128], the $SU(2)_R$ triplet scalar masses being even allowed to be smaller than the heaviest right-handed neutrino mass. Right-handed neutrinos could nevertheless be indirectly constrained by neutrinoless double-beta decays and cosmology [129–131].

With the above assignments, the only parameters left to be considered are the mass parameters of the heavy and light neutrinos, M_{N_i}, with $i = 1, 2, 3, 4, 5, 6$. We consider the lighter degrees of freedom (*i.e.*, the left-handed neutrinos corresponding to $i = 1, 2, 3$) to have a mass of the order of 0.1 eV to agree with cosmological data. For simplicity,

we assume a unified scenario for the right-handed neutrino sector,

$$M_{N_4} = M_{N_5} = M_{N_6} \equiv M_{N_R} = 12 \text{ TeV} \ , \tag{3.16}$$

which allows one to evade all the above-mentioned bounds and feature perturbative Yukawa couplings of $\mathcal{O}(1)$.

In addition, the heavy-light neutrino mixing is constrained from neutrino oscillation data. After having fixed all physical masses of the neutrinos and assuming that $|fv_L| \ll |M_D| \ll |M_R|$, the M_R mass matrix can be read off these masses, in a first approximation, and the Type-II seesaw contribution to the light neutrino masses can be deduced from the (inputted) M_ν matrix [132],

$$M_D = M_{N_R} \left(\frac{v_L}{v_R} - \frac{M_\nu}{M_{N_R}} \right)^{1/2} \ . \tag{3.17}$$

The Dirac mass is of about 100 GeV with an assumed $M_\nu \sim 0.1$ eV for the considered scenario. The cancellation in Eq. (3.17) between the Type I and Type II seesaw contributions are hence fine-tuned to the level of 10^{10}, such a fine-tuning being stable against quantum corrections [133]. This further impacts the light-heavy neutrino mixing matrix,

$$T = -R^\dagger U_L = -(M_R^{-1})^\dagger M_D^\dagger U_L \approx 0.018 U_L \ , \tag{3.18}$$

which also dictates the strength of the heavy neutrino decays into left-handed leptons and a Standard Model W-boson. The rest of the neutrino mixing matrix stems from the unitarity properties of that matrix, which subsequently fixes the strength of the heavy neutrino decays into a final state system made of a right-handed lepton and a possibly off-shell heavy gauge boson. The heavy-light neutrino mixing is actually rather large, as v_L is large, which opens the door for unusual heavy neutrino decays into the left-handed sector.

3.2.3 Main feature of our benchmark scenario

In order to determine the experimental signatures associated with the production of two scalar bosons or one vector and one scalar boson at the LHC, we first present, in Table 3.2, the decay table related to the relevant (lighter) fields. The large right-handed neutrino masses have deep consequences on the couplings of the $SU(2)_L$ doubly-charged and singly-charged Higgs bosons to leptons, as they are proportional to M_{N_R}/v_R. This impacts the decay pattern of the scalar fields which will rarely decay into non-leptonic final states. The $H_L^{\pm\pm}$ boson, hence, decays almost exclusively into a same-sign dileptonic system and the H_1^+ Higgs boson into a lepton-neutrino pair. Other non negligibly small H_L^{++} decay modes include a virtual H_1^+ boson, and these sum up to a branching ratio of 3% after considering all three lepton flavours. The $SU(2)_R$ doubly-charged H_R^{++} boson in contrast only decays into a same-sign lepton pair, the potential decay modes into an $SU(2)_R$ gauge boson and another scalar being kinematically closed. Finally, the lighter neutral H_3^0 and A_2^0 bosons almost exclusively decay invisibly, the neutral scalar boson H_3^0 nevertheless undergoing rare visible decays into electroweak gauge bosons, whilst the singly-charged W_R boson always decays into a dijet system.

Doubly-charged bosons

$\mathrm{BR}(H_R^{++} \to \ell^+\ell^+)$	33.3%
$\mathrm{BR}(H_L^{++} \to \ell^+\ell^+)$	32.3%
$\mathrm{BR}(H_L^{++} \to W^+\ell^+\nu_\ell)$	1.0%

Singly-charged bosons

$\mathrm{BR}(H_1^+ \to \ell^+\nu_\ell)$	33.26%
$\mathrm{BR}(H_1^+ \to W^+Z)$	0.22%
$\mathrm{BR}(W_R^+ \to q\bar{q}')$	100%

Neutral bosons

$\mathrm{BR}(H_3^0 \to \nu_\ell\nu_\ell)$	31.8%
$\mathrm{BR}(H_3^0 \to Z\nu_\ell\nu_\ell)$	0.83%
$\mathrm{BR}(H_3^0 \to W\ell\nu_\ell)$	0.38%
$\mathrm{BR}(H_3^0 \to ZZ)$	0.52%
$\mathrm{BR}(H_3^0 \to WW)$	0.26%
$\mathrm{BR}(A_2^0 \to \nu_\ell\nu_\ell)$	32.1%
$\mathrm{BR}(A_2^0 \to Z\nu_\ell\nu_\ell)$	0.85%
$\mathrm{BR}(A_2^0 \to W\ell\nu_\ell)$	0.38%

Table 3.2: *Branching ratios (BR) associated with the different decay channels of the light scalar and vector bosons within the considered MLRSM realisation. We independently denote by $\ell = e, \mu, \tau$ any lepton flavor, and omit any channel whose branching ratio is smaller than 0.1%.*

As the considered new particles significantly decay into leptonic final states, natural

collider probes include final-state systems made of three or four leptons, as the corresponding SM background is additionally small. We thus focus on the production of two doubly-charged Higgs bosons and on the associated production of a doubly-charged Higgs boson and a singly-charged gauge or Higgs boson,

$$pp \to H_{L/R}^{++} H_{L/R}^{--} \,, \qquad pp \to H_L^{\pm\pm} H_1^{\mp} \qquad \text{and} \qquad pp \to H_R^{\pm\pm} W_R^{\mp} \,, \tag{3.19}$$

for which representative leading-order Feynman diagrams are shown in Figure 3.1. Other hard-scattering processes involving new Higgs and gauge bosons could also possibly lead to multi-leptonic final states, but with suppressed and negligible rates. For instance, $H_L^{\pm\pm} W^{\mp}$ production suffers from a strong v_L suppression, and the large mass of the heavier Higgs bosons yields to a severe phase-space suppression for any process in which they could be produced.

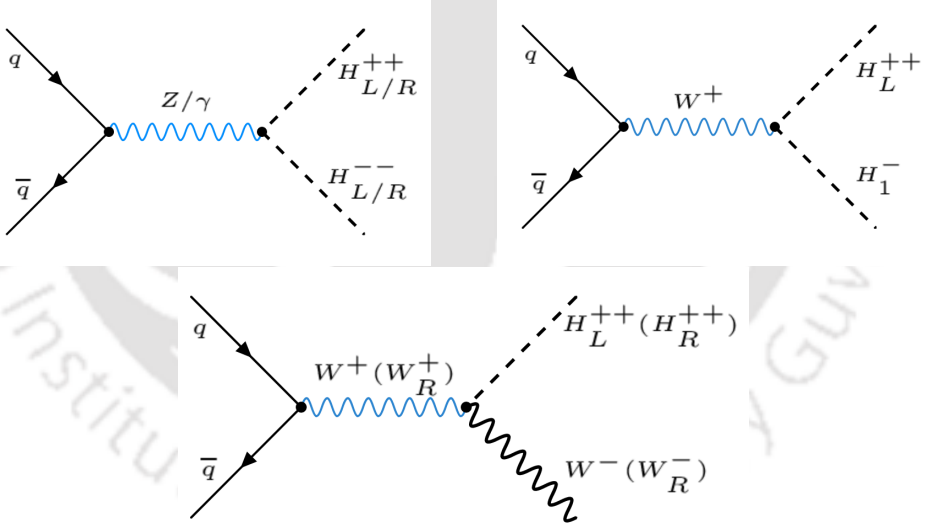

Figure 3.1: *Representative Feynman diagram of the various MLRSM processes giving rise to multileptonic final states.*

Leading-order cross sections are given in the top panel of Table 3.3 for LHC proton-proton collisions at a centre-of-mass energy $\sqrt{s} = 14$ TeV. The production of a pair of doubly-charged Higgs bosons proceeds via a Drell-Yan-like process and the exchange of an s-channel neutral gauge or Higgs boson. By virtue of the smallness of the SM Yukawa couplings and the heavy mass of the Z_R and extra Higgs bosons, virtual Z-boson and photon contributions dominate and lead to a cross section of about 0.197 fb and

Total rate at $\sqrt{s} = 14$ TeV	
$pp \to H_L^{++} H_L^{--}$	0.197 fb
$pp \to H_R^{++} H_R^{--}$	0.076 fb
$pp \to H_L^{++} H_1^{-}$	0.28 fb
$pp \to H_L^{--} H_1^{+}$	0.10 fb

Total rate at $\sqrt{s} = 14$ TeV	
$pp \to H_{L/R}^{++} H_{L/R}^{--} \to \ell^+\ell^+\ell^-\ell^-$	0.12 fb
$pp \to H_L^{\pm\pm} H_1^{\mp} \to \ell^\pm\ell^\pm\ell^\mp + \not{E}_T$	0.17 fb

Table 3.3: *Production cross sections associated with the set of processes shown in Eq. (3.19), for proton-proton collisions at a centre-of-mass energy of 14 TeV and in the context of the adopted benchmark scenario. The cross sections are obtained by multiplying the results returned by MG5_aMC [**?**], when leading-order matrix elements are convoluted with the leading-order set of NNPDF 2.3 parton densities [**?**], with an NLO K-factor of 1.25 [**?**]. Total production rates are presented on the left panel, whereas branching ratios into the two final states of interests are included on the right panel. We independently denote by $\ell = e, \mu$ any light lepton flavour (and the lepton flavours can be different within any given process).*

0.076 fb for the production of a pair of $SU(2)_L$ and $SU(2)_R$ doubly-charged Higgs bosons respectively, including in both case a next-to-leading order (NLO) K-factor of 1.25 [**?**]. Doubly-charged Higgs bosons can also be produced in association with a singly-charged Higgs or gauge boson. While the $H_R^{\pm\pm} W_R^{\mp}$ production cross section is negligible by virtue of the heavy mass of the W_R boson, a $H_L^{\pm\pm} H_1^{\mp}$ system can be produced via the exchange of a lighter SM W-boson, other diagrams contributing to a smaller extent. The associated cross section is of about 0.38 fb.

Including the relevant branching ratios, four-lepton final states arise from the production and decay of a pair of doubly-charged Higgs bosons each decaying into a same-sign dilepton, the associated cross section being of about 0.12 fb. On the other hand, trileptonic final states originate from the associated production of a doubly-charged and a singly-charged Higgs boson, with a similar total rate of 0.17 fb. Other leptonic final states, like those featuring a same-sign dilepton system, cannot be produced with a sufficiently large rate to be relevant. Despite the smallness of these cross sections, we demonstrate in Section 3.3 that the associated MLRSM signals can potentially be observed (or excluded) at the HL run of the LHC.

3.3 LHC phenomenology

For our analysis, we have used the FeynRules package [134] and the existing implementation of the MLRSM model [49] to generate a UFO model [135] that can be used within the MG5_aMC platform [**?**]. We have generated hard-scattering events both for the signal processes of Eq. (3.19) and for the SM background, the tree-level matrix elements being convoluted with the leading-order set of NNPDF 2.3 parton distributions [**?**]. The simulation of the QCD environment (parton showering and hadronisation) has been performed with Pythia 6 [83], and we have included the response of a CMS-like detector with Delphes 3 [85] that internally relies on FastJet [84] for the reconstruction of the physics objects, using the anti-k_T algorithm with a radius parameter $R = 0.4$ [136].

We require, at the matrix-element level, that all leptons and jets have a transverse momentum $p_T^{\rm gen}$ and pseudorapidity $\eta^{\rm gen}$ satisfying

$$p_T^{\rm gen}(j) > 10 \text{ GeV}, \qquad p_T^{\rm gen}(\ell) > 10 \text{ GeV}, \qquad |\eta^{\rm gen}(j)| < 2.5 \qquad \text{and} \qquad |\eta^{\rm gen}(\ell)| < 2.5 \ , \tag{3.20}$$

and are separated in the transverse plane by an angular distance of at least 0.4,

$$\Delta R^{\rm gen}(j,j) > 0.4 \ , \qquad \Delta R^{\rm gen}(j,\ell) > 0.4 \qquad \text{and} \qquad \Delta R^{\rm gen}(\ell,\ell) > 0.4 \ . \tag{3.21}$$

We analyse the reconstructed events with MadAnalysis 5 [82] and impose a basic event preselection where the reconstructed leptons and jets are required to be central and to have a transverse momentum larger than 20 GeV,

$$p_T(j) > 20 \text{ GeV}, \qquad p_T(\ell) > 20 \text{ GeV}, \qquad |\eta(j)| < 2.5 \qquad \text{and} \qquad |\eta(\ell)| < 2.5 \ . \tag{3.22}$$

We furthermore ignore any lepton lying within a cone of radius $R = 0.4$ centred on a jet.

The SM background contributing to the $\ell^+\ell^+\ell^-\ell^-$ final state is mainly pair production of Z boson, associated production of WW with a Z boson and a top quark-antiquark pair with a Z boson. On the other hand, WZ, ZZ, WWW, ttZ and ttW are main SM

backgrounds contributing to $\ell^{\pm}\ell^{\pm}\ell^{\mp}\not{E}_T$ final states. We discuss about these backgrounds in detail in the next section.

3.3.1 Four-lepton probes

After simulating all the potential contributions to the SM background (except for fake and charge-misidentification contributions), our preselection implies that the main background to a four-lepton signal are events issued from the production of a pair of (possibly off-shell) Z-bosons where both weak bosons decay leptonically. Subdominant contributions are expected to originate from the production of a WWZ system and the associated production of a top quark-antiquark pair with a Z-boson. These last components of the background could potentially be rejected by (at least loosely) vetoing the presence of missing energy and b-tagged jets in the final state. The signal fiducial cross section, normalised at the NLO accuracy and including the basic preselection is of 0.11 fb, for a corresponding background cross section of 18.9 fb, 1.3 fb and 0.13 fb for the Z-boson pair, $t\bar{t}Z$ and tribosonic components, respectively. These last numbers include a QCD next-to-next-to-leading-order (NNLO) K-factor of 1.72 for the diboson case [137] and NLO ones of 1.38 and 1.04 for the two other processes [138**?**] respectively.

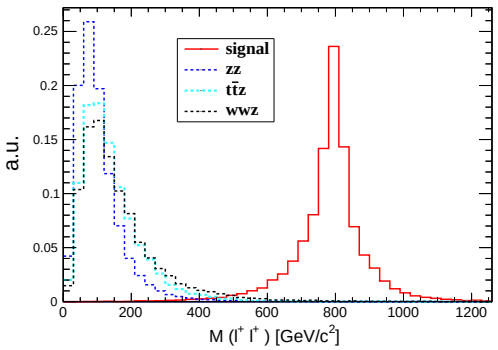

Figure 3.2: *Normalized invariant mass spectrum of the system made of the two positively-charged leptons, after selecting events containing two pairs of same-sign leptons and vetoing the presence of b-tagged jets for the signal and the background.*

To optimise the signal significance, we select events featuring exactly two pairs of opposite-charged leptons and veto those exhibiting any b-tagged jet. Signal leptons being originating from the decay of heavy Higgs bosons, we further impose that the p_T of the

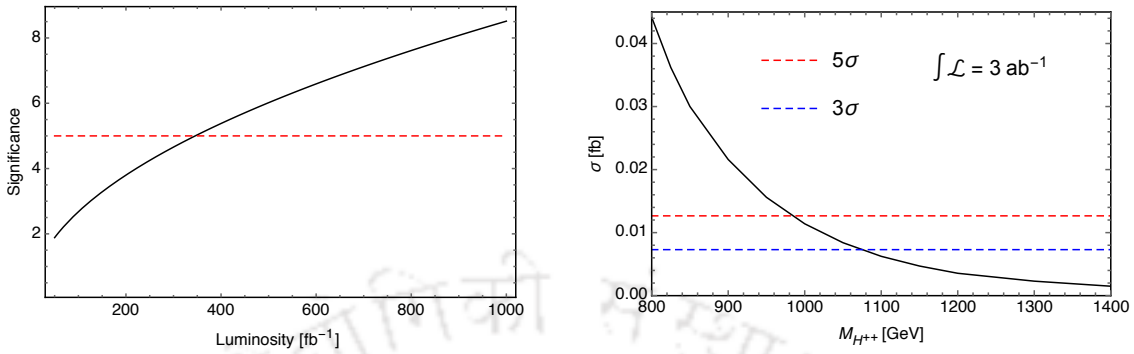

Figure 3.3: Left: *Dependence of the LHC sensitivity to the four-leptonic MLRSM signal on the integrated luminosity.* Right: *Dependence of the signal fiducial cross section after all selections on the double-charged Higgs boson mass $M_{H^{++}}$. The corresponding 3σ (blue) and 5σ (red) reference lines are indicated, assuming an integrated luminosity of 3 ab^{-1}.*

three leading leptons $p_T(\ell_1)$, $p_T(\ell_2)$ and $p_T(\ell_3)$ satisfy

$$p_T(\ell_1) > 200 \text{ GeV}, \qquad p_T(\ell_2) > 150 \text{ GeV} \qquad \text{and} \qquad p_T(\ell_3) > 60 \text{ GeV}. \tag{3.23}$$

We then use, as an extra handle on the new physics signal, the invariant masses of the systems formed by the two pairs of same-sign leptons $M(\ell^+\ell^+)$ and $M(\ell^-\ell^-)$. As in any resonance search, the shape of the signal spectrum is expected to show peaks corresponding to the physical masses of the parent particles, *i.e.*, the doubly-charged Higgs bosons in our case, as illustrated in Figure 3.2. By imposing that these invariant masses fulfil

$$M(\ell^+\ell^+) > 300 \text{ GeV} \qquad \text{and} \qquad M(\ell^-\ell^-) > 300 \text{ GeV}, \tag{3.24}$$

we are able to make the selection almost free from any background contamination, with about 15 background events being expected for a luminosity of 1 ab^{-1}.

In the left panel of Figure 3.3, we present the sensitivity of the LHC to the MLRSM four-leptonic signal for different luminosity goals, the sensitivity s (expressed in σ) being defined by [139]

$$s = \sqrt{2} \times \left((S+B) \ln\left[\frac{(S+B)\,(B+x^2)}{B^2+(S+B)\,x^2}\right] - \frac{B^2}{x^2}\ln\left[1+\frac{x^2\,S}{B\,(B+x^2)}\right]\right)^{\frac{1}{2}}, \tag{3.25}$$

where S and B, respectively, indicate the number of surviving signal and background

events, and x represents the systematic uncertainties on the background. Assuming $x = 0.1B$, a discovery could occur for about 350 fb^{-1}, whilst a signal significance of $s = 8.5\sigma$ could be expected for 1 ab^{-1}. Conversely, assuming that exclusion statements could be achieved for a sensitivity of about 2σ, the considered benchmark scenario could be excluded at the very beginning of the LHC Run 3. In order to assess the stability of our predictions with respect to the systematics, we vary the x parameter to up to 20% of the background, and investigate the induced modifications on the predictions. The latter are found robust and almost agnostic of such a change. In right panel of Figure 3.3, we generalise our conclusions to heavier scenarios and present the dependence of the fiducial cross section associated with the production of the four-lepton signal on the mass of the doubly-charged Higgs boson. We compare it to the cross sections yielding potential 3σ (blue) and 5σ (red) observations for an integrated luminosity of 3 ab^{-1}. Whilst the discovery reach can in principle be pushed above 980 GeV regime, it is clear that hints for new physics could be observed for much heavier scales. Four-leptonic probes consist thus of key MLRSM signals, both by virtue of the associated background-free environment and by the moderate value of the signal cross sections.

3.3.2 Trileptonic probes

With a larger signal cross section, trileptonic probes are expected to provide good handles on any potential new physics signal. In our case, trileptonic signal events originate from the associated production of a doubly-charged and a singly-charged scalar. The signal production rate after preselection is of about 0.14 fb. Such a signal rate must compete with diboson and triboson backgrounds as well as with top backgrounds through the associated production of a top-antitop pair with a weak boson, any other background contribution having been found negligible after requesting the presence of three leptons. The corresponding cross sections are of 214.5 fb, 32.5 fb, 1 fb, 2.77 fb and 1.71 fb for WZ, ZZ, WWW, ttZ and ttW production, after including NNLO QCD K-factors in the diboson cases ($K_{WZ} = 2.01$ and $K_{ZZ} = 1.72$ [137, 140]), an NLO QCD and electroweak K-factor in the triboson case (we have conservatively chosen $K_{WWW} = 2.27$ [141], which differs from the much smaller K-factor of Ref. [142]), an NLO QCD K-factor in the ttZ

case ($K_{ttZ} = 1.38$ [138]) and an NLO K-factor including the resummation of the threshold logarithms in the ttW case ($K_{ttW} = 1.07$ [143]).

Our selection requires events to contain two leptons carrying the same electric charge and a third lepton with an opposite charge. We moreover veto the presence of any reconstructed b-tagged jet to control the top-quark-induced background. As in the previous section, we impose a stringent selection of the lepton properties, and constrain the transverse-momentum of the two leading leptons to satisfy

$$p_T(\ell_1) > 250 \text{ GeV} \qquad \text{and} \qquad p_T(\ell_2) > 80 \text{ GeV}. \tag{3.26}$$

The signal selection efficiency is practically of 100%, while the dominant diboson background is reduced by a factor of 50. We then reconstruct the invariant mass of the same-sign dilepton system and use it as an extra handle on the signal, requiring

$$M_{\ell^\pm\ell^\pm} > 300 \text{ GeV}, \tag{3.27}$$

which reduces the triboson and remaining top-induced background to a barely visible level. Although a veto on events featuring an opposite-sign dilepton system compatible with a Z-boson could help in reducing the remaining background, we instead require the selected events to contain a large amount of missing transverse energy,

$$\not{E}_T > 150 \text{ GeV}. \tag{3.28}$$

These selections are sufficient to get a decent sensitivity to the signal, as shown in the left panel of Figure 3.4 in which we present the dependence of the significance s calculated as in Eq. (3.25) on the integrated luminosity. Both the $\ell^+\ell^+\ell^-$ and $\ell^-\ell^-\ell^+$ channels are expected to yield promising results, a 5σ discovery being reachable within about $800 - 1200$ fb^{-1} of proton-proton collisions at $\sqrt{s} = 14$ TeV in both cases. Combining the two channels, a signal may even be observed during the earlier phase of the LHC Run 3, with a luminosity of about 500 fb^{-1}. While promising, the trilepton channel is not as competitive as the four-lepton one. Nevertheless, the option of a combination is conceivable and could potentially lead to an even better expectation. Our results are

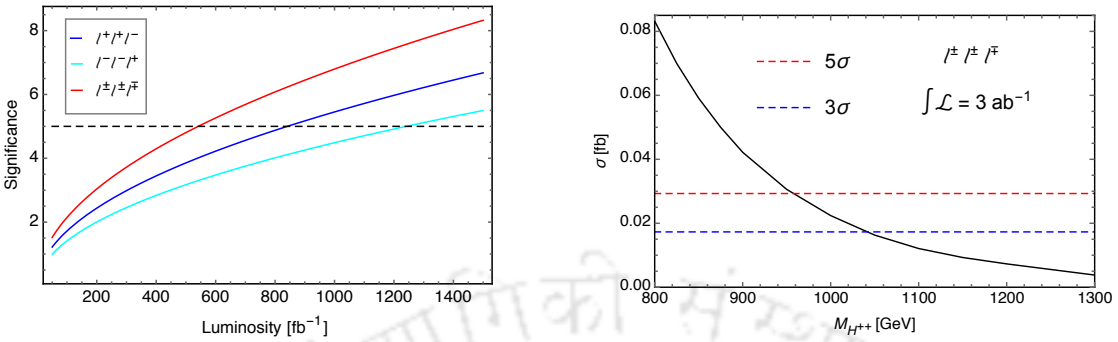

Figure 3.4: Left: *Dependence of the LHC sensitivity to the trileptonc MLRSM signal on the integrated luminosity. We separately indicate results for the $\ell^+\ell^+\ell^-$ (blue) and $\ell^-\ell^-\ell^+$ (cyan) channels, as well as for their combination (red).* Right: *Dependence of the signal fiducial cross section after all selections on the double-charged Higgs boson mass $M_{H^{++}}$. The corresponding 3σ (blue) and 5σ (red) reference lines are indicated, assuming an integrated luminosity of 3 ab^{-1}.*

generalised in the heavier mass scale case on the right panel of Figure 3.4, in which we present the dependence of the trilepton fiducial cross section (including thus the selection efficiency) on the mass of the doubly-charged Higgs boson. In contrast to the four-leptonic channel, the entire luminosity expected to be collected during the high-luminosity run of the LHC will only allow us to barely reach the TeV mass regime.

3.4 Conclusions

Left-Right Symmetric Models offer natural explanations for parity violation at the electroweak scale and an elegant way to address neutrino masses through the embedding of a seesaw mechanism. As a consequence of their symmetry breaking pattern, they feature additional scalar fields including $SU(2)_L$ and $SU(2)_R$ triplets. Such an enriched scalar sector offers various handles for discovering Left-Right Symmetric new physics and to distinguish it from other extensions of the Standard Model. In this work, we have focused on the multi-leptonic collider signatures of this scalar sector and estimated how the LHC could be sensitive to it in the upcoming years. By carefully designing first a benchmark configuration viable relatively to present data, we have found that the production of four-lepton and trilepton systems is enhanced and could be as used the main discovery mode

of the model, even if current constraints already push the new physics masses to a high scale.

For our study, we consider a scenario with doubly-charged scalar masses fixed to 800 GeV, heavy right-handed neutrinos with masses of 12 TeV and a W_R boson of 10 TeV. With all other model parameters set to guarantee consistency with flavour data, we obtain a scenario featuring one light singly-charged and two light neutral scalar bosons with large triplet components. Although the cross sections associated with the production of these light doubly-charged and singly-charged states have been found to be of about 0.1–1 fb, we have shown, by relying on state-of-the-art Monte Carlo simulations, that a simple selection strategy could allow for observing the resulting four-leptonic and trileptonic signals within the reach of the High-Luminosity phase of the LHC. In other words, MLRSM singly-charged and doubly-charged Higgs bosons lying in the TeV range could be reached in a not too far future thanks to an analysis strategy yielding an almost background-free environment.

Chapter 4

Study of charged dark fermions at ILC250

In this chapter, we study the $2\tau + MET$ final state to probe the charged fermions arising in Dark Matter Models at 250 GeV ILC. We perform a detailed signal versus SM background analysis using ILC software package (ILCsoft) and show that charged fermion of 100-124 GeV mass can be probed with significance larger than 5σ using appropriate beam polarisation combinations. Manuscript under review by the collaborators.

4.1 Introduction

The heaviest of the leptons present in the particle spectrum of the SM is the tau lepton with mass a little above a GeV. However, many models beyond SM included heavy fermions, especially non-coloured fermions, in their spectrum. With the tiny neutrino mass now established, heavier neutral leptons are somewhat accepted as a reality to make the seesaw mechanism possible. On the other hand, presence of heavy charged leptons are not as compelling. At the same time, there are many interesting BSM scenarios where

such particles are necessary for various reasons. For example, with the experimental observations suggesting that about 27% of the total energy of the universe can be categorised as DM [51, 144], some of the recent scenarios have proposed fermionic or scalar DM candidates with charged fermion partners. An attractive model among the simple scaler DM scenarios is the so-called IHDM [145–149] with an additional scalar doublet compared to the SM, which does not interact with the SM fields other than their gauge interactions. This inertness owes to their oddness under a Z_2 symmetry under which all other particles are considered to be even. The stability of the neutral component of this doublet field is also ensured by the same Z_2 symmetry. The DM thus gauge produced can get annihilated before freezing out at a later temperature. The annihilation is typically mediated by the SM Higgs boson in the s-channel or with the gauge bosons in the t-channel. The former can have SM fermions or gauge bosons in the final state, whereas the latter can have only gauge bosons in the final state. Thus, for lighter DM with mass less than M_W, the relevant s-channel process is proportional to the square of the effective scalar quartic coupling, usually denoted as λ_L. However, the same coupling controls the nuclear scattering of DM in the direct detection experiments, and therefore are stringently constrained. This severely restricts the annihilation cross section, making the dark matter over-abundant in this region. On the other hand, once kinematically allowed (with dark matter mass larger than M_W), the gauge boson annihilation channels overkill the dark matter making it under abundant in this region of parameter space. Thus, the simple IHDM is pushed to a corner with the push and pull arising from the direct detection constraints on the one hand, and the relic density consideration on the other. However, as shown in a recent work [150] the presence of a charged fermion partner to the inert doublet along with the addition of another (fermionic) dark matter can effortlessly accommodate both the relic density constraint and the direct detection limits. The charged fermion in this case can have mass a few 100 GeV to a TeV compatible with all DM measurements. Apart from this, there are many studies with fermionic or scalar DM candidates along with additional charged fermions suitably chosen to be compatible with all the experimental constraints [151–157]. The other context in which models with heavy fermions arise are supersymmetric models with heavy charginos and neutralinos and the extensions of SM addressing electroweak baryogenesis [158–160]. LHC search for the presence of heavy fermions are

mostly limited to those arising in supersymmetric models. ATLAS [161] and CMS [162] search for chariginos and neutralinos lead to exclusion of about 650-750 GeV assuming massless neutralino, which is considerably relaxed to 125 GeV for the lightest chargino when the mass splitting with the neutralinos is close to Z mass.

In this study, we consider the possible presence of heavy charged fermions ($\chi^{\pm}$) existing in association with the scalar DM. Being Z_2 odd such fermions allow Yukawa couplings with the dark scalar field along with standard fermions. $\chi^{\pm}$ being considered as gauge singlets, the left-handed SM doublet is present in the Yukawa interaction, allowing the heavy fermions to decay directly to the charged leptons. We assume that the couplings to the first two generations of leptons are quite suppressed so as not to run into trouble with the $g-2$ measurements. Moreover, we consider only diagonal Yukawa interactions, avoiding lepton flavour violating interactions. Thus, we focus on the tau decay of $\chi^{\pm}$ along with large missing energy. With the pair production and decay, the signal of a tau-pair with large missing energy closely mimics the pair production of stau ($\tilde{\tau}$) and its decay to tau and neutralino (χ_1^0). CMS search for stau with 35.6 fb^{-1} data at 13 TeV in this channel has restricted the production cross section of around 3 pb for $M_{\tilde{\tau}} \sim 100$ GeV, which is reduced to around 30 fb for higher masses of 200 GeV at 95% C.L. [163], considering the mass of the missing neutralino to be 50 GeV. In their HL projection with 3000 fb^{-1} luminosity at 14 TeV centre of mass, ATLAS has presented the exclusion regions in the $m_{\tilde{\tau}} - m_{\chi_1^0}$ plane, showing that $m_{\tilde{\tau}} \sim 100$ GeV with $m_{\chi_1^0} > 60$ GeV will not be restricted, whereas restrictions on larger mass regions are more stringent [164]. One may note that these studies have two distinctions with the case proposed in the present study. Firstly, while $\tilde{\tau}$ is a scalar, we have a heavy fermion, χ^+. This means, the selection criteria tuned to the supersymmetric search may not be applicable as it is.[1] Secondly, unlike the 100% branching ratio (BR) of $\tilde{\tau}$ to τ, in the present case there are other equally competing channels, which can reduce the BR to one-third. Moreover, it is precisely the low mass regions of around a 100 GeV, which are comparatively difficult at the LHC what we focus on here. We show that the proposed ILC with a baseline centre of mass energy of 250 GeV is quite capable of exploring the presence of χ^+ with small luminosity. For specificity, we consider the model studied in Ref.[150]. However the results of this study

[1] A recast of this search with χ^+ channel as the signal is being performed.

do not depend on the details of the model, and can be adapted easily to other similar models with a charged fermion decaying to tau and missing energy. While carrying out a detailed analysis at the 250 GeV ILC with close-to-realistic collider-detector simulation including all the relevant backgrounds considered, we also indicate what may be expected at possible higher energy versions of the e^+e^- collider. We may add that with low centre of mass energy, the baseline design of ILC is limited in its explorations of particle dynamics beyond the SM. New particles in most BSM scenarios are already restricted by the LHC or will be explored by its HL version, with masses beyond the production threshold of 250 GeV ILC. In this backdrop, the scenario we discuss in this chapter with heavy leptons of mass around 100 GeV comes as an attractive possibility at the ILC. As we demonstrate, ILC will be able to probe its presence within a short period of its commissioning.

We proceed with a brief description of the model in Section 4.2 followed by the introduction to the simulation tools, with ILC detector concept and the signal and SM background processes in Section 4.3. Section 4.4 presents the analysis and discussions and then we conclude the results in Section 4.5.

4.2 Model description

While charged fermions present in many extensions of the SM, we focus on the case where such a fermion decays predominantly to charged leptons and missing particles. For definiteness we consider the DM model briefly indicated in the Introduction. The framework presented in the model discussed here introduce of an $SU(2)_L$ singlet charged fermion $\chi^{\pm}$ to the standard IHDM scenario, with the same Z_2 charge as that of the inert doublet, Φ_2, the neutral component of which (H^0) is the scalar DM candidate. This, while taking care of the regions with DM mass $m_{H^0} < m_W$, the mass of weak gauge boson, does not address the issue with over-killing due to the annihilation into gauge boson pairs resulting in under-abundance in the regions $m_{H^0} \geq m_W$. In the proposed set up sufficiently large presence of another DM candidate (considered here as a fermion, ψ, and made stable with another discrete symmetry Z_2') takes care of the under-abundance of the scalar component. In addition, possible interactions between ψ and H^0 brings in

an altogether new dimension to the dynamics by allowing conversion of ψ to H^0 whenever kinematically allowed. In addition, considering the collider signatures of DM models, the presence of charged fermion and the additional interactions lead to signatures that could be distinct from the typical IHDM scenario. We focus on the collider study of $\chi^{\pm}$ in this work. Below we present the relevant details of the model. The Lagrangian of the model is given by

$$\begin{aligned}\mathcal{L} &= \mathcal{L}_{\rm SM} + (D_\mu \Phi_2)^\dagger (D^\mu \Phi_2) + \bar{\chi} i\gamma^\mu D'_\mu \chi + \bar{\psi} i\gamma^\mu \partial_\mu \psi \\ &\quad - M_\chi \bar{\chi}\chi - M_\psi \bar{\psi}\psi - (y_1 \bar{L}\Phi_2 \chi_R + h.c) - y_2 \bar{\chi}\chi\phi - y_3 \bar{\psi}\psi\phi - V, \end{aligned} \tag{4.1}$$

where the covariant derivatives are given by $D_\mu = \partial^\mu + ig\frac{\tau}{2}.W^\mu + ig'\frac{Y}{2}B^\mu$ and $D'^\mu = \partial^\mu + ig'\frac{Y}{2}B^\mu$. The scalar potential V can be written as ,

$$\begin{aligned} V &= \mu_2^2 \Phi_2^\dagger \Phi_2 + \lambda_2 (\Phi_2^\dagger \Phi_2)^2 + \lambda_3 (\Phi_1^\dagger \Phi_1)(\Phi_2^\dagger \Phi_2) + \lambda_4 |(\Phi_1^\dagger \Phi_2)|^2 \\ &\quad + \frac{1}{2}[\lambda_5 (\Phi_1^\dagger \Phi_2)^2 + h.c] + \mu_3^2\, \phi^\dagger\phi + \lambda_6 (\phi^\dagger\phi)^2 + \frac{1}{2}[\mu_4 \phi (\Phi_1^\dagger \Phi_1) + \mu_5 \phi (\Phi_2^\dagger \Phi_2) + h.c] \\ &\quad + \frac{1}{2}[\mu_6 \phi^3 + \mu_7 \phi + \mu_8 (\phi^\dagger\phi)\phi + h.c] + \lambda_7 (\phi^\dagger\phi)(\Phi_1^\dagger \Phi_1) + \lambda_8 (\phi^\dagger\phi)(\Phi_2^\dagger \Phi_2). \end{aligned} \tag{4.2}$$

Here Φ_1 is the SM Higgs field. We have introduced another singlet scalar field ϕ which mediate the interaction of ψ to the visible spectrum through its mixing with SM Higgs field. The inert doublet in terms of the physical charged and neutral fields may be written as $\Phi_2 = \begin{pmatrix} H^+ \\ \frac{H^0 + iA^0}{\sqrt{2}} \end{pmatrix}$. With this, the physical spectrum of the model has two charged scalars $H^{\pm}$, one is neutral scalar, H^0 and the other is neutral pseudo scalar A^0 coming from the Φ_2 filed. The lighter of H^0 or A^0 and ψ are the DM candidates. We consider H^0 to be lighter, and thus the DM candidate. In addition, masses of the charged fermion, $\chi^{\pm}$ and the charged scalar, $H^{\pm}$ should be larger than that of H^0 so as to enable their decay.

We study the possible presence of $\chi^{\pm}$ through its production at the ILC in its baseline centre of mass energy of 250 GeV. The production is controlled by the gauge coupling and the mass of the particle with the cross section lying in the order of pb. Depending on the mass hierarchy with $H^{\pm}$ and A^0, the decay of $\chi^{\pm}$ can be through $\chi^{\pm} \to H^0\tau,\ H^{\pm}\nu_\tau,\ A^0\tau$, with further decays of $H^{\pm}$ and A^0 as detailed in the following discussions.

4.3 Signal background processes, event generation, detector simulation

We discuss the signal and background processes, event generation and the analysis with ILD detector simulation in this section.

4.3.1 Signal processes

We assume a scenario where $\chi^{\pm}$ is Z_2 odd, like the inert Higgs doublet, and therefore can be pair produced or produced in association with $H^{\mp}$, H^0, A^0. In this study we consider its pair production through the s-channel mediated by Z or γ in e^+e^- annihilation. Possible t-channel process mediated by H^0/A^0 enabled by y_1 Yukawa coupling require $\chi - e$ mixing. Considering this mixing to be tiny to suppress possible dangerous contributions to $g-2$, this channel is negligible. The Feynman diagrams corresponding to the s-channel gauge production is given in Figure 4.1. Further, with negligible $\chi - \mu$ mixing, the only

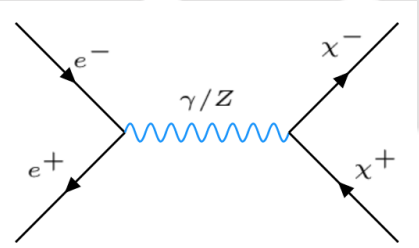

Figure 4.1: *Feynman diagrams for the production of the process $e^-e^+ \to \chi^+\chi^-$ at 250 GeV ILC.*

possible decays of χ are to the final state involving τ and ν_τ, with the decay widths given by

$$\Gamma(\chi^+ \to \tau^+ H^0) = \frac{y_1^2}{64\pi} M_\chi \left(1 - \frac{m_{H^0}^2}{m_{\chi^+}^2}\right)^2 \tag{4.3}$$

$$\Gamma(\chi^+ \to \tau^+ A^0) = \frac{y_1^2}{64\pi} M_\chi \left(1 - \frac{m_{A^0}^2}{m_{\chi^+}^2}\right)^2 \tag{4.4}$$

$$\Gamma(\chi^+ \to \nu_\tau H^+) \;=\; \frac{y_1^2}{64\pi}\, M_\chi \left(1 - \frac{m_{H^+}^2}{m_{\chi^+}^2}\right)^2 . \tag{4.5}$$

The only distinction between the three channels are due to the masses of the inert Higgs bosons. Thus, depending on the mass hierarchy, one or all channels are possible. We consider H^0 to be the lightest of all the Z_2 odd particles, and therefore, stable and a candidate DM. On the other hand, A^0 and H^+ further decays through the IHDM channels to H^0 and the gauge bosons Z and W^+, respectively. Whenever kinematically disfavoured, the gauge bosons would be produced off-shell. In the present model with the additional heavy fermion, both A^0 and H^+ pick up additional decay channels of $A^0 \to \tau\chi$ and $H^+ \to \nu_\tau \chi^+$, both depending on the Yukawa coupling, y_1. This clear distinction from the pure IHDM case would be a helpful discriminator in the phenomenological studies.

BP's	M_{H^0}	M_{A^0}	M_{H^+}	M_{χ^+}	y_1	Ωh^2	σ_{SI} in pb
BP1	59.1	119.1	124.1	122.3	1.91	0.120	3.723×10^{-12}
BP2	67.1	127.1	132.1	110.9	1.56	0.117	5.723×10^{-12}
BP3	63.6	94.9	92.9	120.0	1.64	0.120	1.124×10^{-11}
BP4	65.8	122.2	120.2	169.5	2.72	0.120	3.086×10^{-12}
BP5	79.2	127.4	125.4	208.9	2.70	0.117	4.768×10^{-12}

Table 4.1: *Parameters satisfying DM relic density and direct detection cross-section.*

We consider a few benchmark scenarios in our study. Our primary criteria is the accessibility of χ at a 250 GeV ILC. This limits us to consider $m_\chi \leq 250$ GeV. The DM candidate H^0 is considered always with $m_{H^0} \sim 60$ GeV. The masses of H^+ and A^0 are chosen so as to enable or disable decay of χ to these states. In order to be specific, we have considered the benchmark points listed in Table 4.1, which are compatible with the DM relic density and direct detection. Before going to our numerical study, we computed the cross section for $pp \to \chi^+\chi^-$ at 13 TeV LHC for different m_χ and made sure that the cross sections are safely below the present LHC bounds as well as the expectations at the HL-LHC, as discussed in the Introduction section. We plot the cross section against m_χ in left panel of Fig. 4.2. On the other hand, the ILC provides much larger cross section

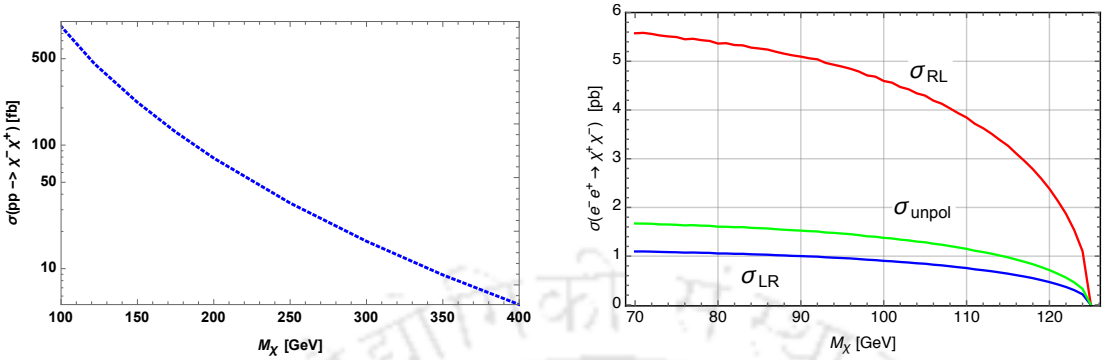

Figure 4.2: *Production cross-section of the process (Left) $pp \to \chi^+\chi^-$ at 13 TeV LHC and (Right) $e^-e^+ \to \chi^+\chi^-$ at 250 GeV ILC for different mass of χ. σ_{RL}, σ_{LR} and σ_{unpol} correspond to 100% Right-polarised electron and left-polarised positron beam, 100% Left-polarised electron beam and right-polarised positron beam, and unpolarised electron and positron beams, respectively.*

for the pair production, as plotted in right panel of Fig. 4.2. Right-handed electron beam has about five times larger cross section compared to that of the left-polarised electron beam. Notice that only the opposite polarisations of electron and positron are relevant in their Z or γ interaction. In practice 100% beam polarisation is not achievable. For the mixed case, degree of polarisation of the beams is defined in terms of the number of left-handed (N_L) and right-handed (N_R) electrons present in the beam as $P_e = \frac{N_R - N_L}{N_R + N_L}$, with $P_e = +1$ corresponds to 100% right-polarised beam ($N_L = 0$) and $P_e = -1$ corresponds to 100% left-polarised beam ($N_R = 0$). A similar definition for the degree of polarisation of positron beam also holds. The cross section with electron beam of degree of polarisation P_e and positron beam of polarisation P_p can be written in terms of the cross section with beam of 100% polarisations as

$$\sigma(P_e, P_p) = \frac{1}{4}\,(1 + P_e)(1 - P_p)\,\sigma_{RL} + \frac{1}{4}\,(1 - P_e)(1 + P_p)\,\sigma_{LR}. \tag{4.6}$$

The cross sections for a selected m_χ for different centre of mass energies of $\sqrt{s}$=250, 350, 500 and 1000 GeV with unpolarised beams are listed in Table 4.2. In all cases, we can see that the cross sections are large enough to probe up to the kinematic limits of masses $m_\chi \sim \frac{\sqrt{s}}{2}$. We first focus on the benchmark points BP1, BP2 and BP3 at the 250 GeV ILC, and take up BP4 and BP5 for higher energy versions. For BP1 and BP2 considered in Table 4.1, charged fermion $\chi^\pm$ decays are restricted to $\tau^\pm H^0$, as the other two possibilities of $A^0\tau$

$\sqrt{s}$ in GeV	$\sigma(e^+e^- \to \chi^+\chi^-)$ in fb			
	$M_\chi = 100$	$M_\chi = 200$	$M_\chi = 300$	$M_\chi = 400$
250	1377	–	–	–
350	837	–	–	–
500	422	337	–	–
1000	106	105	100	89

Table 4.2: *Production cross section of the process $e^+e^- \to \chi^+\chi^-$ at different centre of mass energies and different mass of χ with unpolarised beams. Masses of χ are expressed in GeV.*

and $H^\pm\nu_\tau$ are not kinematically accessible. On the other hand, for BP3, both of these channels open up, with further decay of A^0 and H^+ to detector level final states. Table 4.3 quotes the branching ratios of the decays of χ for the three benchmark scenarios, and that of H^+ and A^0 for the relevant BP3. With these BR's, the final state with $\tau^+\tau^- + \not{E}_T$

Dark fermion χ

BP1	$\mathrm{BR}(\chi^+ \to \tau^+ H^0)$	100%
BP2	$\mathrm{BR}(\chi^+ \to \tau^+ H^0)$	100%
BP3	$\mathrm{BR}(\chi^+ \to H^0\tau^+)$	52.79 %
	$\mathrm{BR}(\chi^+ \to H^+\nu_\tau)$	32.86 %
	$\mathrm{BR}(\chi^+ \to A^0\tau^+)$	14.34%

scalar boson H^+

BP3	$\mathrm{BR}(H^+ \to \tau^+\nu_\tau H^0)$	80.9 %
	$\mathrm{BR}(H^+ \to \mu^+\nu_\mu H^0)$	2.38 %
	$\mathrm{BR}(H^+ \to e^+\nu_e H^0)$	2.38 %
	$\mathrm{BR}(H^+ \to qqH^0)$	14.27 %

psedo scalar A^0

BP3	$\mathrm{BR}(A^0 \to \tau^+\tau^- H^0)$	88.87 %
	$\mathrm{BR}(A^0 \to \mu^+\mu^- H^0)$	0.407 %
	$\mathrm{BR}(A^0 \to e^+e^- H^0)$	0.413 %
	$\mathrm{BR}(A^0 \to qqH^0)$	7.8 %
	$\mathrm{BR}(A^0 \to \nu\nu H^0)$	2.44%

Table 4.3: *Branching ratios (BR) associated with the different decay channels of the scalar and fermion*

arising from $e^-e^+ \to \chi^+\chi^-$ have the cross sections listed in Table 4.4. The ILC is expected to have ±80% electron beam polarisation and ±30% positron beam polarisation [54]. We use these polarisation combinations in our analysis. The τ will further decay to

leptons and hadrons, with BR's of 32% and 68%, respectively [165]. ILD is expected to have very efficient hadronic tau reconstruction [166], and we consider all possible decay channels of tau in our analysis. The final state of our signal event contains two opposite charge τ leptons and missing energy. Both τs decaying hadronically to $\tau^{\pm} \to \pi^{\pm}\pi^{0}\nu_{\tau}$ with 26%, $\tau^{\pm} \to \pi^{\pm}\nu_{\tau}$ with 11%, $\tau^{\pm} \to \pi^{\pm}\pi^{0}\pi^{0}\nu_{\tau}$ with 9.26%, $\tau^{\pm} \to \pi^{\pm}\pi^{\pm}\pi^{\mp}\nu$ with 9%, and last decay of hadronic mode is $\tau^{\pm} \to \pi^{\pm}\pi^{0}\pi^{0}\pi^{0}\nu$ with 1.04 % which accounts for total hadronic decay of τ is around 64.79%. Apart from hadronic decay modes, there are two leptonic decay modes of τ, one is to $\tau^{\pm} \to e^{\pm}\bar{\nu}_{e}\nu_{\tau}$ and another is to $\tau^{\pm} \to \mu^{\pm}\bar{\nu}_{\mu}\nu_{\tau}$ accounts for 17.85% and 17.36%, respectively. Before the detailed discussion of our analysis,

Final state	BP's	$\sigma_{100\%pol}$ in fb		$\sigma(P_e, P_p)$ in fb	
		σ_{LR}	σ_{RL}	$(-80\%, +30\%)$	$(+80\%, -30\%)$
$e^+e^- \to \chi^+\chi^-$ $\to \tau^+\tau^-\not{E}_T$	BP1	306	1562	233	924
	BP2	709	3597	540	2129
	BP3	145	734	110	435

Table 4.4: *Final state cross section of the process $e^-e^+ \to \chi^+\chi^- \to \tau^+\tau^-\not{E}_T$ at 250 GeV ILC with 100 % left-right (LR) and right-left (RL) polarised electron-positron beams, along with the expected $(-80\%, +30\%)$ and $(+80\%, -30\%)$ polarizations for different benchmark points mentioned in Table 4.1.*

we consider the SM background to this process.

4.3.2 Background selection

Background can be broadly categorized into 2-fermionic and 4-fermionic, with major contributions from two and four-fermions at the parton level final states, with bremsstrahlung radiation included wherever significant. The backgrounds are further classified into leptonic, hadronic and semi-leptonic, depending on the final states. Below we list all 2-fermion, 4-fermion (leptonic, semileptonic and hadronic) SM backgrounds to the signal of opposite charged τ lepton pair and missing energy:

- **2-fermion leptonic** $(e^+e^- \to Z \to 2f)$: This background comes from the pair production of charged lepton with the intermediate state of Z boson.

- **2-fermion hadronic** ($e^+e^- \to Z \to q\bar{q}$): The final state of this background is the pair production of quarks with the intermediate state of Z boson.

- **2-fermion bhabhag** ($e^+e^- \to e^-e^+\gamma$): The production of electron and positron along with a photon (bhabha scattering).

- **4-fermion leptonic** ($e^+e^- \to W^+W^- \to \ell^+\nu_l\ell^-\bar{\nu}_l / e^+e^- \to ZZ \to \ell^+\ell^-\nu_l\bar{\nu}_l$): Final states of 4 leptons consisting of mainly processes through ZZ and WW intermediate states. Those events containing a pair of lepton and missing energy are background of our signal.

- **4-fermion leptonic** ($e^+e^- \to W^-W^+\_ZZ_{mix} \to 4f$): Production of 4 leptons mainly coming from processes with both ZZ and WW intermediate states. Those events containing a pair of lepton and missing energy are background to our signal.

- **4-fermion leptonic** ($e^+e^- \to Ze^+e^- \to \ell^+\ell^-\nu_\ell\bar{\nu_\ell}$): Final states of 4 leptons consisting of mainly processes through Z and electron, positron production. Those events containing a pair of lepton and missing energy are background of our signal.

- **4-fermion leptonic** ($e^+e^- \to W^\pm e^\mp\nu_\ell \to \ell^+\ell^-\nu_\ell\bar{\nu_\ell}$): Final states of 4 leptons consisting of mainly processes through W boson and either electron, electron type neutrino or positron and positron type neutrino production. Those events containing a pair of lepton and missing energy are background of our signal.

- **4-fermion leptonic** ($e^+e^- \to Z\nu_\ell\bar{\nu_\ell} \to \ell^+\ell^-\nu_\ell\bar{\nu_\ell}$): Final states of 4 leptons consisting of mainly processes through Z and neutrino and anti-neutrino production. Those events containing a pair of lepton and missing energy are background of our signal.

- **4-fermion leptonic** ($e^+e^- \to Zee/W^\pm e^\mp\nu_\ell \to 4f$): Production of four leptons consisting of mainly processes through single Z along with a pair of electron positron or W boson and lepton and a neutrino. Those events containing a pair of lepton and missing energy are background of our signal.

- **4-fermion semileptonic** ($e^+e^- \to W^+W^- \to 4f$/ $e^-e^+ \to ZZ \to 4f$): A pair of charged leptons and pair of quarks, consisting of mainly processes through ZZ

and WW intermediate states. In ZZ boson case, one Z boson decays to a pair of charged leptons and the other Z boson decays to a pair of quarks. In the latter case, one W boson decays to a charged lepton and a neutrino and other W boson decays to quarks.

- **4-fermion semileptonic** ($e^+e^- \to Zee \to 2j\ell\ell$): Final state of 4 fermions consisting of mainly processes through Z and electron, positron production. Those events containing a pair of lepton and two jets are background of our signal.

- **4-fermion semileptonic** ($e^+e^- \to W^\pm e^\mp \nu \to 2j\ell\nu_\ell$): Final state of 4 fermions consisting of mainly processes through W boson and either electron, electron type neutrino or positron and positron type neutrino production. Those events containing a pair of lepton and two quarks are background of our signal.

- **4-fermion semileptonic** ($e^+e^- \to Z\nu_\ell\bar{\nu_\ell} \to 2j\nu_\ell\bar{\nu_\ell}$): Final state of 4 fermions consisting of mainly processes through Z and neutrino and anti-neutrino production. Those events containing a pair of neutrino anti-neutrino and two jets are background of our signal.

- **4-fermion hadronic** ($e^+e^- \to W^+W^- \to 4j / e^-e^+ \to ZZ \to 4j$): Final state of 4 fermion consisting of quarks, consisting of mainly processes through ZZ and WW intermediate states. In both ZZ case or WW case, both Z boson and W boson decays to quarks.

- **4-fermion hadronic** ($e^+e^- \to W^-W^+\_ZZ_{mix} \to 4f$): Production of 4 quarks, mainly coming from processes with both ZZ and WW intermediate states. Those events containing a pair of light quark jets and missing energy are background to our signal.

In addition, $e^+e^- \to \nu\bar{\nu}h$, where h is the SM Higgs boson with its all possible decays can potentially contribute to the background. We have considered this in our analysis as well. In Table 4.5 we present the cross section of all the above background process for the two different polarisation combinations considered. For convenience we have also included the corresponding cross sections for 100% beam polarisations.

SM background		poln	$\sigma_{100\%pol}$ in fb	σ^{tot} in fb	
				$(-80\%,+30\%)$	$(+80\%,-30\%)$
$2f\_leptonic$	$2f\_Z\_l$	LR	21226.35	12993.8	10377.8
		RL	16470.02		
	$2f\_z\_bhabhag$	LR	25286.93	25183.36	24605.9
		RL	24228.04		
		LL	25183.35		
		RR	25128.28		
$2f\_hadronic$	$2f\_Z\_h$	LR	129148.58	78046.46	46214.8
		RL	71272.8		
$\nu\nu h$	nnh	LR	128.64	77.53	42.58
		RL	65.09		
$4f\_leptonic$	$4f\_ZZWWMIX\_l$	LR	1636.03	958.96	88.82
		RL	53.96		
	$4f\_WW\_l$	LR	1564.21	915.57	63.34
		RL	14.6		
	$4f\_ZZ\_l$	LR	157.96	95.88	63.73
		RL	99.51		
	$4f\_singleZee\_l$	LR	1084.08	1053.4	1017.63
		RL	1019.53		
		LL	1009.6		
		RR	1008.41		
	$4f\_singleW\_l$	LR	3334.66	1966.9	148.7
		RL	29.09		
		LL	39.95		
		RR	39.9		
	$4f\_singleZnunu\_l$	LR	192.75	114.14	29.75
		RL	39.3		
	$4f\_sZsWMix\_l$	LR	922.048	550.6	55.40
		RL	21.59		
		LL	27.67		
		RR	27.6		
$4f\_semileptonic$	$4f\_WW\_sl$	LR	18780.9	10992.91	758.38
		RL	172.7		
	$4f\_ZZ\_sl$	LR	1422.1	856.92	467.2
		RL	713.5		
	$4f\_singleW\_sl$	LR	9999.5	5898.16	445.42
		RL	85.6		
		LL	119.6		
		RR	119.28		
	$4f\_singleZee\_sl$	LR	459.05	378.28	299.68
		RL	316.5		
		LL	259.75		
		RR	258.95		
	$4f\_singleZnunu\_sl$	LR	456.7	271.80	92.5
		RL	130.7		
$4f\_hadronic$	$4f\_ZZWWMIX\_h$	LR	12383.3	7252	564.9
		RL	224.84		
	$4f\_WW\_h$	LR	14874.3	8706.2	600.36
		RL	136.35		
	$4f\_ZZ\_h$	LR	1402.05	841.4	402.93
		RL	604.9		
	signal				
BP1	$e^-e^+ \to \chi^+\chi^-$ $\to \tau^+\tau^- H^0H^0$	LR	305.7	233.5	924.4
		RL	1562		
BP2	$e^-e^+ \to \chi^+\chi^-$ $\to \tau^+\tau^- H^0H^0$	LR	709	540.66	2129
		RL	3597		
BP3	$e^-e^+ \to \chi^+\chi^-$ $\to \tau^+\tau^- H^0H^0$, $e^-e^+ \to \chi^+\chi^-$ $\to \tau\tau\nu_\tau\nu_\tau H^0H^0$	LR	144.5	110.26	434.6
		RL	734.4		

Table 4.5: *Cross section list of SM background for the signal final state $\tau^+\tau^- MET$ at ILC250 for three different Benchmark Point (BP), for $(-80\%, 30\%)$ and $(80\%, -30\%)$ polarization.*

4.3.3 Event generation and simulation

We conduct this study at 250 GeV ILC with two beam polarizations of $(P_e, P_p) = (-80\%, +30\%)$ and $(+80\%, -30\%)$. The Monte Carlo samples for both signal and background are generated with 100% polarizations in appropriate combinations. From this we obtained the cross section for the above polarization combination using the expression given in Eq.4.6, generalised to include other polarisation combinations also for the backgrounds which require those. Coming to the background, we take a set of full two fermion and four fermion samples, which are centrally generated by ILC Physics group using WHIZARD version 1.95 [167], which includes the effects of initial state radiation. In table 4.5 we present the background samples used in this analysis along with the statistics. The table also gives the signal and background cross sections. For hadronization and showering including τ decay, we used PYTHIA (version 8.212) [83, 168]. Each τ is allowed to decay by TAUOLA++ v1.1.4 [169] at ILC. The τ leptons in the signal are allowed to decay to all possible modes. For simulation and reconstruction of the events, tools are used from software package called ILCSoft[170]. The generated events are passed through the ILD [171] with GEANT4-based MOKKA toolkit [172] for detector simulation. The simulated energy deposits are digitised and reconstructed using MARLINRECO in Marlin Framework [173]. After the event reconstruction, the output is collected in the form of Particle Flow Object (PFO), each of which corresponds to individual final state particle. Charged PFOs are classified as electrons, muons and charged hadrons, while neutral PFOs are neutrinos, photons and neutral hadrons. All photon PFOs in the proximity of charged particles are considered as being induced by FSR or Bremsstrahlung. We explain the methods and performance of the signal selection and background rejection in section 4.4.

4.4 Analysis and discussion

We now go through the details of analysis including the kinematic selection to improve the signal significance over the background.

4.4.1 Reconstruction and event selection

Preselection for τ decays

For the preselection, the first requirement is to form two isolated oppositely charged jets originating from two oppositely charged τ leptons. We prepare an algorithm to generate two jets (which would be identified as originating from the two τ's) from reconstructed PFOs as follows. First of all, we find the most energetic charged PFO and collect other PFO's making a cone of radius 0.2 radian around this. This we consider as the first τ jet ($\mathbf{jet}_1$). While forming the second τ jet ($\mathbf{jet}_2$), we find the second most energetic charged PFO which is not assigned in $\mathbf{jet}_1$. Then other nearby PFOs are collected around this second most energetic charged PFO making an angle less than or equal to 0.2 radian. It is made sure that the same PFO will not be part of both the jets. The jets thus formed are further required to have opposite average electric charge.

Event reconstruction and selection

Optimised for Particle Flow Algorithm (PFA), ILD has a high precision silicon vertex detector (VTX) made of three extremely fine silicon pixel sensors with the innermost radius of the sensor 15 mm. It can measure the particle tracks with spatial resolution of 2.8 μm. The arrangement is followed by a large volume Time Projection Chamber (TPC), which provides upto 224 points per track. TPC is optimised for 3D point resolution with spatial resolution better than 100 μm and an energy loss ($-\frac{dE}{dx}$) based particle identification. Additional silicon strip tracking detectors are placed outside the TPC, one behind the end-plate of the TPC (ETD) and one in between the TPC and the Electromagnetic Calorimeter (ECAL). This is done with the motivation to provide high precision space points, which improves the tracking performance of the momentum resolution. An *Si-W* based highly segmented ECAL is placed outside the tracking system with the inner radius of 1.8 m and 30 longitudinal layers and small transverse cell size of 5×5 mm^2. ECAL is followed by steel scintillator type highly segmented Hadron Calorimeter (HCAL) with upto 48 longitudinal layers, corresponding to 5.9 interaction lengths. HCAL surrounds the ECAL and has its outer radius of 3.4 m. There are two options based on Steel-based

absorber structure. An analogue based read out system uses the scintillator tiles of 3×3 cm^2 and the gas based readout uses a 1×1 cm^2 cell geometry with a binary or semi-digital readout of each cell. A system of high precision radiation hard calorimetric detectors are installed outside the forward region of the ECAL and HCAL to measure the luminosity and to monitor the quality of the colliding beams. This whole system of tracking set up and calorimeters are surrounded by a large volume superconducting coils to provide an axial magnetic field of 3.5 Tesla. In order to return the magnetic flux of the solenoid, an iron yoke is instrumented with scintillator type strips and at the same time this serves as a muon detector. With such arrangements, the ILD is capable of high precision τ tracking and reconstruction [166].

Along with the distribution of number of PFOs, the kinematic distributions including the total visible energy, individual PFO energy, invariant mass distributions of the jets, projected angle between the jets in the XY-plain (ϕ_{jet1jet2}) and $\cos\theta_{\text{visible}} = P_z/P$, where P corresponds to the magnitude of the sum of all visible momenta, for BP1 are given in Fig. 4.3, and 4.4, for the two polarisation combinations of $(-80\%, +30\%)$ and $(+80\%, -30\%)$, respectively. As listed in Table 4.5, we have combined the background into six different groups of

1. *2f-leptonic*: This include $e^+e^- \to 2\ell$ and $e^+e^- \to e^+e^-\gamma$ events, with a combined cross section of more than 38 pb (220 pb) for the polarisation combinations of $P_e = -80\%,\ P_p = +30\%$ $(+80\%, -30\%)$.

2. *2f-hadronic*: This is mainly the $e^+e^- \to q\bar{q}$ process with cross sections of 78 pb (46 pb).

3. $\nu\nu h$: The $e^+e^- \to \nu\bar{\nu}h$ process with all possible decays of h is included in this background, with a cross section of 78 fb (43 fb).

4. *4f-leptonic*: Major contributions arise from $e^+e^- \to ZZ \to 4\ell$, $e^+e^- \to WW \to 2\ell 2\nu$, $e^+e^- \to ZZ \to 2\ell 2\nu$, $e^+e^- \to Ze^+e^- \to 2e\ 2\nu$, $e^+e^- \to Z\nu\nu \to 2\ell 2\nu$, $e^+e^- \to We\nu \to 2\ell 2\nu$. The combined cross section is about 5.6 (1.5) pb.

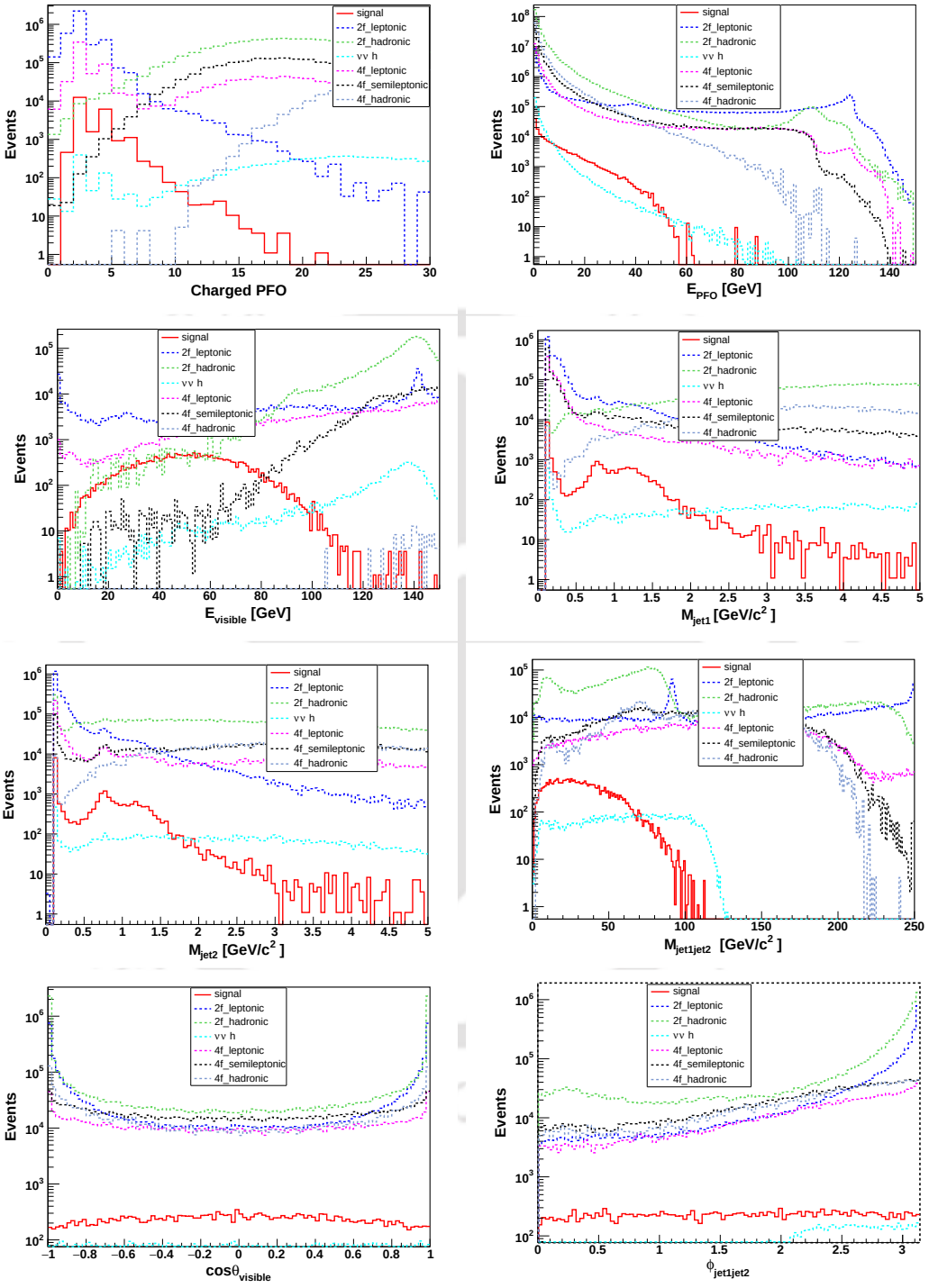

Figure 4.3: *Kinematic distributions of $\tau^+\ \tau^- + \not{E}_T$ final state for BP1 (-80%, 30%) polarization, with all backgrounds before applying any selection cuts with 100 fb^{-1} integrated luminosity.*

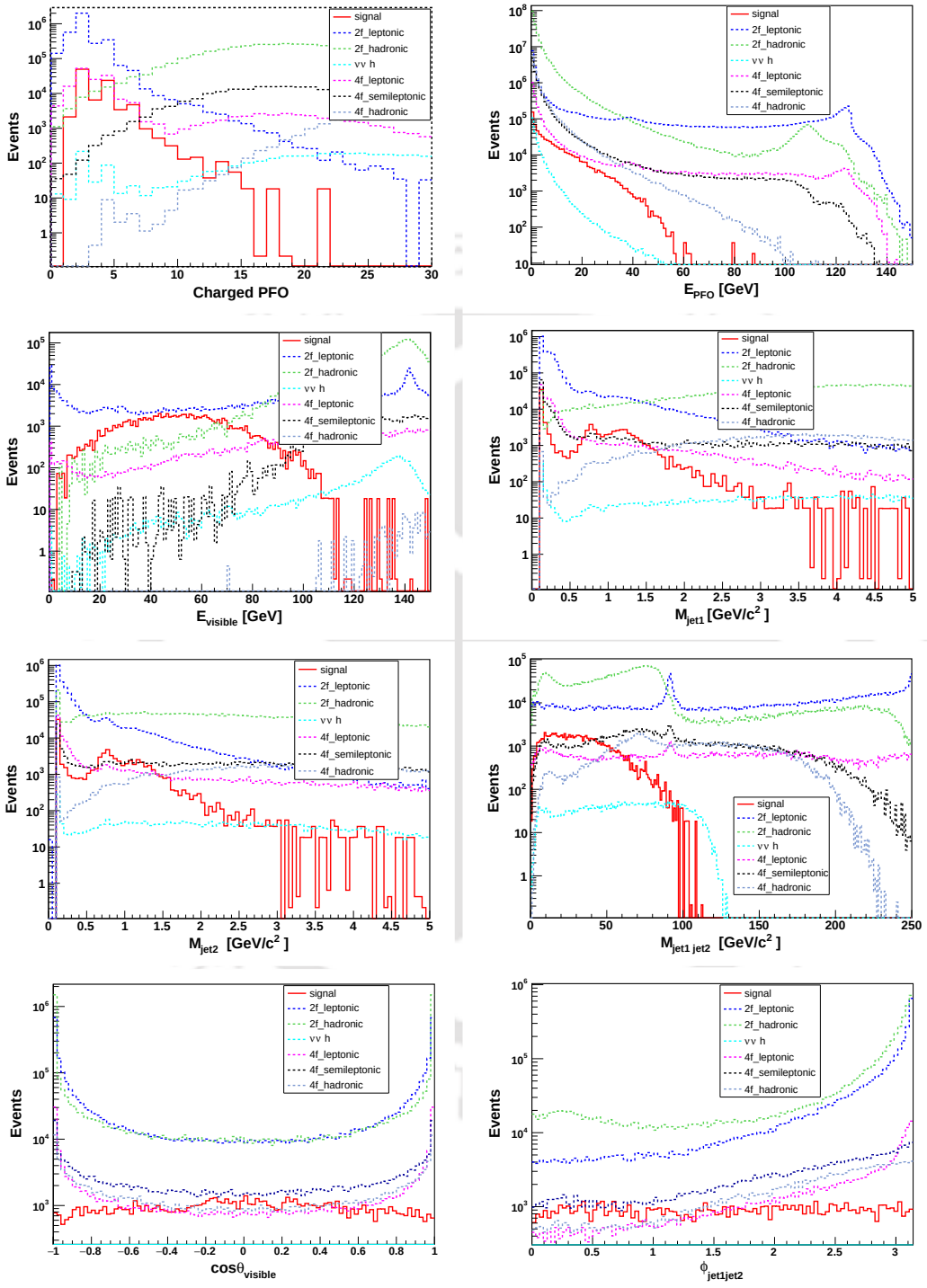

Figure 4.4: *Kinematic distributions of $\tau^+\ \tau^- + \not{E}_T$ final state for BP1 (80%,- 30%) polarization polarization, with all backgrounds before applying any selection cuts with 100 fb^{-1} integrated luminosity.*

Cut1	No. of jets ≥ 2
Cut2	No. of charged PFO's ≤ 14.
Cut3	The visible energy $E_{\text{visible}} < 105$ GeV.
Cut4	Energy of PFO $E_{\text{PFO}} < 55$ GeV.
Cut5	$M_{\text{jet1jet2}} < 100$ GeV.
Cut 6	$M_{\text{jet1}},\ M_{\text{jet2}} < 2.5$ GeV
Cut 7	The projected angle of jet1 and jet2 on the X-Y plane, $\phi_{\text{jet1jet2}} \leq 3.0$ radian.

Table 4.6: *Event selection criteria adopted for both the combinations of beam polarisations considered.*

5. *4f-semileptonic*: The total cross section in this group of backgrounds including $e^+e^- \to WW/ZZ \to 4f$, $e^+e^- \to ZZ \to 4f$, $e^+e^- \to Zee \to 2j2\ell$, $e^+e^- \to We\nu \to 2je\nu$, $e^+e^- \to Z\nu\nu \to 2j2\nu$ is 18.4 (2.1) pb

6. *4f-hadronic*: This group of backgrounds include $e^+e^- \to WW/ZZ \to 4j$ with total cross section of 16.8 (1.6) pb.

For the distributions given in Fig. 4.3, and 4.4 we have considered an integrated luminosity of 100 fb^{-1}. While larger fraction of the signal events in both the polarisation combinations have relatively small number of charged PFO's of less than 10, most of the background processes, except the *2f-leptonic* background, mostly have much larger number of charged PFO's. Thus we considered an optimised selection of events with smaller than 14 charged PFO's as our first criteria, after demanding that every event has at least 2 jets. Left side plot in the second row of Fig. 4.3, and 4.4 shows the distribution of total visible energy E_{visible} obtained by summing over the energies of all the PFO's in a particular event. Cut-flow table with number of signal and background events after every selection cut discussed above is given in Table 4.7 and 4.8 for the two beam polarisation combinations of $(-80\%, +30\%)$ and $(+80\%, -30\%)$, respectively. For the signal events, most of the events have the total visible energy less than around 100 - 120 GeV, whereas for all the backgrounds have a large fraction of events with larger energies. This trend is also true for the energy E_{PFO} of individual PFO's shown in the right side plot in the first row.We have, therefore, selected events with $E_{\text{visible}} < 105$ GeV and $E_{\text{PFO}} < 55$ GeV. The jets in

the signal events originating from τ is expected to have the invariant mass ($M_{\text{jet1,2}}$) close to the mass of τ, whereas for the background this is not the case. We have introduced a cut of $M_{\text{jet1,2}} < 2.5$ GeV as another selection criteria. The invariant mass of the two jets (M_{jet1jet2}) do not go beyond around 100 GeV. This is because of the presence of the two missing particles (H^0) of mass around 60 GeV. On the other hand, almost all backgrounds have a good fraction of events with much larger M_{jet1jet2}. Exception is $\nu\nu h$ background events, where the M_{jet1jet2} is expected to be not more than the Higgs mass. We introduce a selection of $M_{\text{jet1jet2}} < 100$ GeV. Considering the angle between the jets in the XY-plain (ϕ_{jet1jet2}) , most of the backgrounds show a peak with back-to-back jets. This is more pronounced in the case of 2-fermion events as expected. This distributions is given in the right side plot of the last row. Notice that the $\nu\nu h$ events with small number of events is not visible in the plot. We considered a selection of $\phi_{\text{jet1jet2}} \leq 3.0$ radian. We have summarised the selection criteria in Table 4.6. The distributions for BP2 and BP3 are

SM background		σ_{cut0}	σ_{cut1}	σ_{cut2}	σ_{cut3}	σ_{cut4}	σ_{cut5}	σ_{cut6}	σ_{cut7}	$\sigma_{tot-bkg}$
$2f\_leptonic$		38177.26	30548.76	30512.70	3020.59	2935.41	2850.20	2790.86	1323.20	
$2f\_hadronic$		78046.45	77920.03	18380.41	2109.51	2106.09	2106.04	1068.35	62.57	
$\nu\nu h$		77.53	77.07	14.39	10.52	10.45	10.32	9.18	8.66	2823.10
$4f\_leptonic$		5655.67	5180.90	5178.48	1710.15	1594.07	1536.03	1518.26	1363.03	
$4f\_semileptonic$		18422.88	18421.22	5088.81	140.92	140.92	140.91	80.15	65.75	
$4f\_hadronic$		16799.70	16799.70	14.53	0.00026	0.00026	0.00026	0.00026	$< 10^{-5}$	
Signal	$BP1$	233.50	226.55	226.30	225.27	225.23	225.14	218.27	208.47	
	$BP2$	540.66	52.46.8	523.99	521.60	521.52	521.41	505.40	482.69	
	$BP3$	110.24	106.96	106.84	106.35	106.33	106.31	103.04	98.42	

Table 4.7: *Cut flow table with cross section (σ_i) in fb after each cut applied for both signal and background for the final state $\tau^+\tau^- MET$ at 250 GeV center of mass energy, with integrated luminosity of 100 fb^{-1} for $(-80\%, 30\%)$ polarization.*

given in Fig. B.1-B.4 in Appendix B. The distributions show similar behaviour as that of BP1. The decay pattern of BP2 is the same as that of the BP1, with the only difference being the reduced m_χ, and a consequent increase in the cross section. In the case of BP3, however, the decay pattern is different as explained in Section 4.3.1. While in the case of BP1 and BP3 the missing energy and momenta are carried by two H^0 produced, in the case of BP3 it is shared by the neutrinos as well. This results in the PFO energy

SM background		σ_{cut0}	σ_{cut1}	σ_{cut2}	σ_{cut3}	σ_{cut4}	σ_{cut5}	σ_{cut6}	σ_{cut7}	$\sigma_{tot-bkg}$
$2f\_leptonic$		34983.78	27483.29	27450.04	2218.70	2161.75	2104.11	2060.67	962.54	
$2f\_hadronic$		46214.80	46092.05	12666.33	1716.93	1710.06	1709.23	877.78	50.74	
$\nu\nu h$		42.58	42.31	7.91	5.76	5.71	5.66	5.14	4.86	1178.89
$4f\_leptonic$		1467.58	1202.84	1201.01	198.86	185.55	181.11	178.10	141.72	
$4f\_semileptonic$		2477.65	2475.14	739.63	63.28	63.22	63.22	28.62	19.02	
$4f\_hadronic$		1568.29	1568.29	3.47	0.0044	0.0044	0.0044	0.0044	$< 10^{-5}$	
Signal	$BP1$	924.46	893.46	892.35	888.10	888.10	887.91	861.09	822.27	
	$BP2$	2129.05	2057.64	2055.10	2045.31	2045.30	2044.88	1983.11	1893.69	
	$BP3$	434.68	420.10	419.58	417.58	417.58	417.49	404.88	386.62	

Table 4.8: *Cut flow table with cross section (σ_i) in fb after each cut applied for both signal and background for the final state $\tau^+\tau^- MET$ at 250 GeV center of mass energy, with integrated luminosity of 100 fb^{-1} for $(+80\%, -30\%)$ polarization.*

distribution and the invariant mass distributions. However, the selection criteria will not change considerably, and therefore, we have employed the same selection criteria for all the benchmark points. The cut-flow for all the BP's are included in Table 4.7 and 4.8. We compute the significance using the formula

$$\sigma_{sig} = \frac{S}{\sqrt{S + B + x^2(S^2 + B^2)}}, \tag{4.7}$$

where S and B are the signal and background number of events, and x is the expected systematic uncertainty. Considering the various uncertainties including those involved in the τ reconstruction, we assume a conservative 20% uncertainty uniformly for all background and signal events.

Significance at 100 fb^{-1}				
Polarisation	$(-80\%, +30\%)$		$(+80\%, -30\%)$	
Systematics	$x = 0.02$	$x = 0.05$	$x = 0.02$	$x = 0.05$
BP1	3.6	1.47	28.2	11.4
BP2	8.3	3.36	42.1	16.9
BP3	1.7	0.69	15.3	6.2

Table 4.9: *Signal significance corresponding to cut flow Table 4.7 and 4.8 at 100 fb^{-1} luminosity with x corresponds to systematic uncertainty of 2% and 5% for both signal and background.*

The signal significance obtainable at 100 fb^{-1} integrated luminosity is quoted in the

right columns of Table 4.9. Beam polarisation with more right-handed electrons favours better, as the background is reduced to about one-third compared to the opposite polarisation combination, while the signal is increased almost four-fold. With the polarisation combination of $(+80\%, -30\%)$ we can reach a significance of more than 5σ at moderate luminosity of 50 fb^{-1}. With large background remaining, at the same time with large signal cross section available, it is the systematics which control the significance. Therefore larger luminosity does not change the significance considerably.

4.4.2 Higher energy collider options

It is expected that the ILC would have an energy upgrade possibly to 350 GeV and 500 GeV, and perhaps also up to 1 TeV centre of mass energies. The CLIC being discussed also is expected to have centre of mass energies of 380 GeV and 1500 GeV. In this section we briefly extend our discussion to possibilities at these collider options. The benchmark points BP4 and BP5 mentioned in Table 4.1 are considered for this. We assume that the beam polarisations remain the same as that of the 250 GeV ILC, and quote the cross sections for the two polarisation combinations for three different centre of mass energies are given in Table 4.10 along with the estimated background. The background processes are obtained from the ILC repository. Apart from all the backgrounds discussed in the 250GeV ILC we have included the background that may arise from $e^+e^- \to t\bar{t}$ process as well. In the absence of full detector study, we have not attempted a detailed analysis here.

Final state	BP's	$\sqrt{s}$ GeV	$\sigma(P_e, P_p)$ in fb and significance (σ)						
			Polarisation	$(-80\%, +30\%)$			$(+80\%, -30\%)$		
				No cut in fb	After cut in fb	σ	No cut in fb	After cut in fb	σ
$e^+e^- \to \chi^+\chi^-$ $\to \tau^+\tau^- \not{E}_T$	BP4	350	Background	104570	1871.8		58940	795.6	
			Signal	39.7	35.6	0.9	141.8	124.8	7.6
	BP5	500	Background	60077	1075.4		46568	628.6	
			Signal	32.2	28.7	1.3	110.3	97.1	7.4

Table 4.10: *SM background and signal cross section for the final state $\tau^+\tau^- MET$ at ILC350 and ILC500. Reduction after selection is assumed from that in the 250GeV ILC study. Significance is obtained for 100 fb^{-1} integrated luminosity and with an assumed systematic uncertainty of $x = 2\%$.*

Instead, we prepared a rough estimate of the significance assuming a similar reduction in the events after the selection as that in the case of 250 GeV ILC above. The signal and background cross sections obtainable after the selection are listed in Table 4.10, along with the corresponding significance, for the two combinations of the beams. This clearly indicates that the high energy versions of ILC are capable of probing the presence of χ up to its kinematic limit.

4.5 Conclusions

In many ways, electron-positron colliders bring in advantages over the hadronic colliders like the LHC in the search for new physics beyond the SM. The advantages include the cleaner environment with the initial state being point-like particles without substructure, and the possibility of beam polarisation. In this work we consider probing the presence of a heavy charged fermion of mass around 100 GeV at the baseline configuration of the ILC with a centre of mass energy of 250 GeV. Such fermions are present in many extensions of the SM. In particular we consider the charged fermions arising in DM models as partner particles of the DM candidates. These fermions, being odd under the same Z_2 symmetry that the DM candidate follows, decay eventually to the DM particle and other SM particles. As a specific example we considered the charged fermion added to the IHDM. In this case the fermion (χ) decays to the scalar DM (H^0) and an SM lepton. Suppressing mixing with the first two generations of the leptons, we consider it interacting predominantly with τ. There are no dedicated search that LHC has performed to look for dark heavy fermions like this. However, the limits drawn from the pair production of supersymmetric particle, $\tilde{\tau}$ decaying to τ and neutralino come close to pair production and decay, $\chi \to \tau H^0$. We have made sure that the parameters we are considering are safely within the experimental limits obtained from these $\tilde{\tau}$ searches at the 13 TeV LHC as well as the expected limits at its HL version, HL-LHC.

We consider the possibility of pair production of χ and further decay of χ at the 250 GeV ILC with two different beam polarisations of $(P_e,\ P_p) = (-80\%, +30\%)$ and $(+80\%, -30\%)$, resulting in a final state with $\tau^+\tau^-$ pair and large missing energy. The

τ's are further allowed to decay to all possible channels. SM backgrounds to this signal arising in all processes are obtained from the ILC repository. The signal events are generated through MadGraph, and processed through Pythia and MOKKA, which is the ILD simulator. Both the signal and background events are then analysed with the help of MARLINRECO, the standard tool used in the ILC studies. The kinematic distributions obtained thus are studied for event selection so as to enhance signal events over the background events. We considered three different benchmark scenarios with m_χ 100 - 124 GeV, around the kinematic limits of the collider. The first and second scenarios (BP1 and BP2) are selected to have χ decay exclusively to $H^0\tau$, whereas the third scenario considered a mass hierarchy with the scalar bosons so that decays to $A^0\nu_\tau$ and $H^+\tau$ also contribute substantially to the width. The study shows that both BP1 and BP2 cases can be probed with a significance of 3.6 and 8.3 for the polarisation combination of $(-80\%, +30\%)$ and an assumed systematics of 2% and integrated luminosity of 50 fb^{-1}, whereas BP3 case is somewhat more difficulty. On the other hand the $(+80\%, -30\%)$ polarisation combination spares much better, where all the three scenarios can be probed with much large significance. The latter polarisation combination is capable of probing the presence of χ in all the three scenarios even with a more conservative systematics of 5%.

Following the same selection method of analysis strategy, we also study BP4 and BP5 with larger mass of χ at ILC350 and ILC500. The polarisation combination of $(+80\%, -30\%)$ can probe a χ of mass around 170 GeV and 200 GeV, respectively, for $\sqrt{s} = 350$ GeV and 500 GeV, with larger than 5σ significance.

Chapter 5

Summary and conclusions

In this chapter, we summarize all the outcome of the studies carried out in the thesis.

The SM particle spectrum is complete with the discovery of the Higgs boson by the ATLAS and CMS collaborations at LHC in 2012. In the history of particle physics, it is the remarkable success of the SM. Therefore it can be said that SM is very successful with its predictions of particle content and the dynamics of fundamental fields. Nevertheless, the SM is unable to explain many of the major issues that arise in nature and hence it has come to picture that the SM is not a complete theory to address particle dynamics at all energies. In the present era, particle physicists are in the hunt for solutions to many of such issues that arise in the SM. Few of the major unexplained phenomena are (i) SM has no mechanism to generate neutrino mass, (ii) no solution to address the DM content of the universe, (iii) the matter and antimatter asymmetry and (iv) hierarchy problem lead by Higgs mechanism.

With a possible prospect to address these issues, one must think beyond the SM and many such models have been proposed beyond the Standard Model. Among these, seesaw models could make a benchmark in the particle physics phenomenology by providing a viable mechanism to generate neutrino mass with the help of heavy scalar or fermion fields

in addition to the particle spectrum of the SM. There are other alternative BSM scenarios with multi Higgs models, which are proposed to address DM issue and hierarchy problem. These multi Higgs models can be simply achieved by adding other Higgs fields along with the SM Higgs doublet. Such multi Higgs models along with exotic fermionic partner particle can solve the issue of DM by providing scalar and fermion component of dark matter candidate. Search of these additional scalars and fermions are of much interest to the particle physics community in experimental as well as in phenomenological studies. This thesis is mainly based on Type III seesaw model, Minimal Left Right Symmetric Model and Multi Component Dark Matter Model with their collider studies of additional scalars and fermions.

In the first chapter, we have provided a brief introduction of the SM of particle physics along with its main difficulties. Further, we have briefly discussed different possible attempts to resolve these difficulties. Out of many possible BSM scenarios, in the thesis we focus on collider phenomenology of Type III seesaw model, Minimal Left Right Symmetric Model and Dark Matter model. Details about these models are presented in this chapter, followed by outline of the rest of the chapters of the thesis.

In the second chapter, we have investigated heavy fermions at high energy electron positron collider arising in Type III seesaw model through their direct production and possible decays using appropriate center of mass energy for both pair production and single production. The electron positron collider brings in specific advantage of possibility to probe the mixing of SM lepton with Type III seesaw fermions, unlike the case of pp-collider. Identifying the SM backgrounds, a detector level simulation and analysis is carried out at center of mass energy of 1 TeV for all possible final states arising in single production of charged and neutral fermion in association with a lepton and a neutrino, respectively. Assuming maximum possible electron type mixing, our study shows that fermion mass reach for single production can be closed to 1 TeV, with the integrated luminosity as small as 100 fb^{-1}. On the other hand, the pair production of charged fermion is studied using the same analysis technique at a center of mass energy of 2 TeV and an integrated luminosity of 300 fb^{-1}, considering the presence of both electron type and muon type mixing, but taking one at a time. It is found that minimum luminosity

required to probe the best final state $4b+2\ell$ is about 50 fb^{-1} with 5σ significance. Larger mass of charged fermion in pair production can be probed with even smaller values of mixings.

In the third chapter, we have focused on the collider signature of the multi leptonic final states arising from the scalar sector in Minimal Left Right Symmetric Model and get an estimate of the sensitivity of 14 TeV HL-LHC in the upcoming years. The four-leptonic final state arising from pair production of doubly charged Higgs boson in the model requires about 350 fb^{-1} integrated luminosity to probe with 5σ significance. Using the same analysis, our study can be extended to an integrated luminosity of 3 ab^{-1} and with this HL-LHC, doubly charged Higgs mass reach can be obtained upto 1080 GeV with 5σ sensitivity. The trileptonic final state arising from the production of doubly charged Higgs boson in association with singly charged Higgs requires larger integrated luminosity ranges from 800 -1200 fb^{-1} to probe with 5σ significance and the mass reach of doubly charged Higgs boson can be obtainable from trileptonic final state is upto 960 GeV at an integrated luminosity of 3 ab^{-1} with 5σ sensitivity. Thus the scenario considered in our study can be probed in the HL versions of LHC.

In chapter 4, we have studied a well motivated BSM scenario to address another contentious issue of the present day particle physics. There are many dark matter models consisting of additional charged fermion or scalar partner particles. In this work of the thesis, we consider searches of such charged fermions of the order of 100 GeV mass at the 250 GeV ILC where the gauge produced heavy fermion decays to τ leptons and DM particle. Close to realistic collider and detector simulation is used to study the significance of the $2\tau + \not{E}_T$ signal events from the SM background events made available by the ILD repository. Our analysis shows that unlike the HL-LHC, 250 GeV ILC would be able to discover such a fermion within its kinematic reach in the very early stages of its data taking.

In summary, we have focused on beyond the Standard Model setup mainly based on seesaw mechanism to generate neutrino masses and some multi component dark matter models. Collider signature of additional scalars and fermions arising in these scenarios are probed by using suitable detector level analysis. We believe that the study detailed

in this thesis will be helpful in deciphering BSM dynamics at the LHC as well as the upcoming electron-positron colliders.

Appendix A

Details of Type III seesaw model

A.1 The Lagrangian

The Lagrangian of the Type III seesaw model, discussed in Section 1.4.2 and 2.2, in the mass basis is given below,

$$\mathcal{L} = \mathcal{L}_{Kin} + \mathcal{L}_{CC} + \mathcal{L}^{\ell}_{NC} + \mathcal{L}^{\nu}_{NC} + \mathcal{L}^{\ell}_{H} + \mathcal{L}^{\nu}_{H} + \mathcal{L}^{\ell}_{\eta} + \mathcal{L}^{\nu}_{\eta} + \mathcal{L}_{\phi^-}, \tag{A.1}$$

where $\mathcal{L}_{Kin}$ is the kinetic part and

$$\mathcal{L}_{CC} = \frac{g}{\sqrt{2}} \begin{pmatrix} \bar{\ell} & \overline{\Psi} \end{pmatrix} \gamma^{\mu} W^{-}_{\mu} \left(P_L \, g^{CC}_{L} + P_R \, g^{CC}_{R} \sqrt{2} \right) \begin{pmatrix} \nu \\ \Sigma \end{pmatrix} + h.c \tag{A.2}$$

$$\mathcal{L}^{\ell}_{NC} = \frac{g}{\cos\theta_W} \begin{pmatrix} \bar{\ell} & \overline{\Psi} \end{pmatrix} \gamma^{\mu} Z_{\mu} \left(P_L \, g^{NC}_{L} + P_R \, g^{NC}_{R} \right) \begin{pmatrix} \ell \\ \Psi \end{pmatrix} \tag{A.3}$$

$$\mathcal{L}^{\nu}_{NC} = \frac{g}{2\cos\theta_W} \begin{pmatrix} \bar{\nu} & \overline{\Sigma}^{0c} \end{pmatrix} \gamma^{\mu} Z_{\mu} \left(P_L \, g^{NC}_{\nu} \right) \begin{pmatrix} \nu_L \\ \Sigma^{0c} \end{pmatrix} \tag{A.4}$$

$$\mathcal{L}^{\ell}_{H} = - \begin{pmatrix} \bar{\ell} & \overline{\Psi} \end{pmatrix} H \left(P_L \, g^{H\ell}_{L} + P_R \, g^{H\ell}_{R} \right) \begin{pmatrix} \ell \\ \Psi \end{pmatrix} \tag{A.5}$$

$$\mathcal{L}_H^{\nu} = -\begin{pmatrix}\overline{\nu} & \overline{\Sigma}^0\end{pmatrix}\frac{H}{\sqrt{2}}\left(P_L\, g_L^{H\nu} + P_R\, g_R^{H\nu}\right)\begin{pmatrix}\nu\\ \Sigma^0\end{pmatrix} \tag{A.6}$$

$$\mathcal{L}_\eta^{\ell} = -\begin{pmatrix}\overline{\ell} & \Psi\end{pmatrix} i\eta\left(P_L\, g_L^{\eta\ell} + P_R\, g_R^{\eta\ell}\right)\begin{pmatrix}\ell\\ \Psi\end{pmatrix} \tag{A.7}$$

$$\mathcal{L}_\eta^{\nu} = -\begin{pmatrix}\overline{\nu} & \overline{\Sigma}^0\end{pmatrix}\frac{i\eta}{\sqrt{2}}\left(P_L\, g_L^{\eta\nu} + P_R\, g_R^{\eta\nu}\right)\begin{pmatrix}\nu\\ \Sigma^0\end{pmatrix} \tag{A.8}$$

$$\mathcal{L}_{\phi^-} = -\begin{pmatrix}\overline{\ell} & \overline{\Psi}\end{pmatrix}\phi^-\left(P_L\, g_L^{\phi^-} + P_R\, g_R^{\phi^-}\right)\begin{pmatrix}\nu\\ \Sigma^0\end{pmatrix} + h.c. \tag{A.9}$$

where, the left and right projection operators are denoted by, $P_{L,R} = \frac{1}{2}(1 \mp \gamma_5)$. The couplings, g_i are explicitly given below in terms of the other parameters of the original Lagrangian. Here, the fields and the couplings, g_i are given in block matrix form, with

$$\begin{pmatrix}\ell\\ \Psi\end{pmatrix} \equiv \begin{pmatrix}e\\ \mu\\ \tau\\ \Psi\end{pmatrix} \text{ and } \begin{pmatrix}\nu\\ \Sigma\end{pmatrix} \equiv \begin{pmatrix}\nu_e\\ \nu_\mu\\ \nu_\tau\\ \Sigma^0\end{pmatrix}$$

$$g_L^{CC} = \begin{pmatrix}\left(1+\frac{\epsilon}{2}\right)U_{PMNS} & -\frac{v}{\sqrt{2}M_\Sigma}Y_\Sigma^\dagger\\ 0 & \sqrt{2}\left(1-\frac{\epsilon'}{2}\right)\end{pmatrix} \tag{A.10}$$

$$g_R^{CC} = \begin{pmatrix}0 & -\frac{m_\ell v}{M_\Sigma^2}Y_\Sigma^\dagger\\ -\frac{v}{\sqrt{2}M_\Sigma}Y_\Sigma^* U_{PMNS}^* & 1-\frac{\epsilon'^\star}{2}\end{pmatrix} \tag{A.11}$$

$$g_L^{NC} = \begin{pmatrix}\frac{1}{2}-\cos^2\theta_W-\epsilon & \frac{v}{2M_\Sigma}Y_\Sigma^\dagger\\ \frac{v}{2M_\Sigma}Y_\Sigma & \epsilon'-\cos^2\theta_W\end{pmatrix} \tag{A.12}$$

$$g_R^{NC} = \begin{pmatrix}1-\cos^2\theta_W & \frac{m_\ell v}{M_\Sigma^2}Y_\Sigma^\dagger\\ \frac{m_\ell v}{M_\Sigma^2}Y_\Sigma & -\cos^2\theta_W\end{pmatrix} \tag{A.13}$$

$$g_\nu^{NC} = \begin{pmatrix}1-U_{PMNS}^\dagger\,\epsilon\,U_{PMNS} & \frac{v}{\sqrt{2}\,M_\Sigma}U_{PMNS}^\dagger Y_\Sigma^\dagger\\ \frac{v}{\sqrt{2}M_\Sigma}Y_\Sigma U_{PMNS} & \epsilon'\end{pmatrix} \tag{A.14}$$

$$g_L^{H\ell} = \begin{pmatrix} \frac{m_\ell}{\upsilon}(1-3\epsilon) & \frac{m_\ell Y_\Sigma^\dagger}{M_\Sigma} \\ Y_\Sigma\left(1-\epsilon+\frac{m_\ell^2}{M_\Sigma^2}\right) & \frac{\upsilon}{M_\Sigma}Y_\Sigma Y_\Sigma^\dagger \end{pmatrix} \tag{A.15}$$

$$g_R^{H\ell} = (g_L^{H\ell})^\dagger \tag{A.16}$$

$$g_L^{H\nu} = \begin{pmatrix} -\frac{\sqrt{2}\ m_\nu^d}{\upsilon} & \frac{m_\nu}{M_\Sigma}U_{PMNS}^T Y_\Sigma^\dagger \\ Y_\Sigma(1-\frac{\epsilon}{2}-\frac{\epsilon'}{2})U_{PMNS} & \frac{\upsilon}{\sqrt{2}M_\Sigma}Y_\Sigma Y_\Sigma^\dagger \end{pmatrix} \tag{A.17}$$

$$g_R^{H\nu} = (g_L^{H\nu})^\dagger \tag{A.18}$$

$$g_L^{\eta\ell} = \begin{pmatrix} -\frac{m_\ell}{\upsilon}(1+\epsilon) & -\frac{m_\ell}{M_\Sigma}Y_\Sigma^\dagger \\ Y_\Sigma(1-\epsilon-\frac{m_\ell^2}{M_\Sigma^2}) & \frac{\upsilon}{M_\Sigma}Y_\Sigma^\dagger Y_\Sigma \end{pmatrix} \tag{A.19}$$

$$g_R^{\eta\ell} = -\left(g_L^{\eta\ell}\right)^\dagger \tag{A.20}$$

$$g_R^{\eta\nu} = -\left(g_L^{\eta\nu}\right)^\dagger \tag{A.21}$$

$$g_L^{\eta\nu} = g_L^{H\nu} \tag{A.22}$$

$$g_L^{\phi^-} = \begin{pmatrix} \sqrt{2}\frac{m_\ell}{\upsilon}(1-\frac{\epsilon}{2})U_{PMNS} & \frac{m_\ell}{M_\Sigma}Y_\Sigma^\dagger \\ \frac{\sqrt{2}m_\ell^2}{M_\Sigma^2}Y_\Sigma U_{PMNS} & 0 \end{pmatrix} \tag{A.23}$$

$$g_R^{\phi^-} = \begin{pmatrix} -\frac{\sqrt{2}m_\nu^{d\star}}{\upsilon}U_{PMNS} & Y_\Sigma^\dagger(1-\epsilon-\frac{\epsilon'^\star}{2}-\frac{2m_\nu^\star}{M_\Sigma}) \\ -\sqrt{2}Y_\Sigma^*(1-\frac{\epsilon^\star}{2})U_{PMNS}^\star & 2\left(-\frac{M_\Sigma}{\upsilon}\epsilon'+\epsilon'\frac{M_\Sigma}{\upsilon}\right) \end{pmatrix} \tag{A.24}$$

Here, $\upsilon \equiv \sqrt{2}\langle\phi^0\rangle$ is the vev of the doublet scalar field, $\epsilon = \frac{\upsilon^2}{M_\Sigma^2}Y_\Sigma^\dagger Y_\Sigma$, $\epsilon' = \frac{\upsilon^2}{2M_\Sigma^2}\sum_\ell Y_{\Sigma\ell}^2$ and U_{PMNS} is the lepton mixing matrix. The Yukawa coupling matrix $Y_\Sigma = (Y_{\Sigma e}\ \ Y_{\Sigma\mu}\ \ Y_{\Sigma\tau})$, where $Y_{\Sigma\ell}$ are the Yukawa couplings appearing in Eq. 1.33. The mixing of Σ with the SM leptons are denoted by $V_\ell = \frac{\upsilon}{\sqrt{2}M_\Sigma}Y_{\Sigma\ell}$, where $\ell = e, \mu, \tau$.

A.2 Cross sections for single and pair productions of fermions

Expressions of the invariant amplitudes for the pair and single production of charged and neutral fermions are given below, with the general expression of cross-section given by,

$$\frac{d\sigma}{dt} = (4\pi\alpha)^2 \frac{|M|^2}{16\pi s^2}.$$

1. Process $e^+e^- \to \Sigma^-\Sigma^+$

The invariant amplitude for the pair production of charged fermion can be written as ,

$$\begin{aligned} |M|^2 &= \frac{|M_{s\gamma}|^2}{s^2} + \frac{1}{\cos^4\theta_W \sin^4\theta_W}\left(\frac{|M_t|^2}{(t-m_Z^2)^2} + \frac{|M_{sz}|^2}{(s-m_Z^2)^2}\right) \\ &+ \frac{1}{\cos^4\theta_W \sin^4\theta_W}\left(\frac{M_{int}^{szt}}{(s-m_Z^2)(t-m_Z^2)}\right) \\ &+ \frac{1}{\cos^2\theta_W \sin^2\theta_W}\left(\frac{M_{int}^{\gamma z}}{s(s-m_Z^2)} + \frac{M_{int}^{\gamma t}}{s(t-m_Z^2)}\right), \end{aligned} \tag{A.25}$$

where

$$|M_t|^2 = \left(g_{L14}^{NC}\right)^4 \left(64\left((s+t)^2 + m_\Sigma^2(m_\Sigma^2 - 2s - 2t)\right) + \frac{s^2}{m_Z^2}\left(4s + t^2 + \frac{m_\Sigma^4}{m_Z^2} - 2t\frac{m_\Sigma^2}{m_Z^2}\right)(1-\beta^2)^2\right)$$

$$\begin{aligned} |M_{sz}|^2 &= 64\ g_{L44}^{NC}\ g_{R44}^{NC}\left(\left(g_{R11}^{NC}\right)^2 + \left(g_{L11}^{NC}\right)^2\right)(m_\Sigma^4 - s\ m_\Sigma^2 - 2tm_\Sigma^2 + t^2) \\ &+64\left((g_{R11}^{NC}\ g_{R44}^{NC})^2 + (g_{L11}^{NC}\ g_{L44}^{NC})^2\right)(m_\Sigma^4 - s\ m_\Sigma^2 - 2t\ m_\Sigma^2 + (s+t)^2) \end{aligned}$$

$$|M_{s\gamma}|^2 = 8s(s+2t) + 16\ (t - m_\Sigma^2)^2$$

$$\begin{aligned} M_{int}^{szt} &= \frac{g_{L11}^{NC}\ \left(g_{L14}^{NC}\right)^2}{m_Z^2}\left(32\ g_{R44}^{NC}\ m_\Sigma^2\left((t-m_\Sigma^2)^2 - 2sm_Z^2\right)\right. \\ &\left. + g_{L44}^{NC}\left(32s\left((2s+2t-1) - (s+t)^2\right) - \frac{s^4}{m_Z^2}(1-\beta^2)^2\right)\right) \end{aligned}$$

$$\begin{aligned} M_{int}^{\gamma z} &= 32\ \left(g_{L11}^{NC}\ g_{L44}^{NC} + g_{R11}^{NC}\ g_{R44}^{NC}\right)\left(s(s - m_\Sigma^2 + 2t) + (m_\Sigma^2 - t)^2\right) \\ &+32\ \left(g_{L11}^{NC}\ g_{R44}^{NC} + g_{L44}^{NC}\ g_{R11}^{NC}\right)\left(s{m_\Sigma}^2 + (m_\Sigma^2 - t)^2\right) \end{aligned}$$

$$M_{int}^{\gamma t} = (g_{L14}^{NC})^2 \left(32 m_\Sigma^2 \ (s + 2t - m_\Sigma^2) - 32(s+t)^2 - \frac{s^3}{m_Z^2}(1-\beta^2)^2 - \frac{16 m_\Sigma^2}{m_Z^2} \ (m_\Sigma^2 - t)^2 \right).$$

Here, M_t is the invariant amplitude for the t-channel process, M_{sz} and $M_{s\gamma}$ are invariant amplitudes for s-channel processes with Z boson and photon propagators, respectively (see Fig. 2.4). M_{int}^{szt} gives the interference of t-channel with s-channel with Z boson propagator. $M_{int}^{\gamma z}$ and $M_{int}^{\gamma t}$ give the interference of s-channel having photon propagator with the s-channel having Z boson, and the t-channel processes, respectively. The factor g_{ij}'s are the corresponding elements of the coupling matrix given in Eq. A.10-A.24, and the boost variable β in the above expressions can be written as $\beta = \sqrt{1 - \frac{4M_\Sigma^2}{s}}$.

2. Process $e^+(p_1)e^-(p_2) \to \Sigma^0(p_3)\nu_\ell(p_4)$

The invariant amplitude for the single production of neutral fermion can be written (with $t = (p_1 - p_3)^2$) as ,

$$|M|^2 = \frac{1}{\cos^4\theta_W \sin^4\theta_W} \left(\frac{|M_t|^2}{(t - m_Z^2)^2} + \frac{|M_s|^2}{(s - m_Z^2)^2} + \frac{M_{int}^{ts}}{(t - m_Z^2)(s - m_Z^2)} \right) \quad \text{(A.26)}$$

where

$$|M_t|^2 = \left((g_{R11}^{NC} \ g_{R14}^{NC})^2 + (g_{L11}^{NC} \ g_{L14}^{NC})^2 \right) \left(\beta^2 \ (64 s^4 - 32 ts) + \beta^4 \ (16 t^2 - 32 ts) \right) + 64 \ s^2 \beta^2 \left(g_{L14}^{NC} \ (g_{R11}^{NC})^2 \ g_{R14}^{NC} + g_{L14}^{NC} \ (g_{L11}^{NC})^2 \ g_{R14}^{NC} \right)$$

$$|M_s|^2 = \left((g_{R11}^{NC} \ g_{R14}^{NC})^2 + (g_{L11}^{NC} \ g_{L14}^{NC})^2 \right) \left(\beta^2 \ (64 \ s^2 - 32 t \ s) + \beta^4 \ (16 \ t^2 - 32 \ t \ s) \right) + \left(g_{L14}^{NC} \ (g_{R11}^{NC})^2 \ g_{R14}^{NC} + (g_{L14}^{NC} \ g_{R11}^{NC})^2 \right) \left(32 \ ts\beta^2 - \beta^4 (16 t^2 - 32 ts) \right)$$

$$M_{int}^{ts} = \left((g_{R11}^{NC} \ g_{R14}^{NC})^2 + (g_{L11}^{NC} \ g_{L14}^{NC})^2 \right) \left((64 \ t \ s - 128 s^2)\beta^2 + (64 \ t \ s - 32 \ t^2)\beta^4 \right)$$

Here again, M_t, M_s are invariant amplitudes for the t-channel, s-channel with Z boson propagator and M_{int}^{ts} is the interference term involving t- and s-channel with Z boson

propagator shown in Fig 2.1. β in the above expressions can be written as $\beta = \frac{s-M_\Sigma^2}{s+M_\Sigma^2}$.

3. Process $e^+(p_1)e^-(p_2) \to \Sigma^-(p_3)e^+(p_4)$

The invariant amplitude for the single production of charged fermion can be written (with $t = (p_1 - p_3)^2$) as ,

$$\begin{aligned} |M|^2 &= \frac{|M_\gamma|^2}{s^2} + \frac{1}{4\sin^4\theta_W}\,\frac{|M_t|^2}{(t-m_W^2)^2} + \frac{1}{4\cos^4\theta_W\sin^4\theta_W}\,\frac{|M_s|^2}{(s-m_Z^2)^2} \\ &+ \frac{1}{2\sin^2\theta_W}\,\frac{M_{int}^{gtW}}{s(t-m_W^2)} + \frac{1}{4\cos^2\theta_W\sin^4\theta_W}\,\frac{M_{int}^{ztW}}{(t-m_W^2)(s-m_Z^2)} \\ &+ \frac{1}{2\cos^2\theta_W\sin^2\theta_W}\,\frac{M_{int}^{gz}}{s(s-m_Z^2)}, \end{aligned} \tag{A.27}$$

where

$$\begin{aligned} |M_t|^2 &= \left((g_{R1\ell}^{CC}\ g_{R14}^{CC})^2 + (g_{L1\ell}^{CC}\ g_{L14}^{CC})^2\right)\left(\beta^2\ (64\ s^2 - 32\ t\ s) + \beta^4\ (16\ t^2 - 32\ t\ s)\right) \\ &\quad + 64\ s^2\beta^2\ \left((g_{R1\ell}^{CC}\ g_{L14}^{CC})^2 + (g_{L1\ell}^{CC}\ g_{R14}^{CC})^2\right) \\ |M_s|^2 &= 16\ t\ \beta^4\ (g_{\nu 14}^{NC})^2(t-2s)\left((g_{R11}^{NC})^2 + (g_{L11}^{NC})^2\right) \\ &\quad +32\ s\ \beta^2\ (g_{\nu 14}^{NC})^2(2s-t)\left((g_{L11}^{NC})^2 + 32ts(g_{R11}^{NC})^2\right) \\ |M_\gamma|^2 &= 4\beta^2(s^2 + t\beta^2(t-2s)) \\ M_{int}^{ztW} &= 32\ \beta^2(2s-\beta^2\ t)(t-2s)\ \ (g_{L1\ell}^{CC}\ g_{L14}^{CC}\ g_{L11}^{NC}\ g_{\nu 14}^{NC}) \\ M_{int}^{gtW} &= 8\ \beta^2(t-2s)(2s-t\beta^2)\left(g_{R1\ell}^{CC}\ g_{R14}^{CC} + g_{L1\ell}^{CC}\ g_{L14}^{CC}\right) \\ M_{int}^{gz} &= \beta^4\ (g_{\nu 14}^{NC})\ (8t^2 - 16\ t\ s)\left(g_{R11}^{NC} + g_{L11}^{NC}\right) + \beta^2\ g_{\nu 14}^{NC}\left(64\ t\ s\ (g_{R11}^{NC} - g_{L11}^{NC}) + 32\ s^2\ g_{L11}^{NC}\right) \end{aligned}$$

Here, M_t, M_s, M_γ are the invariant amplitudes with the propagator of W boson (t-channel), Z boson and photon, respectively . M_{int}^{ztW} is the invariant amplitude of interference terms of the s-channel with Z boson propagator and the t-channel with W boson propagator. M_{int}^{gtW} is the invariant amplitude of interference term with s-channel containing photon propagator and the t-channel containing W boson propagator. M_{int}^{gz} is

the invariant amplitude of interference term having s-channel with Z boson and photon propagator (see Fig 2.1). β in the above expressions is given by $\beta = \frac{s-M_\Sigma^2}{s+M_\Sigma^2}$.

Appendix B

Kinematic distributions of $\tau^+\tau^- + \not{E}_T$ final state in Chapter 4

We study the charged dark fermions at 250 GeV ILC in Chapter 4 considering two different type of polarization combinations. The behaviour of different kinematic distributions are almost same for BP1, BP2 and BP3. Therefore, the selection cuts mentioned in Table 4.6 are employed in all of the benchmark points considered at 250 GeV center-of-mass energy. We show the kinematic distributions for BP2 and BP3 in Fig. B.1-B.4 for two different set of polarizations below which are discussed in Section 4.4.1 of the Chapter 4.

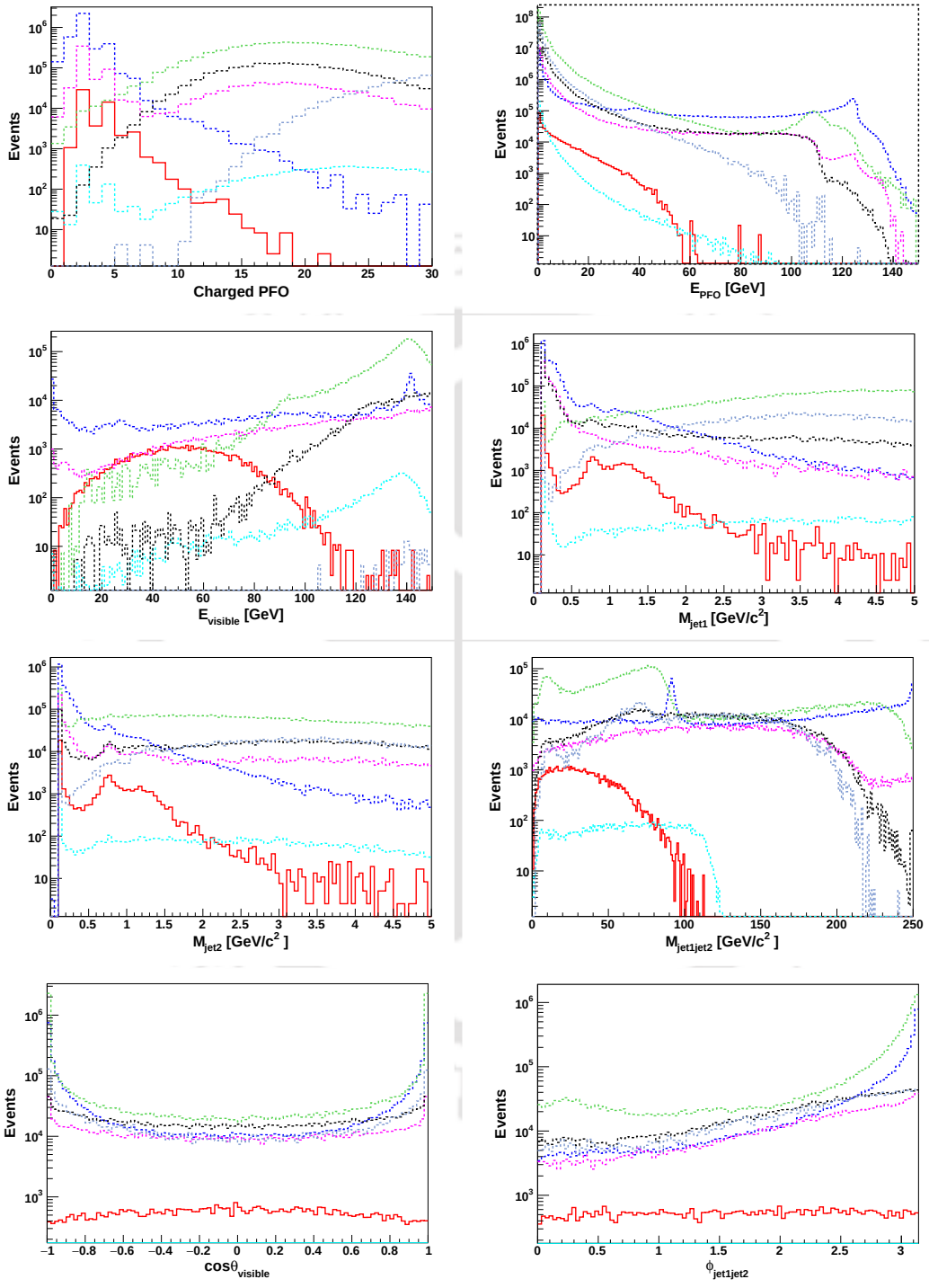

Figure B.1: *Kinematic distributions of τ^+ τ^- + $\not{E}_T$ final state for BP2 (-80%, 30%) polarization polarization, with all backgrounds before applying any selection cuts with 100 fb^{-1} integrated luminosity.*

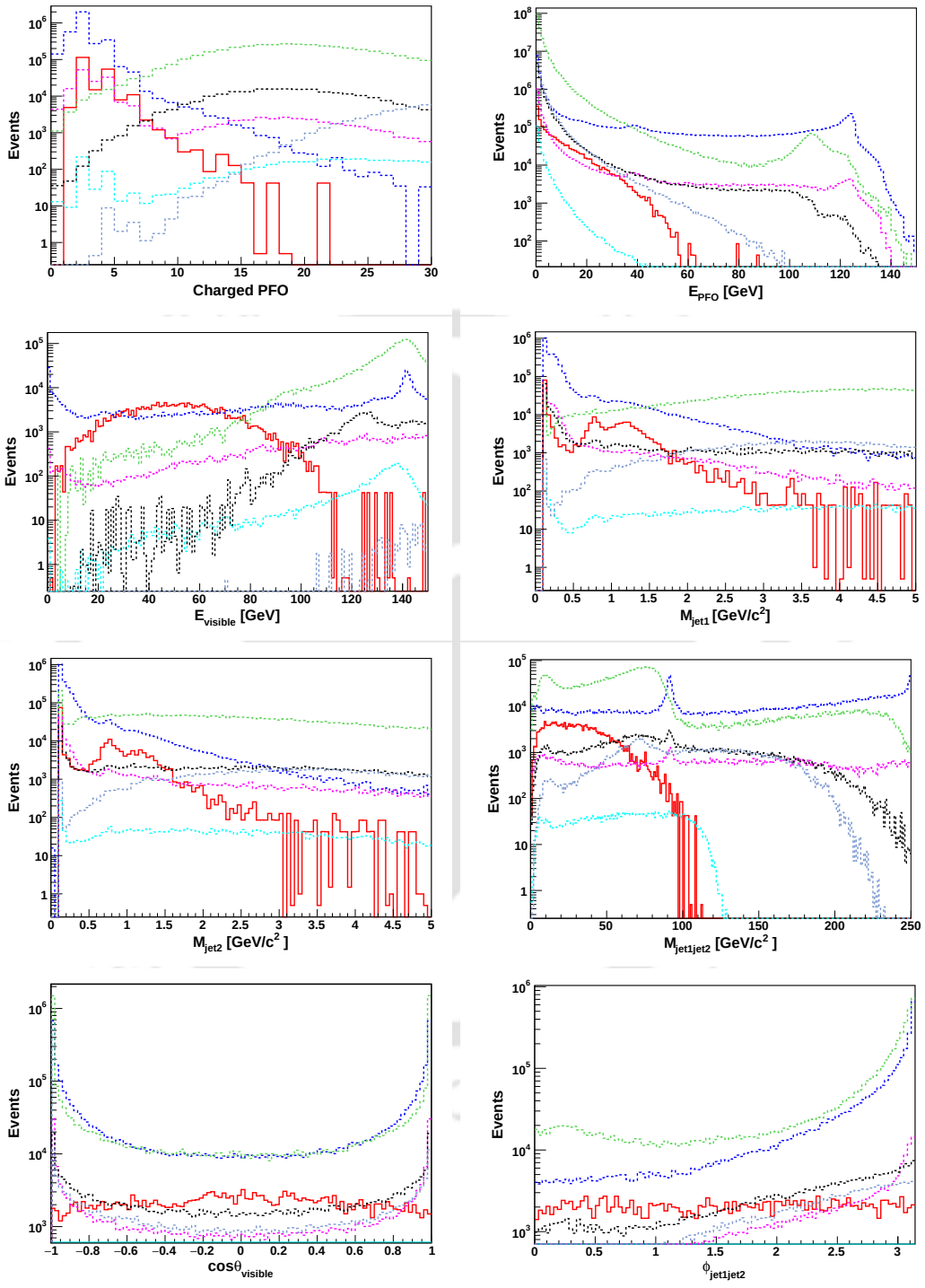

Figure B.2: *Kinematic distributions of $\tau^+\ \tau^- + \not{E}_T$ final state for BP2 (80%, -30%) polarization polarization, with all backgrounds before applying any selection cuts with 100 fb^{-1} integrated luminosity.*

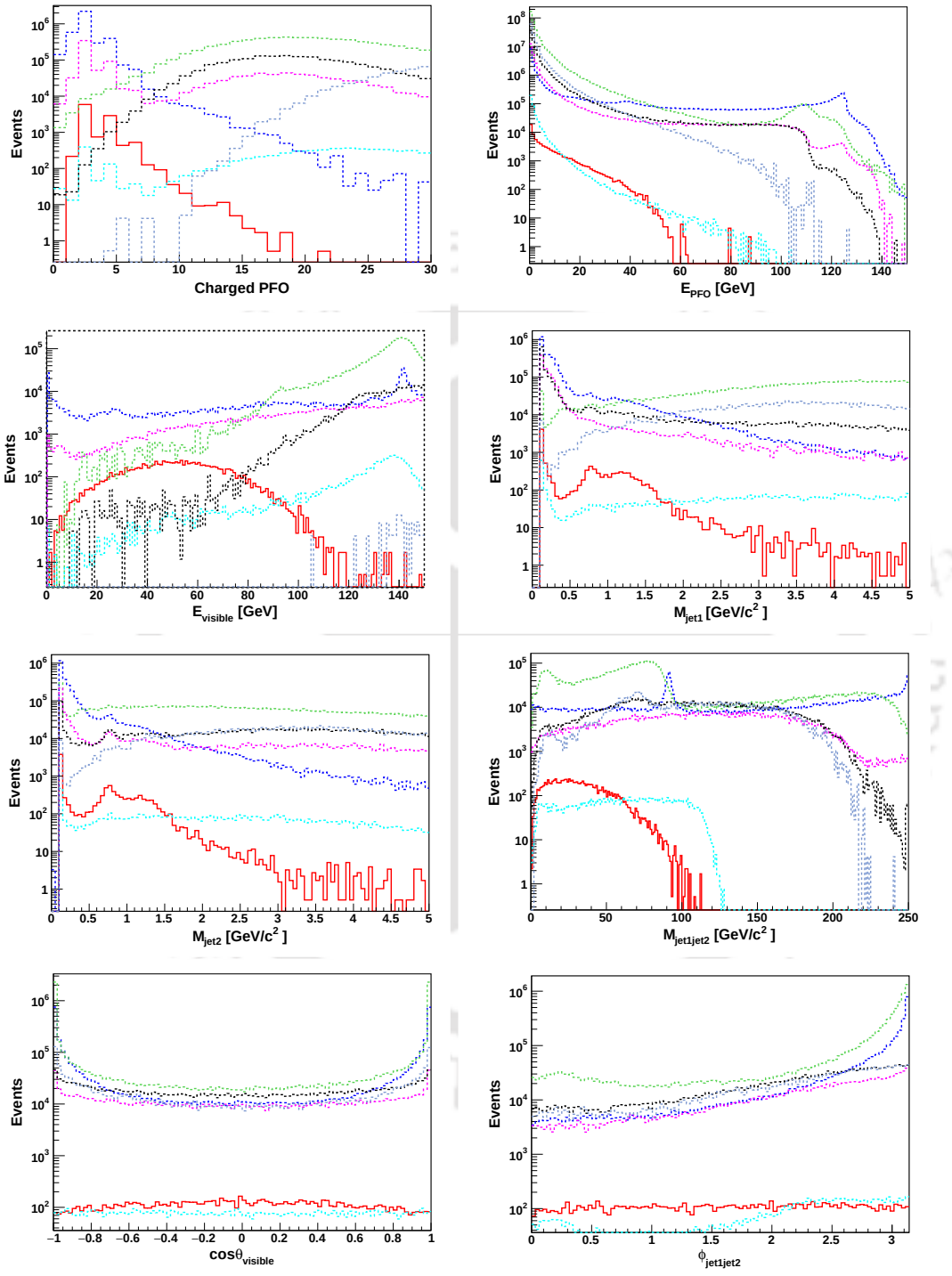

Figure B.3: *Kinematic distributions of τ^+ τ^- + $\not{E}_T$ final state for BP3 (-80%, 30%) polarization polarization, with all backgrounds before applying any selection cuts with 100 fb^{-1} integrated luminosity.*

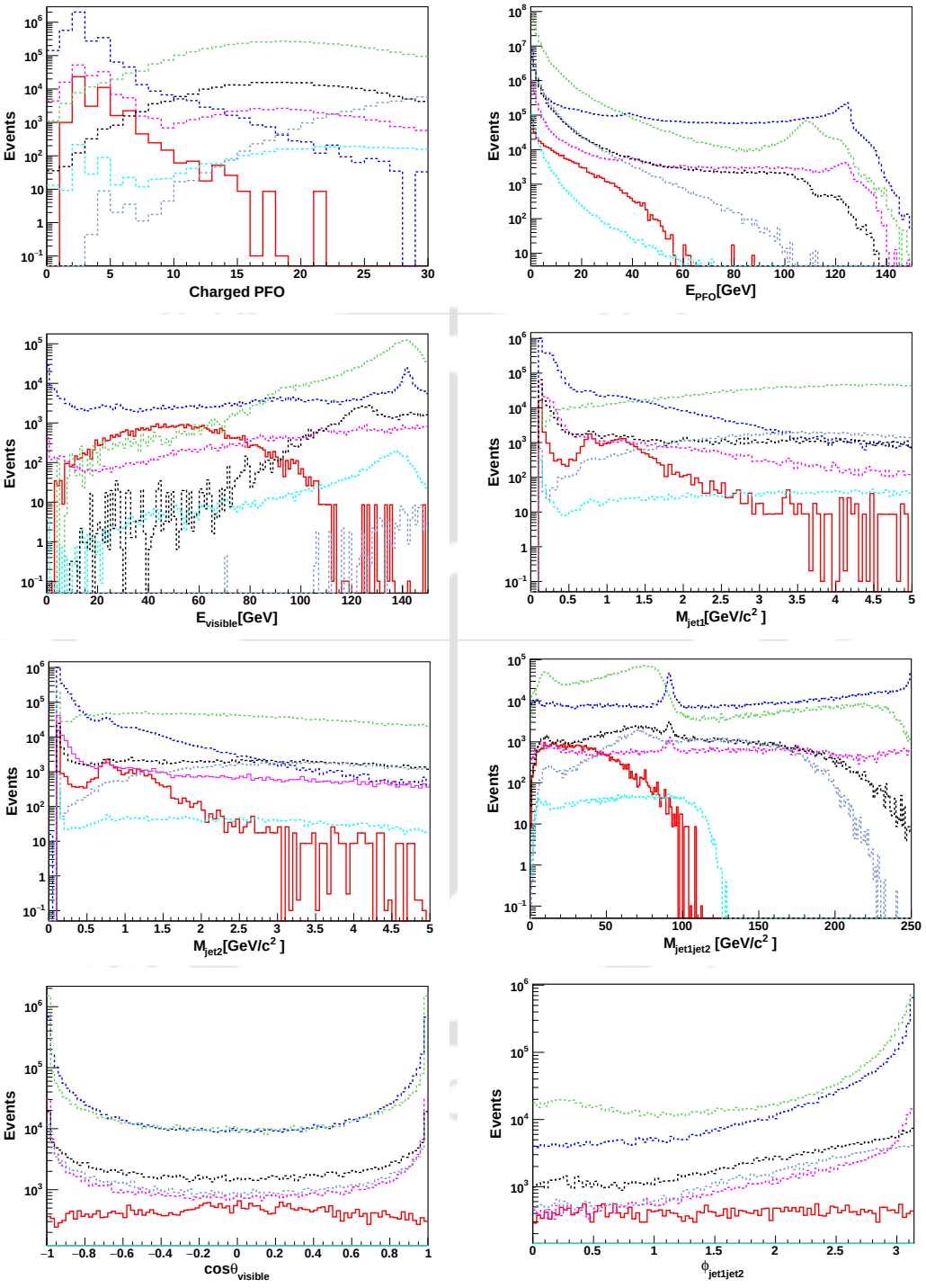

Figure B.4: *Kinematic distributions of $\tau^+\ \tau^- + \not{E}_T$ final state for BP3 (80%,-30%) polarization polarization, with all backgrounds before applying any selection cuts with 100 fb^{-1} integrated luminosity.*

Appendix C

Acronyms and abbreviations

SM	: Standard Model
BSM	: Beyond Standard Model
LHC	: Large Hadron Collider
QCD	: Quantum CromoDynamics
VEV	: Vacuum Expectation Value
ATLAS	: A Toroidal LHC ApparatuS
e	: Electron
μ	: Muon
τ	: Tau
CMS	: Compact Muon Solenoid
GeV	: Giga electron Volt
TeV	: Tera electron Volt
EM	: Electromagnetic
EW	: Electroweak

EWSB : Electroweak Symmetry Breaking

DM : Dark Matter

GUT : Grand Unified Theory

MLRSM : Minimal Left Right Symmetric Model

THDM : Two Higgs Doublet Model

IHDM : Inert Higgs Doublet Model

ILC : International Linear Collider

CLIC : Compact Linear Collider

FLC : Future Leptonic Collider

MCDM : Multi Component Dark Matter

BR : Branching Ratio

fb : femto barn

pb : pico barn

$\not{E}$: Missing Energy

MET : Missing Transverse Energy

$\not{E}_T$: Missing Transverse Energy

ISR : Initial State Radiation

FSR : Final State Radiation

ILD : International Linear Detector

MC : Monte Carlo

FCNC : Flavour Changing Neutral Current

PMNS : Pontecorvo-Maki-Nakagawa-Sakata

NLO : Next-to-Leading Order

NNLO : Next-to-Next-to-Leading Order

UFO : Universal FeynRule Output

WIMP : Weakly Interacting Massive Particle

BP : Benchmark Point

PFO : Particle Flow Object

LR : Left Right

RL : Right Left

HL : High Luminosity

Bibliography

[1] S. L. Glashow. Partial Symmetries of Weak Interactions. *Nucl. Phys.*, 22:579–588, 1961.

[2] Abdus Salam. Weak and Electromagnetic Interactions. *Conf. Proc.*, C680519:367–377, 1968.

[3] F. Englert and R. Brout. Broken Symmetry and the Mass of Gauge Vector Mesons. *Phys. Rev. Lett.*, 13:321–323, 1964. [157(1964)].

[4] Peter W. Higgs. Broken Symmetries and the Masses of Gauge Bosons. *Phys. Rev. Lett.*, 13:508–509, 1964. [160(1964)].

[5] G. S. Guralnik, C. R. Hagen, and T. W. B. Kibble. Global Conservation Laws and Massless Particles. *Phys. Rev. Lett.*, 13:585–587, 1964. [162(1964)].

[6] Serguei Chatrchyan et al. Observation of a new boson at a mass of 125 GeV with the CMS experiment at the LHC. *Phys. Lett.*, B716:30–61, 2012.

[7] Georges Aad et al. Observation of a new particle in the search for the Standard Model Higgs boson with the ATLAS detector at the LHC. *Phys. Lett.*, B716:1–29, 2012.

[8] Vera C. Rubin and W. Kent Ford, Jr. Rotation of the Andromeda Nebula from a Spectroscopic Survey of Emission Regions. *Astrophys. J.*, 159:379–403, 1970.

[9] Wayne Hu and Scott Dodelson. Cosmic microwave background anisotropies. *Ann. Rev. Astron. Astrophys.*, 40:171–216, 2002.

[10] Gianfranco Bertone, Dan Hooper, and Joseph Silk. Particle dark matter: Evidence, candidates and constraints. *Phys. Rept.*, 405:279–390, 2005.

[11] Andrew G. Cohen, A. De Rujula, and S. L. Glashow. A Matter - antimatter universe? *Astrophys. J.*, 495:539–549, 1998.

[12] Y. Fukuda et al. Evidence for oscillation of atmospheric neutrinos. *Phys. Rev. Lett.*, 81:1562–1567, 1998.

[13] Peter Minkowski. $\mu \to e\gamma$ at a Rate of One Out of 10^9 Muon Decays? *Phys. Lett.*, 67B:421–428, 1977.

[14] Murray Gell-Mann, Pierre Ramond, and Richard Slansky. Complex Spinors and Unified Theories. *Conf. Proc.*, C790927:315–321, 1979.

[15] Rabindra N. Mohapatra and Goran Senjanovic. Neutrino Mass and Spontaneous Parity Nonconservation. *Phys. Rev. Lett.*, 44:912, 1980. [231(1979)].

[16] Rabindra N. Mohapatra and Goran Senjanovic. Neutrino Masses and Mixings in Gauge Models with Spontaneous Parity Violation. *Phys. Rev.*, D23:165, 1981.

[17] J. Schechter and J. W. F. Valle. Neutrino Masses in SU(2) x U(1) Theories. *Phys. Rev.*, D22:2227, 1980.

[18] Y. Chikashige, Rabindra N. Mohapatra, and R. D. Peccei. Are There Real Goldstone Bosons Associated with Broken Lepton Number? *Phys. Lett.*, 98B:265–268, 1981.

[19] George Lazarides, Q. Shafi, and C. Wetterich. Proton Lifetime and Fermion Masses in an SO(10) Model. *Nucl. Phys.*, B181:287–300, 1981.

[20] J. Schechter and J. W. F. Valle. Neutrino Decay and Spontaneous Violation of Lepton Number. *Phys. Rev.*, D25:774, 1982.

[21] Robert Foot, H. Lew, X. G. He, and Girish C. Joshi. Seesaw Neutrino Masses Induced by a Triplet of Leptons. *Z. Phys.*, C44:441, 1989.

[22] Jogesh C. Pati and Abdus Salam. Lepton Number as the Fourth Color. *Phys. Rev.*, D10:275–289, 1974. [Erratum: Phys. Rev.D11,703(1975)].

[23] Rabindra N. Mohapatra and Jogesh C. Pati. Left-Right Gauge Symmetry and an Isoconjugate Model of CP Violation. *Phys. Rev.*, D11:566–571, 1975.

[24] R. N. Mohapatra and Jogesh C. Pati. A Natural Left-Right Symmetry. *Phys. Rev.*, D11:2558, 1975.

[25] G. Senjanovic and Rabindra N. Mohapatra. Exact Left-Right Symmetry and Spontaneous Violation of Parity. *Phys. Rev.*, D12:1502, 1975.

[26] Rabindra N. Mohapatra, Frank E. Paige, and D. P. Sidhu. Symmetry Breaking and Naturalness of Parity Conservation in Weak Neutral Currents in Left-Right Symmetric Gauge Theories. *Phys. Rev.*, D17:2462, 1978.

[27] Goran Senjanovic. Spontaneous Breakdown of Parity in a Class of Gauge Theories. *Nucl. Phys.*, B153:334–364, 1979.

[28] Rabindra N. Mohapatra and R. E. Marshak. Local B-L Symmetry of Electroweak Interactions, Majorana Neutrinos and Neutron Oscillations. *Phys. Rev. Lett.*, 44:1316–1319, 1980. [Erratum: Phys. Rev. Lett.44,1643(1980)].

[29] C. S. Lim and T. Inami. Lepton Flavor Nonconservation and the Mass Generation Mechanism for Neutrinos. *Prog. Theor. Phys.*, 67:1569, 1982.

[30] J. F. Gunion, J. Grifols, A. Mendez, Boris Kayser, and Fredrick I. Olness. Higgs Bosons in Left-Right Symmetric Models. *Phys. Rev.*, D40:1546, 1989.

[31] N. G. Deshpande, J. F. Gunion, Boris Kayser, and Fredrick I. Olness. Left-right symmetric electroweak models with triplet Higgs. *Phys. Rev.*, D44:837–858, 1991.

[32] Pavel Fileviez Perez. Type III Seesaw and Left-Right Symmetry. *JHEP*, 03:142, 2009.

[33] Goran Senjanovi and Vladimir Tello. Probing Seesaw with Parity Restoration. *Phys. Rev. Lett.*, 119(20):201803, 2017.

[34] T. D. Lee. A Theory of Spontaneous T Violation. *Phys. Rev.*, D8:1226–1239, 1973. [,516(1973)].

[35] G. C. Branco, P. M. Ferreira, L. Lavoura, M. N. Rebelo, Marc Sher, and Joao P. Silva. Theory and phenomenology of two-Higgs-doublet models. *Phys. Rept.*, 516:1–102, 2012.

[36] Nilendra G. Deshpande and Ernest Ma. Pattern of Symmetry Breaking with Two Higgs Doublets. *Phys. Rev.*, D18:2574, 1978.

[37] James Brau, Yasuhiro Okada, Nicholas J. Walker, Abdelhak Djouadi, Joseph Lykken, Klaus Monig, Mark Oreglia, Satoru Yamashita, Nan Phinney, Nobukazu Toge, et al. International Linear Collider reference design report. 1: Executive summary. 2: Physics at the ILC. 3: Accelerator. 4: Detectors. 2007.

[38] T. K. Charles et al. The Compact Linear Collider (CLIC) - 2018 Summary Report. *CERN Yellow Rep. Monogr.*, 1802:1–98, 2018.

[39] Toshinori Abe et al. The International Large Detector: Letter of Intent. 2010.

[40] H. Aihara, P. Burrows, M. Oreglia, E. L. Berger, V. Guarino, J. Repond, H. Weerts, L. Xia, J. Zhang, Q. Zhang, et al. SiD Letter of Intent. 2009.

[41] Muhammd Ahmad et al. CEPC-SPPC Preliminary Conceptual Design Report. 1. Physics and Detector. 2015.

[42] CEPC-SPPC Study Group. CEPC-SPPC Preliminary Conceptual Design Report. 2. Accelerator. 2015.

[43] CEPC Conceptual Design Report: Volume 1 - Accelerator. 2018.

[44] A. Blondel et al. LEP3: A High Luminosity e^+e^- Collider to Study the Higgs Boson. 2012.

[45] M. Bicer et al. First Look at the Physics Case of TLEP. *JHEP*, 01:164, 2014.

[46] Carla Biggio and Florian Bonnet. Implementation of the Type III Seesaw Model in FeynRules/MadGraph and Prospects for Discovery with Early LHC Data. *Eur. Phys. J.*, C72:1899, 2012.

[47] A. Abada, C. Biggio, F. Bonnet, M. B. Gavela, and T. Hambye. mu —¿ e gamma and tau —¿ l gamma decays in the fermion triplet seesaw model. *Phys. Rev.*, D78:033007, 2008.

[48] Adam Alloul, Jorgen D'Hondt, Karen De Causmaecker, Benjamin Fuks, and Michel Rausch de Traubenberg. Automated mass spectrum generation for new physics. *Eur. Phys. J.*, C73(2):2325, 2013.

[49] Aviad Roitgrund, Gad Eilam, and Shaouly Bar-Shalom. Implementation of the left-right symmetric model in FeynRules. *Comput. Phys. Commun.*, 203:18–44, 2016.

[50] K. A. Olive et al. Review of Particle Physics. *Chin. Phys.*, C38:090001, 2014.

[51] P. A. R. Ade et al. Planck 2013 results. XVI. Cosmological parameters. *Astron. Astrophys.*, 571:A16, 2014.

[52] T. Barklow, J. Brau, K. Fujii, J. Gao, J. List, N. Walker, and K. Yokoya. ILC Operating Scenarios. 2015.

[53] Ties Behnke, James E. Brau, Brian Foster, Juan Fuster, Mike Harrison, James McEwan Paterson, Michael Peskin, Marcel Stanitzki, Nicholas Walker, and Hitoshi Yamamoto. The International Linear Collider Technical Design Report - Volume 1: Executive Summary. 2013.

[54] Howard Baer, Tim Barklow, Keisuke Fujii, Yuanning Gao, Andre Hoang, Shinya Kanemura, Jenny List, Heather E. Logan, Andrei Nomerotski, Maxim Perelstein, et al. The International Linear Collider Technical Design Report - Volume 2: Physics. 2013.

[55] Chris Adolphsen, Maura Barone, Barry Barish, Karsten Buesser, Philip Burrows, John Carwardine, Jeffrey Clark, Hlne Mainaud Durand, Gerry Dugan, Eckhard Elsen, et al. The International Linear Collider Technical Design Report - Volume 3.I: Accelerator & in the Technical Design Phase. 2013.

[56] Chris Adolphsen, Maura Barone, Barry Barish, Karsten Buesser, Philip Burrows, John Carwardine, Jeffrey Clark, Hlne Mainaud Durand, Gerry Dugan, Eckhard

Elsen, et al. The International Linear Collider Technical Design Report - Volume 3.II: Accelerator Baseline Design. 2013.

[57] Gerald Aarons et al. ILC Reference Design Report Volume 1 - Executive Summary. 2007.

[58] Christoph Bartels, Anthony Hartin, Christian Helebrant, Daniela Kafer, and Jenny List. Precision Polarimetry at the ILC: Concepts, Simulations and experiments. *Nucl. Instrum. Meth.*, A623:570–572, 2010.

[59] B. Vormwald. Polarisation and Beam Energy Measurement at a Linear e^+e^- Collider. *JINST*, 9:C08012, 2014.

[60] C. Helebrant, D. Kafer, and J. List. Precision Polarimetry at the International Linear Collider. In *Proceedings, 34th International Conference on High Energy Physics (ICHEP 2008): Philadelphia, Pennsylvania, July 30-August 5, 2008*, 2008.

[61] G. Moortgat-Pick et al. The Role of polarized positrons and electrons in revealing fundamental interactions at the linear collider. *Phys. Rept.*, 460:131–243, 2008.

[62] Andre Sailer. CLIC: Status and Plan. *EPJ Web Conf.*, 70:00085, 2014.

[63] H. Abramowicz et al. Physics at the CLIC e+e- Linear Collider – Input to the Snowmass process 2013. In *Proceedings, 2013 Community Summer Study on the Future of U.S. Particle Physics: Snowmass on the Mississippi (CSS2013): Minneapolis, MN, USA, July 29-August 6, 2013*, 2013.

[64] M Aicheler, P Burrows, M Draper, T Garvey, P Lebrun, K Peach, N Phinney, H Schmickler, D Schulte, and N Toge. A Multi-TeV Linear Collider Based on CLIC Technology. 2012.

[65] P. Lebrun, L. Linssen, A. Lucaci-Timoce, D. Schulte, F. Simon, S. Stapnes, N. Toge, H. Weerts, and J. Wells. The CLIC Programme: Towards a Staged e^+e^- Linear Collider Exploring the Terascale : CLIC Conceptual Design Report. 2012.

[66] Borut Bajc, Miha Nemevsek, and Goran Senjanovic. Probing seesaw at LHC. *Phys. Rev.*, D76:055011, 2007.

[67] Roberto Franceschini, Thomas Hambye, and Alessandro Strumia. Type-III see-saw at LHC. *Phys. Rev.*, D78:033002, 2008.

[68] F. del Aguila and J. A. Aguilar-Saavedra. Distinguishing seesaw models at LHC with multi-lepton signals. *Nucl. Phys.*, B813:22–90, 2009.

[69] Tong Li and Xiao-Gang He. Neutrino Masses and Heavy Triplet Leptons at the LHC: Testability of Type III Seesaw. *Phys. Rev.*, D80:093003, 2009.

[70] Priyotosh Bandyopadhyay, Suyong Choi, Eung Jin Chun, and Kyungnam Min. Probing Higgs bosons via the type III seesaw mechanism at the LHC. *Phys. Rev.*, D85:073013, 2012.

[71] O. J. P. Eboli, J. Gonzalez-Fraile, and M. C. Gonzalez-Garcia. Neutrino Masses at LHC: Minimal Lepton Flavour Violation in Type-III See-saw. *JHEP*, 12:009, 2011.

[72] Federico von der Pahlen, Guillermo Palacio, Diego Restrepo, and Oscar Zapata. Radiative Type III Seesaw Model and its collider phenomenology. *Phys. Rev.*, D94(3):033005, 2016.

[73] Richard Ruiz. QCD Corrections to Pair Production of Type III Seesaw Leptons at Hadron Colliders. *JHEP*, 12:165, 2015.

[74] CMS Collaboration. Search for Type-III Seesaw Heavy Fermions with Multilepton Final States using 2.3/fb of 13 TeV proton-proton Collision Data. 2016.

[75] The ATLAS collaboration. Search for type-III seesaw heavy leptons in proton-proton collisions at $\sqrt{s} = 13$ TeV with the ATLAS detector. 2018.

[76] Albert M Sirunyan et al. Search for Evidence of the Type-III Seesaw Mechanism in Multilepton Final States in Proton-Proton Collisions at $\sqrt{s} = 13$ TeV. *Phys. Rev. Lett.*, 119(22):221802, 2017.

[77] Han Liang, Xiao-Gang He, Wen-Gan Ma, Shao-Ming Wang, and Ren-You Zhang. Seesaw Type I and III at the LHeC. *JHEP*, 09:023, 2010.

[78] Chong-Xing Yue, Hao-Lin Feng, and Wei Ma. Heavy charged leptons from type-III seesaw and pair production of the Higgs boson H at the International Linear e+ e- Collider. *Chin. Phys. Lett.*, 27:011202, 2010.

[79] Ernest Ma. Radiative inverse seesaw mechanism for nonzero neutrino mass. *Phys. Rev.*, D80:013013, 2009.

[80] A. Abada, C. Biggio, F. Bonnet, M. B. Gavela, and T. Hambye. Low energy effects of neutrino masses. *JHEP*, 12:061, 2007.

[81] F. del Aguila, J. de Blas, and M. Perez-Victoria. Effects of new leptons in Electroweak Precision Data. *Phys. Rev.*, D78:013010, 2008.

[82] Eric Conte, Benjamin Fuks, and Guillaume Serret. MadAnalysis 5, A User-Friendly Framework for Collider Phenomenology. *Comput. Phys. Commun.*, 184:222–256, 2013.

[83] Torbjorn Sjostrand, Stephen Mrenna, and Peter Z. Skands. PYTHIA 6.4 Physics and Manual. *JHEP*, 05:026, 2006.

[84] Matteo Cacciari, Gavin P. Salam, and Gregory Soyez. FastJet User Manual. *Eur. Phys. J.*, C72:1896, 2012.

[85] J. de Favereau, C. Delaere, P. Demin, A. Giammanco, V. Lematre, A. Mertens, and M. Selvaggi. DELPHES 3, A modular framework for fast simulation of a generic collider experiment. *JHEP*, 02:057, 2014.

[86] Steven Weinberg. Baryon and Lepton Nonconserving Processes. *Phys. Rev. Lett.*, 43:1566–1570, 1979.

[87] Tsutomu Yanagida. Horizontal symmetry and masses of neutrinos. *Conf. Proc.*, C7902131:95–99, 1979.

[88] C. Wetterich. Neutrino Masses and the Scale of B-L Violation. *Nucl. Phys.*, B187:343–375, 1981.

[89] Gabriela Barenboim, Martin Gorbahn, Ulrich Nierste, and Martti Raidal. Higgs sector of the minimal left-right symmetric model. *Phys. Rev.*, D65:095003, 2002.

[90] J. Polak and M. Zralek. Higgs sector influence on left-right symmetric model parameters. *Phys. Lett.*, B276:492–496, 1992.

[91] Georges Azuelos, K. Benslama, and J. Ferland. Prospects for the search for a doubly-charged Higgs in the left-right symmetric model with ATLAS. *J. Phys.*, G32(2):73–91, 2006.

[92] Dong-Won Jung and Kang Young Lee. Production of the charged Higgs bosons at the CERN Large Hadron Collider in the left-right symmetric model. *Phys. Rev.*, D78:015022, 2008.

[93] G. Bambhaniya, J. Chakrabortty, J. Gluza, M. Kordiaczyńska, and R. Szafron. Left-Right Symmetry and the Charged Higgs Bosons at the LHC. *JHEP*, 05:033, 2014.

[94] Adam Alloul, Mariana Frank, Benjamin Fuks, and Michel Rausch de Traubenberg. Doubly-charged particles at the Large Hadron Collider. *Phys. Rev.*, D88:075004, 2013.

[95] Bhaskar Dutta, Ricardo Eusebi, Yu Gao, Tathagata Ghosh, and Teruki Kamon. Exploring the doubly charged Higgs boson of the left-right symmetric model using vector boson fusionlike events at the LHC. *Phys. Rev.*, D90:055015, 2014.

[96] G. Bambhaniya, J. Chakrabortty, J. Gluza, T. Jeliński, and M. Kordiaczynska. Lowest limits on the doubly charged Higgs boson masses in the minimal left-right symmetric model. *Phys. Rev.*, D90(9):095003, 2014.

[97] Alessio Maiezza, Miha Nemevek, and Fabrizio Nesti. Lepton Number Violation in Higgs Decay at LHC. *Phys. Rev. Lett.*, 115:081802, 2015.

[98] G. Bambhaniya, J. Chakrabortty, J. Gluza, T. Jelinski, and R. Szafron. Search for doubly charged Higgs bosons through vector boson fusion at the LHC and beyond. *Phys. Rev.*, D92(1):015016, 2015.

[99] P. S. Bhupal Dev, Rabindra N. Mohapatra, and Yongchao Zhang. Probing the Higgs Sector of the Minimal Left-Right Symmetric Model at Future Hadron Colliders. *JHEP*, 05:174, 2016.

[100] K. S. Babu and Sudip Jana. Probing Doubly Charged Higgs Bosons at the LHC through Photon Initiated Processes. *Phys. Rev.*, D95(5):055020, 2017.

[101] Alessio Maiezza, Goran Senjanovi, and Juan Carlos Vasquez. Higgs sector of the minimal left-right symmetric theory. *Phys. Rev.*, D95(9):095004, 2017.

[102] Tao Han, Biswarup Mukhopadhyaya, Zongguo Si, and Kai Wang. Pair production of doubly-charged scalars: Neutrino mass constraints and signals at the LHC. *Phys. Rev.*, D76:075013, 2007.

[103] Pavel Fileviez Perez, Tao Han, Gui-yu Huang, Tong Li, and Kai Wang. Neutrino Masses and the CERN LHC: Testing Type II Seesaw. *Phys. Rev.*, D78:015018, 2008.

[104] A. G. Akeroyd, Cheng-Wei Chiang, and Naveen Gaur. Leptonic signatures of doubly charged Higgs boson production at the LHC. *JHEP*, 11:005, 2010.

[105] Eung Jin Chun, Kang Young Lee, and Seong Chan Park. Testing Higgs triplet model and neutrino mass patterns. *Phys. Lett.*, B566:142–151, 2003.

[106] Zhi-Long Han, Ran Ding, and Yi Liao. LHC Phenomenology of Type II Seesaw: Nondegenerate Case. *Phys. Rev.*, D91:093006, 2015.

[107] Zhi-Long Han, Ran Ding, and Yi Liao. LHC phenomenology of the type II seesaw mechanism: Observability of neutral scalars in the nondegenerate case. *Phys. Rev.*, D92(3):033014, 2015.

[108] M. Chabab, M. C. Peyranere, and L. Rahili. Degenerate Higgs bosons decays to $\gamma\gamma$ and $Z\gamma$ in the type II seesaw model. *Phys. Rev.*, D90(3):035026, 2014.

[109] G. Ecker, W. Grimus, and H. Neufeld. Higgs Induced Flavor Changing Neutral Interactions in SU(2)-l X SU(2)-r X U(1). *Phys. Lett.*, B127:365, 1983. [Erratum: Phys. Lett.B132,467(1983)].

[110] Rabindra N. Mohapatra, Goran Senjanovic, and Minh D. Tran. Strangeness Changing Processes and the Limit on the Right-handed Gauge Boson Mass. *Phys. Rev.*, D28:546, 1983.

[111] M. E. Pospelov. FCNC in left-right symmetric theories and constraints on the right-handed scale. *Phys. Rev.*, D56:259–264, 1997.

[112] Yue Zhang, Haipeng An, Xiangdong Ji, and Rabindra N. Mohapatra. General CP Violation in Minimal Left-Right Symmetric Model and Constraints on the Right-Handed Scale. *Nucl. Phys.*, B802:247–279, 2008.

[113] Alessio Maiezza, Miha Nemevsek, Fabrizio Nesti, and Goran Senjanovic. Left-Right Symmetry at LHC. *Phys. Rev.*, D82:055022, 2010.

[114] G. Beall, Myron Bander, and A. Soni. Constraint on the Mass Scale of a Left-Right Symmetric Electroweak Theory from the $K(L)$ $K(S)$ Mass Difference. *Phys. Rev. Lett.*, 48:848, 1982.

[115] Alessio Maiezza, Miha Nemevek, and Fabrizio Nesti. Perturbativity and mass scales in the minimal left-right symmetric model. *Phys. Rev.*, D94(3):035008, 2016.

[116] Morad Aaboud et al. Search for a new heavy gauge boson resonance decaying into a lepton and missing transverse momentum in 36 fb^{-1} of pp collisions at $\sqrt{s} = 13$ TeV with the ATLAS experiment. 2017.

[117] Morad Aaboud et al. Search for new phenomena in dijet events using 37 fb^{-1} of pp collision data collected at $\sqrt{s}$ =13 TeV with the ATLAS detector. *Phys. Rev.*, D96(5):052004, 2017.

[118] Albert M Sirunyan et al. Search for dijet resonances in protonproton collisions at $\sqrt{s} = 13$ TeV and constraints on dark matter and other models. *Phys. Lett.*, B769:520–542, 2017. [Erratum: Phys. Lett.B772,882(2017)].

[119] Vardan Khachatryan et al. Search for heavy gauge W' boson in events with an energetic lepton and large missing transverse momentum at $\sqrt{s} = 13$ TeV. *Phys. Lett.*, B770:278–301, 2017.

[120] Albert M Sirunyan et al. Search for high-mass resonances in final states with a lepton and missing transverse momentum at $\sqrt{s} = 13$ TeV. *Submitted to: JHEP*, 2018.

[121] Morad Aaboud et al. Search for doubly charged Higgs boson production in multi-lepton final states with the ATLAS detector using protonproton collisions at $\sqrt{s} =$ 13 TeV. *Eur. Phys. J.*, C78(3):199, 2018.

[122] Wai-Yee Keung and Goran Senjanovic. Majorana Neutrinos and the Production of the Right-handed Charged Gauge Boson. *Phys. Rev. Lett.*, 50:1427, 1983.

[123] Lorenzo Basso, Benjamin Fuks, Manuel E. Krauss, and Werner Porod. Doubly-charged Higgs and vacuum stability in left-right supersymmetry. *JHEP*, 07:147, 2015.

[124] Albert M Sirunyan et al. Search for a heavy right-handed W boson and a heavy neutrino in events with two same-flavor leptons and two jets at $\sqrt{s} = 13$ TeV. *Submitted to: JHEP*, 2018.

[125] Vladimir Tello, Miha Nemevsek, Fabrizio Nesti, Goran Senjanovic, and Francesco Vissani. Left-Right Symmetry: from LHC to Neutrinoless Double Beta Decay. *Phys. Rev. Lett.*, 106:151801, 2011.

[126] Gulab Bambhaniya, P. S. Bhupal Dev, Srubabati Goswami, and Manimala Mitra. The Scalar Triplet Contribution to Lepton Flavour Violation and Neutrinoless Double Beta Decay in Left-Right Symmetric Model. *JHEP*, 04:046, 2016.

[127] Debasish Borah and Arnab Dasgupta. Neutrinoless Double Beta Decay in Type I+II Seesaw Models. *JHEP*, 11:208, 2015.

[128] Debasish Borah and Arnab Dasgupta. Charged lepton flavour violcxmation and neutrinoless double beta decay in left-right symmetric models with type I+II seesaw. *JHEP*, 07:022, 2016.

[129] Debasish Borah. Light sterile neutrino and dark matter in left-right symmetric models without a Higgs bidoublet. *Phys. Rev.*, D94(7):075024, 2016.

[130] Mariana Frank, Benjamin Fuks, Katri Huitu, Santosh Kumar Rai, and Harri Waltari. Resonant slepton production and right sneutrino dark matter in left-right supersymmetry. *JHEP*, 05:015, 2017.

[131] Jack Y. Araz, Mariana Frank, and Benjamin Fuks. Differentiating $U(1)'$ supersymmetric models with right sneutrino and neutralino dark matter. *Phys. Rev.*, D96(1):015017, 2017.

[132] Miha Nemevsek, Goran Senjanovic, and Vladimir Tello. Connecting Dirac and Majorana Neutrino Mass Matrices in the Minimal Left-Right Symmetric Model. *Phys. Rev. Lett.*, 110(15):151802, 2013.

[133] M. J. Luo and Q. Y. Liu. Small Neutrino Masses From Structural cancellation In Left-Right Symmetric Model. *JHEP*, 12:061, 2008.

[134] Adam Alloul, Neil D. Christensen, Cline Degrande, Claude Duhr, and Benjamin Fuks. FeynRules 2.0 - A complete toolbox for tree-level phenomenology. *Comput. Phys. Commun.*, 185:2250–2300, 2014.

[135] Celine Degrande, Claude Duhr, Benjamin Fuks, David Grellscheid, Olivier Mattelaer, and Thomas Reiter. UFO - The Universal FeynRules Output. *Comput. Phys. Commun.*, 183:1201–1214, 2012.

[136] Matteo Cacciari, Gavin P. Salam, and Gregory Soyez. The Anti-k(t) jet clustering algorithm. *JHEP*, 04:063, 2008.

[137] F. Cascioli, T. Gehrmann, M. Grazzini, S. Kallweit, P. Maierhfer, A. von Manteuffel, S. Pozzorini, D. Rathlev, L. Tancredi, and E. Weihs. ZZ production at hadron colliders in NNLO QCD. *Phys. Lett.*, B735:311–313, 2014.

[138] Adam Kardos, Zoltan Trocsanyi, and Costas Papadopoulos. Top quark pair production in association with a Z-boson at NLO accuracy. *Phys. Rev.*, D85:054015, 2012.

[139] Glen Cowan, Kyle Cranmer, Eilam Gross, and Ofer Vitells. Asymptotic formulae for likelihood-based tests of new physics. *Eur. Phys. J.*, C71:1554, 2011. [Erratum: Eur. Phys. J.C73,2501(2013)].

[140] Massimiliano Grazzini, Stefan Kallweit, Dirk Rathlev, and Marius Wiesemann. $W^{\pm}Z$ production at hadron colliders in NNLO QCD. *Phys. Lett.*, B761:179–183, 2016.

[141] Shen Yong-Bai, Zhang Ren-You, Ma Wen-Gan, Li Xiao-Zhou, and Guo Lei. NLO QCD + EW corrections to WWW production with leptonic decays at the LHC. 2016.

[142] F. Campanario, V. Hankele, C. Oleari, S. Prestel, and D. Zeppenfeld. QCD corrections to charged triple vector boson production with leptonic decay. *Phys. Rev.*, D78:094012, 2008.

[143] Hai Tao Li, Chong Sheng Li, and Shi Ang Li. Renormalization group improved predictions for $t\bar{t}W^{\pm}$ production at hadron colliders. *Phys. Rev.*, D90(9):094009, 2014.

[144] G. Hinshaw et al. Nine-Year Wilkinson Microwave Anisotropy Probe (WMAP) Observations: Cosmological Parameter Results. *Astrophys. J. Suppl.*, 208:19, 2013.

[145] Laura Lopez Honorez, Emmanuel Nezri, Josep F. Oliver, and Michel H. G. Tytgat. The Inert Doublet Model: An Archetype for Dark Matter. *JCAP*, 0702:028, 2007.

[146] T. Hambye, F. S. Ling, L. Lopez Honorez, and J. Rocher. Scalar Multiplet Dark Matter. *JHEP*, 07:090, 2009. [Erratum: JHEP05,066(2010)].

[147] Laura Lopez Honorez and Carlos E. Yaguna. The inert doublet model of dark matter revisited. *JHEP*, 09:046, 2010.

[148] Alexander Belyaev, Giacomo Cacciapaglia, Igor P. Ivanov, Felipe Rojas-Abatte, and Marc Thomas. Anatomy of the Inert Two Higgs Doublet Model in the light of the LHC and non-LHC Dark Matter Searches. *Phys. Rev.*, D97(3):035011, 2018.

[149] P. Poulose, Shibananda Sahoo, and K. Sridhar. Exploring the Inert Doublet Model through the dijet plus missing transverse energy channel at the LHC. *Phys. Lett.*, B765:300–306, 2017.

[150] Sreemanti Chakraborti and Poulose Poulose. Interplay of Scalar and Fermionic Components in a Multi-component Dark Matter Scenario. 2018.

[151] Debasish Borah, Soumya Sadhukhan, and Shibananda Sahoo. Lepton Portal Limit of Inert Higgs Doublet Dark Matter with Radiative Neutrino Mass. *Phys. Lett.*, B771:624–632, 2017.

[152] Aqeel Ahmed, Mateusz Duch, Bohdan Grzadkowski, and Michal Iglicki. Multi-Component Dark Matter: the vector and fermion case. 2017.

[153] Andrei Angelescu and Giorgio Arcadi. Dark Matter Phenomenology of SM and Enlarged Higgs Sectors Extended with Vector Like Leptons. *Eur. Phys. J.*, C77(7):456, 2017.

[154] Subhaditya Bhattacharya, Nirakar Sahoo, and Narendra Sahu. Minimal vectorlike leptonic dark matter and signatures at the LHC. *Phys. Rev.*, D93(11):115040, 2016.

[155] Subhaditya Bhattacharya, Nirakar Sahoo, and Narendra Sahu. Singlet-Doublet Fermionic Dark Matter, Neutrino Mass and Collider Signatures. *Phys. Rev.*, D96(3):035010, 2017.

[156] Basabendu Barman, Debasish Borah, Lopamudra Mukherjee, and Soumitra Nandi. Correlating the anomalous results in $b \to s$ decays with inert Higgs doublet dark matter and muon $(g-2)$. 2018.

[157] Subhaditya Bhattacharya, Purusottam Ghosh, and Narendra Sahu. Multipartite Dark Matter with Scalars, Fermions and signatures at LHC. 2018.

[158] Marcela Carena, Ariel Megevand, Mariano Quiros, and Carlos E. M. Wagner. Electroweak baryogenesis and new TeV fermions. *Nucl. Phys.*, B716:319–351, 2005.

[159] Hooman Davoudiasl, Ian Lewis, and Eduardo Ponton. Electroweak Phase Transition, Higgs Diphoton Rate, and New Heavy Fermions. *Phys. Rev.*, D87(9):093001, 2013.

[160] Daniel Egana-Ugrinovic. The minimal fermionic model of electroweak baryogenesis. *Journal of High Energy Physics*, 2017(12):64, Dec 2017.

[161] Morad Aaboud et al. Search for the direct production of charginos and neutralinos in final states with tau leptons in $\sqrt{s} = 13$ TeV pp collisions with the ATLAS detector. *Eur. Phys. J.*, C78(2):154, 2018.

[162] A. M. Sirunyan et al. Combined search for electroweak production of charginos and neutralinos in proton-proton collisions at $\sqrt{s} = 13$ TeV. *JHEP*, 03:160, 2018.

[163] Albert M. Sirunyan et al. Search for supersymmetry in events with a τ lepton pair and missing transverse momentum in proton-proton collisions at $\sqrt{s} = 13$ TeV. *JHEP*, 11:151, 2018.

[164] Prospects for searches for staus, charginos and neutralinos at the high luminosity LHC with the ATLAS Detector. Technical Report ATL-PHYS-PUB-2018-048, CERN, Geneva, Dec 2018.

[165] http://pdg.lbl.gov/2019/reviews/rpp2018-rev-tau-branching-fractions.pdf . Technical report.

[166] Trong Hieu Tran, Vladislav Balagura, Vincent Boudry, Jean-Claude Brient, and Henri Videau. Reconstruction and classification of tau lepton decays with ILD. *Eur. Phys. J.*, C76(8):468, 2016.

[167] Wolfgang Kilian, Thorsten Ohl, and Jurgen Reuter. WHIZARD: Simulating Multi-Particle Processes at LHC and ILC. *Eur. Phys. J.*, C71:1742, 2011.

[168] Torbjrn Sjstrand, Stefan Ask, Jesper R. Christiansen, Richard Corke, Nishita Desai, Philip Ilten, Stephen Mrenna, Stefan Prestel, Christine O. Rasmussen, and Peter Z. Skands. An Introduction to PYTHIA 8.2. *Comput. Phys. Commun.*, 191:159–177, 2015.

[169] N. Davidson, G. Nanava, T. Przedzinski, E. Richter-Was, and Z. Was. Universal Interface of TAUOLA Technical and Physics Documentation. *Comput. Phys. Commun.*, 183:821–843, 2012.

[170] iLCsoft (2018), http://ilcsoft.desy.de/portal.

[171] Halina Abramowicz et al. The International Linear Collider Technical Design Report - Volume 4: Detectors. 2013.

[172] P. Mora de Freitas and H. Videau. Detector simulation with MOKKA / GEANT4: Present and future. In *Linear colliders. Proceedings, International Workshop on physics and experiments with future electron-positron linear colliders, LCWS 2002, Seogwipo, Jeju Island, Korea, August 26-30, 2002*, pages 623–627, 2002.

[173] F. Gaede. Marlin and LCCD: Software tools for the ILC. *Nucl. Instrum. Meth.*, A559:177–180, 2006.